Modern Aspects of Electrochemistry 60

Stojan Djokić *Editor*

Biomedical and Pharmaceutical Applications of Electrochemistry

Springer

Stojan Djokić
Editor

Biomedical and Pharmaceutical Applications of Electrochemistry

Editor
Stojan Djokić
Elchem Consulting Ltd.
Edmonton, AB, Canada

ISSN 0076-9924 ISSN 2197-7941 (electronic)
Modern Aspects of Electrochemistry
ISBN 978-3-319-31847-9 ISBN 978-3-319-31849-3 (eBook)
DOI 10.1007/978-3-319-31849-3

Library of Congress Control Number: 2016943423

Printed on acid-free paper

This Springer imprint is published by Springer Nature
The registered company is Springer International Publishing AG Switzerland

Contents

Chapter 2
Contribution to the Recent Advances in Electrochemical Analysis of Pharmaceuticals

Milka L. Avramov Ivić, Slobodan D. Petrović, and Dušan Ž. Mijin

2.1 Introduction

Electrochemistry is rapidly growing area with a number of possible applications in the pharmaceutical analysis. Modern electrochemical methods are selective, sensitive, rapid, and provide easy techniques applicable to analyses in the pharmaceutical field. It is evident that the electroanalytical techniques at varying levels of sensitivity are required to solve analytical–pharmaceutical problems. The advantages of electrochemical methods are the simple procedures of the sample preparation and in most cases lack of interferences from excipients in the pharmaceutical dosage forms.

M.L.A. Ivić (✉)
ICTM-Institute of Electrochemistry, University of Belgrade, Njegoševa 12, P.O. Box 473, 11000 Belgrade, Serbia
e-mail: milka@tmf.bg.ac.rs

S.D. Petrović • D.Ž. Mijin
Faculty of Technology and Metallurgy, University of Belgrade, Karnegijeva 4, P.O. Box 3503, 11001 Belgrade, Serbia
e-mail: sloba@tmf.bg.ac.rs; kavur@tmf.bg.ac.rs

S. Djokić (ed.), *Biomedical and Pharmaceutical Applications of Electrochemistry*, Modern Aspects of Electrochemistry 60,
DOI 10.1007/978-3-319-31849-3_2

The electroanalysis of pharmaceutically active compounds is actively involved in new research areas of different techniques due to the progress in electronics and computer sciences [1]. Many new electroanalytical techniques that have been successfully applied for trace measurements of important pharmaceutically active compounds due to the high sensitivity and selectivity that they provide.

This review concerns on recent advances in the application of various modern electrochemical techniques to the analysis of pharmaceuticals and biological samples. It is known that different highly sensitive electrochemical techniques are well established in the analysis of selected drugs. The application and choice of the most preferred electrochemical techniques applied to the analysis is closely related on physicochemical properties of the organic functional groups that comprise any given drug structure, especially on redox properties of the pharmaceuticals and biomolecules in real samples.

Cyclic voltammetry (CV) is often the first experiment performed in an electrochemical study of pharmaceutical compound. It is effectively used in the fields of organic chemistry, biochemistry, and environmental electrochemistry. The effectiveness of CV is in capability for rapidly observing the redox behavior over a wide potential range and for the initial information about electrode/pharmaceutical compound interface. CV has become a popular tool for more than 40 years for studying electrochemical reaction. CV is the most versatile electroanalytical technique in pharmaceutical analysis [2].

A pulse technique was proposed by Barker and Gardner in order to increase the sensitivity of the technique and to lower the detection limits for electroactive species. Differential pulse voltammetry (DPV) is very useful for the determination of trace amounts of electroactive compound in pharmaceuticals and biological fluids. There are numerous studies related to the electrochemical aspects of antimicrobial drugs. Generally, these are focused on the electroanalytical determination of antimicrobial drugs of importance in medicine [2]. The used electroanalytical methods were rapid, requiring less than 5 min to perform. It showed the possibility of monitoring this drug compound, making

the method useful for pharmacokinetic and pharmacodynamic purposes. It requires no complex pretreatment of the active principle to be determined. Easy applicability and availability of low-cost instruments are the important advantages of DPV. DPV/DPP (Differential Pulse Polarography) is often the method of choice for therapeutic dose analysis because of the low limit of detection of approximately 10^{-8} M. Square wave voltammetry (SWV) is a large amplitude differential technique in which a waveform is composed of symmetrical square waves. Excellent sensitivity in SWV is gained from the fact that net current is large compared to either forward or backward current, coupled with effective discrimination against the charging current. The peak currents obtained are about four times higher than the differential pulse response. The major advantage of SWV is its speed. The effective scan rate is of the order of 500 mVs^{-1}. As a result, the analysis time is drastically reduced. A complete voltammogram can be recorded within a few seconds, compared to 2–3 min in differential pulse voltammetry. So, the entire voltammogram can be recorded with a single mercury drop. In addition, SWV is also more sensitive than DPV, because both forward and reverse currents are measured in the former, but only the forward currents are measured in the latter. Frequencies of 1–100 square-wave cycles per second permit the use of extremely fast potential scan rates. The analysis time is reduced; a complete voltammogram can be recorded within a few seconds, compared to about 3 min time required for DPV [2].

Electroanalytical techniques, especially modern stripping voltammetry, have been used for the sensitive determination of a wide range of pharmaceuticals. Such techniques enjoy the advantages that there is no need for derivatization and that these methods are less sensitive to matrix effects than other analytical techniques.

It is well known that anodic stripping voltammetry (ASV) is the most widely used form of stripping analysis. In this case, the metals are preconcentrated by electrodeposition onto a small-volume mercury electrode (thin mercury film or a hanging mercury drop).

Cathodic stripping voltammetry (CSV) is the “mirror image” of ASV. It involves anodic deposition of the analyte followed by stripping in a negative potential scan (cathodic scan). The method is generally applied to organic compounds and anions that are

capable of forming insoluble salts with mercury. During the stripping step, as the potential attains a value equal to the reduction potential of the analyte, it is stripped out in the form of anion. The resulting reduction peak current provides the desired quantitative information. Other electrodes, like rotating silver disk electrodes, can be used for halides. The method has a large number of applications in the field of organic and medicinal chemistry [2].

Higher sensitivity and selectivity compared to other voltammetric techniques are the important features of Adsorptive stripping voltammetry (AdSV). The main advantages of the stripping voltammetric method are its speed and simplicity. Each voltammetric run takes a few seconds. It involves no clean-up procedures, and simple dilution of the biological fluid with suitable solvent nearly eliminates most of the published chromatographic and spectroscopic methods requiring lengthy and tedious extraction procedures, such as liquid–liquid and solid-phase extraction. The sensitivity is significantly enhanced by adsorption of the drug on the electrode surface and after careful choice of the operating parameters extremely low detection limits can be reached. Compared with other techniques the DPAdSV and SWAdSV methods are cheap and the measurements are not time consuming, leading to results for analytical purposes of certain drugs in pharmaceutical formulation and biological fluids [2].

Modern electrochemical instrumentation, especially voltammetric techniques, provides reliable and reproducible data for the quantification of analyte. Further, use of modified electrodes proved to have excellent electroanalytical properties, such as wide potential windows, low background current, and good biocompatibility.

The new electrode materials were characterized by broader potential window, higher signal-to-noise ratio, mechanical stability enabling their application in flowing systems, and resistance toward passivation. The last requirement is especially important because electrode fouling is probably the biggest obstacle to more frequent applications of electroanalytical methods in environmental analysis. Last but not least the scientific word search for nontoxic electrode material friendly toward the environment and thus compatible with the concept of so-called green analytical chemistry.

It is obvious that mercury is the best electrode material for voltammetric determinations based on cathodic reduction [3]. However, because of fears of mercury toxicity (although unsubstantiated according to our opinion), there is a tendency to substitute mercury with other nontoxic materials. For that reason, new types of metal solid amalgam electrodes (MeSAE) and dental amalgam electrodes were introduced.

Carbon paste electrodes (CPE) and their utilization in analytical electrochemistry of pharmaceuticals are documented in [2] and [4]. Their use is driven by low cost of the measurements, wide working potential window in both positive and negative direction, ease of working surface renewal, low background currents, and reasonable repeatability.

Nearly all sp^2 carbon electrodes are susceptible to strong adsorption of polar species mainly due to the presence of polar functionalities on the surface. Over the past 15 years, advanced sp^3 carbon materials, conductive diamond thin films, have been prepared and studied thoroughly [4]. During this time, it has become apparent that these films are in many ways ideal as electrode materials for electrochemistry and thus can be used for high-sensitivity analytical measurements of a wide variety of organic and inorganic species.

Solid composite electrodes belong to the group of composite electrodes with randomly distributed two or more compounds, which exhibit after their mixing solid consistency. They are composed of at least one conductor phase and at least one insulator phase, particles of which are mutually mixed.

Portability and nontoxicity of Me-SAE make them useful substitute of mercury electrodes for on spot electroanalytical monitoring of electrochemically reducible substances and their mechanical properties make them compatible with measurements in flowing systems. SCE can be useful because of low cost, easy fabrication, and easy electrochemical pretreatment. Further attention must be paid to electrode pretreatment and to other means minimizing the electrode passivation complicating practical environmental applications of electroanalytical methods [4].

In recent years, various chemically modified electrodes were used in electroanalysis of drugs. Electrode surfaces are modified

by coating them with different types of polymers mainly conducting polymer, ion exchange, and redox polymers. Often chemical groups are attached to these coatings in order to introduce particular electrochemical effects.

They are based on an ion selective membrane that separates the sample from the inner electrolyte. The nature of the membrane determines the selectivity of the electrode. A membrane is considered to be any material that separates two solutions.

In recent years, nanomaterials have become extremely popular theme in electrochemical sensing research due to their electrical conductivity, unique structural and catalytic properties, high loading of biocatalysts, good stability, and excellent penetrability. Carbon nanotubes (CNTs) are used as electrode materials with useful properties for various potential applications.

The electrocatalytic properties of the oxides of noble metals in the electrooxidation of numerous organic molecules are well known. For example, oxidation of malic acid on a gold electrode proceeds only in the region where the electrode is covered by gold oxide. On a glassy carbon electrode modified by silver, reactivation of the formaldehyde anodic oxidation is observed in the region where the electrode is covered by silver oxide. On the bulk silver electrode and on the glassy carbon electrode modified by silver, alcohols such as methanol, ethylene glycol, and glycerol are oxidized only in the region where the electrodes are covered by silver oxide [5]. The electrochemical behavior of biological compounds such as glucose, hormones, and therapeutic drugs is frequently investigated on noble metal electrodes (Au, Pt, Ag).

2.2 Recent Trends in Development of Electrochemical Methods for Analysis of Pharmaceutical

In the following, the application of various electrochemical methods for analyzing of pharmaceuticals will be discussed in more details. For this review (chapter), the pharmaceuticals are grouped to their pharmacological activity, in several groups: antibiotics,

cardiovascular, central nervous system, anticancer, anti-inflammatory, and miscellaneous. The papers are presented, as much as possible, in their chronological order of their publication.

2.2.1 Antibiotics

The outstanding application of antibiotics in the human and veterinary medicine, for successful treatment of different diseases, and in the other fields, has made them one of the most important products of pharmaceutical industry from 1942 to these days. Antibiotics are among the most frequently prescribed medications today, although is evident the growth of microbial resistance. This fact is a serious medical problem and affects on successful control of diseases caused by resistant strains of bacteria. In this part, the several important groups of antibiotics are presented (cephalosporins, macrolides, tetracyclines, quinolones, etc.) with great spectrum of activity.

Azithromycin is a 15-cyclic lactone antibiotic (Fig. 2.1) and a semisynthetic erythromycin derivative. It exhibits some advantages over erythromycin, including better oral bioavailability, higher tissue concentrations, and fewer side effects. Azithromycin is active against some gram-positive and gram-negative microorganisms and functions by binding to the 50S subunit of the bacterial ribosome.

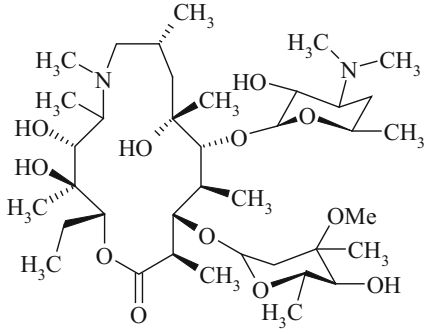

Fig. 2.1 Chemical structure of azithromycin

Azithromycin has been used to treat respiratory infections, skin and soft tissue infections, and some sexually transmitted diseases.

The oxidative properties and the assay of azithromycin and Hemomycin® at a gold electrode using cyclic linear sweep voltammetry were examined [6]. An aqueous solution of $NaHCO_3$ was used in one set of experiments, and methanol–aqueous $NaHCO_3$ mixture was used in the second one. Azithromycin (pure and as a content of capsules, Hemomycin®) was examined in both sets of experiments.

It is obvious from the cyclic voltammograms of pure azithromycin and of Hemomycin® in 0.05 M $NaHCO_3$ (Fig. 2.2) that the potential was cycled between −1.2 and 1.0 V vs. SCE in order to obtain the electrochemical reaction of antibiotic. In the first stage, after the addition of the antibiotic into the electrolyte, the potential was cycled between −0.6 and 1.0 V, but this was not sufficient for the electrochemical activation of azithromycin in 0.05 M $NaHCO_3$.

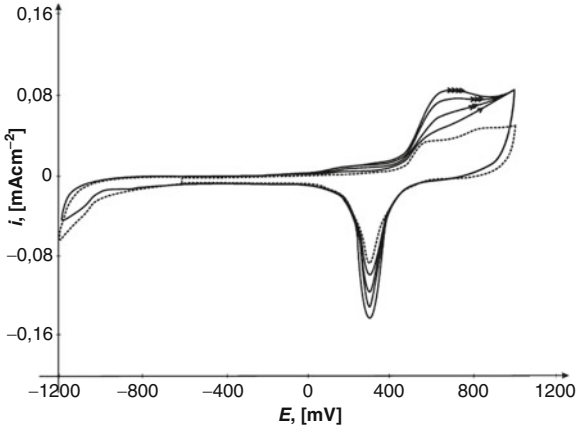

Fig. 2.2 Cyclic voltammogram of an Au electrode in 0.05 M $NaHCO_3$ (*dashed line*) and after the addition of 0.235, 0.353, 0.471, and 0.588 mg cm^{-3} pure azithromycin dihydrate (*full line*), the lowest concentration is indicated by *one arrow*, and the highest one with *four arrows*, sweep rate: 50 mVs^{-1}. Only the first sweep was recorded (Reproduced with a permission from Elsevier) [6]

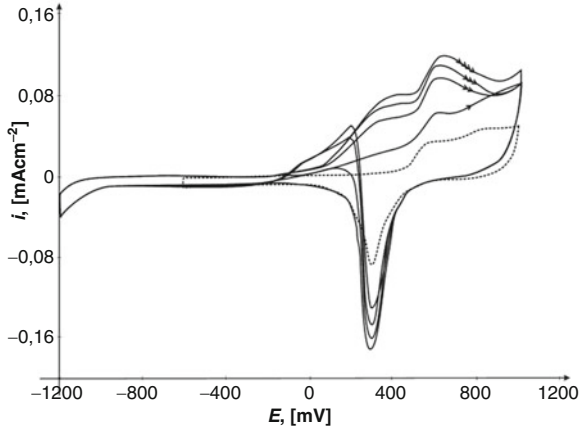

Fig. 2.3 Cyclic voltammogram of Au electrode in 0.05 M $NaHCO_3$ (*dashed line*) and after the addition of Hemomycin® from capsule of 0.235, 0.353, 0.471, and 0.588 mg cm^{-3} (*full line*), the lowest concentration is indicated by *one arrow*, and the highest one with *four arrows*, sweep rate: 50 mVs^{-1}. Only the first sweep was recorded (Reproduced with a permission from Elsevier) [6]

By extending the negative limit of the potential to −1.2 V vs. SCE, in the first (reverse) anodic sweep, the azithromycin was oxidized (both pure and Hemomycin®) and the observed anodic peak of the first cycle was described earlier for azithromycin dihydrate. On reaching the potential of −1.2 V vs. SCE, hydrogen evolution at the gold electrode occurred. The cyclic voltammograms of the pure gold electrode in the supporting electrolyte (Figs. 2.2 and 2.3) show that the hydrogen evolution was suppressed by azithromycin and Hemomycin® adsorption. Only the beginning of the electroactivity of azithromycin and Hemomycin® was affected by hydrogen evolution at a sweep rate of 50 mVs^{-1}. As will be presented later, the electrooxidation of azithromycin and Hemomycin® coincides with AuO formation but for this effect to occur, it seems that it is necessary to commence with azithromycin and Hemomycin® adsorption caused by hydrogen evolution. The suppressed hydrogen evolution resulting from the presence of both kinds of antibiotic in electrolyte supports this assumption. The purging of H_2 into the electrolyte had no effect. The experiment with $NaHCO_3$/

Na_2CO_3 buffer (pH 8) shows the activation of azithromycin did not occur on reaching a value of −1.2 V vs. SCE, because the buffer inhibited the production of electroactive hydrogen species. Measurements show that the pH value of the electrolyte (0.05 M $NaHCO_3$) was 8.48 at the beginning of all experiments but after 2 h it had increased to 8.72. It is interesting that the electrochemical oxidation of azithromycin and Hemomycin® was promoted by the electrochemical production of H species and that the anodic peak (in both cases) was quite stable during 2 h of cycling without a decrease in the peak current. It is quite possible that the solubility of azithromycin dihydrate and Hemomycin® in 0.05 M $NaHCO_3$ was improved by the evolution of hydrogen, which was probably the main cause for the initialization of azithromycin electrooxidation. A couple of patent applications concerning the improvement of the solubility of the azithromycin by ionization of the pure molecule in order to facilitate the application of this antibiotic in ophthalmology can be found in the literature [7, 8].

The assumption for the electrochemically improved solubility of azithromycin in 0.05 M $NaHCO_3$ is supported by the fact that the same reaction in an electrolyte containing methanol proceeded in the range of potentials from −0.6 to 1.0 V vs. SCE and did not require a potential of −1.2 V. This will be discussed later with the analysis of the role of CH_3OH:0.05 M $NaHCO_3$ electrolyte in the electrooxidation of azithromycin and Hemomycin®.

The quantitative electrochemical determination of azithromycin from capsules was successfully applied for the assay of the drug in the tested dosages with, as in the case of azithromycin dihydrate, the possibility for the development of the method for any dosage which may be needed to be detected, including biological samples.

Another set of experiments was performed with an electrolyte containing methanol in order to investigate the influence of methanol on oxidation of azithromycin dihydrate and Hemomycin® in 0.05 M $NaHCO_3$ at a gold electrode and to analyze possible differences in the electrochemical reactivity of the antibiotic in the two different electrolytes. The anodic oxidation of azithromycin dihydrate in the concentration range of 0.235–0.588 mg cm^{-3} is presented in Fig. 2.4. The consequences for the anodic oxidation of

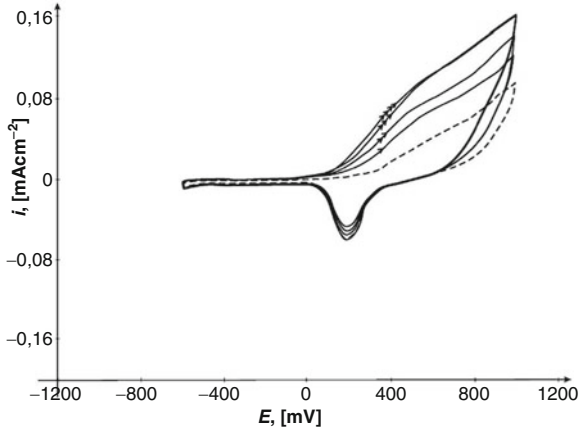

Fig. 2.4 Cyclic voltammogram of an Au electrode in 0.05 M $NaHCO_3$ (*dashed line*) and methanol in the ratio 50 %:50 % after the addition of 0.235, 0.353, 0.471, and 0.588 mg cm^{-3} of pure azithromycin dihydrate (*full line*), lowest concentration is indicated by *one arrow*, and the highest one by *four arrows*, sweep rate: 50 mVs^{-1}. Only the first sweep was recorded (Reproduced with a permission from Elsevier) [6]

azithromycin dihydrate in the presence of methanol are seen in the deformed anodic oxidation peak for each concentration, compared to the very well shaped peak in the absence of methanol, which appear at the same values of the potential for the same range of concentrations (Fig. 2.4).

This work showed that gold electrode can be successfully employed for the qualitative and quantitative electrochemical determination of azithromycin dihydrate and azithromycin from capsule (Hemomycin®) via its oxidation in the tested dosages. Also, there is a possibility for the application of this method for any dosage which is required to be analyzed, including biological samples.

Erythromycin is a natural compound metabolized by a strain of *Streptomyces erythreus*. It has proved invaluable for the treatment of bacterial infections in patients with β-lactam hypersensitivity. If the 6-hydroxy group is methylated, *clarithromycin* is obtained, which has an improved pharmacokinetic profile

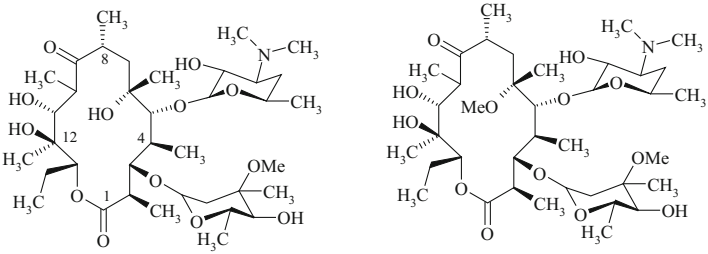

Fig. 2.5 Chemical structures of erythromycin (*left*) and clarithromycin (*right*)

compared to the parent molecule (Fig. 2.5). Azithromycin and clarithromycin present several clinical advantages over erythromycin, including enhanced spectrum activity, higher tissue concentrations, and improved tolerability. Clarithromycin is widely used for the eradication of *Helicobacter pylori* that causes gastritis and gastric ulcers.

The qualitative determination of the pure clarithromycin using its reactivity at a gold electrode in neutral electrolyte by cyclic linear sweep voltammetry was performed [9].

As in a case of azithromycin, for clarithromycin, our choice was 0.05 M $NaHCO_3$ as the supporting electrolyte. The solubility of clarithromycin in water is very poor, and it is slightly soluble in methanol. The methanol is avoided as the solvent (in a mixture with water) because of its activity on the oxides of gold and silver electrodes in different electrolytes.

In the first stage, after addition of the antibiotic into the electrolyte, the potential was cycled between −0.6 and 1.0 V. The electrochemical activation of clarithromycin is not observed as was the case with azithromycin. It was necessary to reach the negative potential value of −1.2 V vs. SCE with the hydrogen evolution occurrence at the gold electrode. The electrochemical activation of clarithromycin and the hydrogen evolution suppression is obvious from Fig. 2.6 and the same effects were already observed with azithromycin [6]. In Fig. 2.6 is also presented that starting from −1.2 V vs. SCE in anodic direction, the cyclic voltammogram first shows one small, wide, and reproducible anodic peak with a current maximum at −0.58 V vs. SCE. The two reproducible anodic

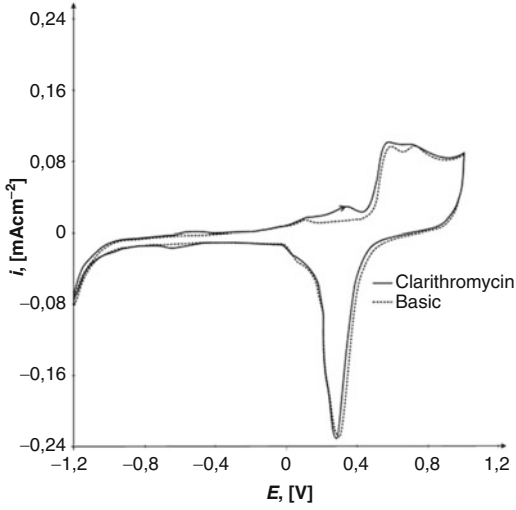

Fig. 2.6 Cyclic voltammogram of the Au electrode in 0.05 M $NaHCO_3$ (*dashed line*) and with the addition of 0.4 mg cm^{-3} of pure clarithromycin, third sweep (*full line*), sweep rate: 50 mVs^{-1} (Reproduced with a permission from Elsevier) [9]

peaks were also observed at +0.10 V vs. SCE and at +0.33 V vs. SCE. In the region of AuO formation, a minor increase of the oxide peaks of the gold electrode was observed. The reproducible cathodic peak is present in the reverse direction with a current maximum at –0.61 V vs. SCE.

It is shown for clarithromycin that observed peaks are not proportional to the concentration of antibiotic in the range of 0.235–0.588 mg cm^{-3}. In this range of concentrations, the four reproducible anodic and one cathodic peaks always qualitatively determine clarithromycin. In order to investigate the structural changes in clarithromycin molecule, electrochemical studies combined with the analysis of the bulk electrolyte after the electrochemical reactions by FTIR spectroscopy and HPLC were performed.

FTIR spectrum of pure clarithromycin and clarithromycin mixed with carbonates, both before the electrochemical experiment, served as reference for the further analysis. The observed changes in the molecule of clarithromycin were tracked with these data.

The potential was held at selected values corresponded to all observed current peaks for 4 h. The first sweep after holding the potential was recorded by cyclic voltammetry and two samples of the electrolyte were analyzed by FTIR and HPLC. The potential was held for 4 h at −0.58 V, at +0.10 V, at +0.33 V, and at −0.61 V vs. SCE.

The significant changes in clarithromycin molecular structure were observed when potential was held for 4 h at −0.61 V, at the cathodic peak, observed in Fig. 2.6. The first sweep after 4 h of holding the potential is presented in Fig. 2.7a and shows that, in addition to the current increase previously described in Fig. 2.6 (around 0.70 V vs. SCE) the anodic current rises by the end of the anodic scan.

A current increase at the potentials corresponding to OH^- adsorption/desorption was observed, not only during the first sweep, but also in the three subsequent sweeps at least. The FTIR spectrum reveals two obvious changes after potential holding (Fig. 2.7b): the disappearance of the 1730 cm^{-1} peak corresponding to the carbonyl group vibration of the lactone, and an intense reduction of the 1170 cm^{-1} peak, probably corresponding to the C–O vibration in the lactone, which implies changes in the ester bond of the lactone. The disappearance of the carbonyl band at 1690 cm^{-1} indicates a change in this group also. No absorptions were recorded in the 1000–1100 cm^{-1} range, which could be the result of changes in the ether and acetal bonds.

The FTIR analysis did not reveal clear changes in the molecule after 4 h of holding the potential at +0.10 V vs. SCE and at +0.33 V vs. SCE, except a minor reduction of the bands in the 1000–1100 cm^{-1} region.

HPLC analysis of the bulk electrolyte showed a significant decrease in the concentration of clarithromycin after the potential was held at selected values for 4 h. The qualitative determination of commercial clarithromycin (provided by Hemofarm and tested in tablets) at gold electrode, followed by FTIR analysis, is already successfully performed.

The reactivity of *erythromycin* [10] (pure) was investigated on a gold electrode in neutral electrolyte by cyclic voltammetry. The resulting structural changes were observed with HPLC and FTIR spectroscopy by analyzing the bulk electrolyte after the

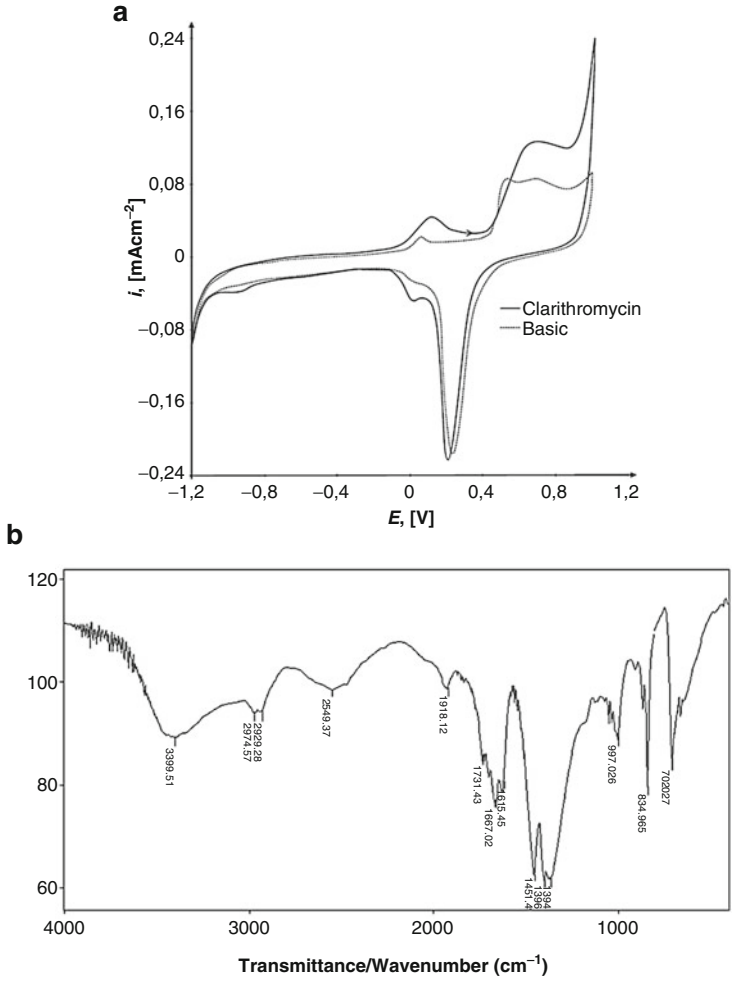

Fig. 2.7 (**a**) Cyclic voltammogram of the first sweep of the Au electrode in the presence of 0.4 mg cm^{-3} pure clarithromycin after the potential had been held for 4 h at –0.61 V vs. SCE in 0.05 M $NaHCO_3$ (*full line*). The voltammogram of the pure gold electrode is presented by the dashed line, sweep rate: 50 mVs^{-1}. (**b**) Infrared spectrum of 0.4 mg cm^{-3} pure clarithromycin in 0.05 M $NaHCO_3$ solution after 4 h electroreduction at –0.61 V vs. SCE under the conditions described in (**a**) (Reproduced with a permission from Elsevier) [9]

electrochemical reactions. The results were compared with those previously obtained for azithromycin and clarithromycin under the same experimental conditions. It was found that the electrochemical behavior of erythromycin A differs from that of azithromycin dihydrate. Comparison with the electrochemical activity of basic clarithromycin suggests that the electrochemical activity of erythromycin is similar but more pronounced than that of clarithromycin.

HPLC analysis confirmed these observations and showed that during the electrochemical oxidation of erythromycin A, the amount of starting macrolide decreased while the amount of starting impurities increased. Also some new products were observed. FTIR spectroscopy confirmed that erythromycin A is more reactive than clarithromycin, although similar changes in their molecular structures were observed.

Under the same experimental conditions, the cyclic voltammogram of erythromycin A exhibits three anodic and one cathodic reaction and one apparent anodic activity in the whole range of the formation of oxides (Fig. 2.8). From Fig. 2.8, it is clear that erythromycin A causes a suppression of the anodic and cathodic currents in the region from −0.35 to 0.0 V and a suppression of hydrogen evolution on a gold electrode. After the addition of antibiotic, pH of the electrolyte was 8.63 and did not change during the further electrochemical examination.

Beckmann rearrangement of erythromycin 9-oxime results in ring expansion to a 15-membered intermediate, the subsequent reduction, and N-methylation of which produce azithromycin with a quite different structure (Fig. 2.1). These structural differences cause the electrochemical behavior of erythromycin A to differ greatly from that of azithromycin dihydrate, which is active only in the oxide formation region and this activity is concentration dependent in the range 0.235–0.588 mg cm^{-3}. Comparing the voltammogram of basic clarithromycin with that of basic erythromycin A presented in Fig. 2.8, it is clear that the three anodic peaks appear at the same potentials. The cathodic reaction is shifted a little to more negative potentials in a case of erythromycin. The activity of clarithromycin is apparent only in the beginning of the region of oxide formation but that of erythromycin covers the

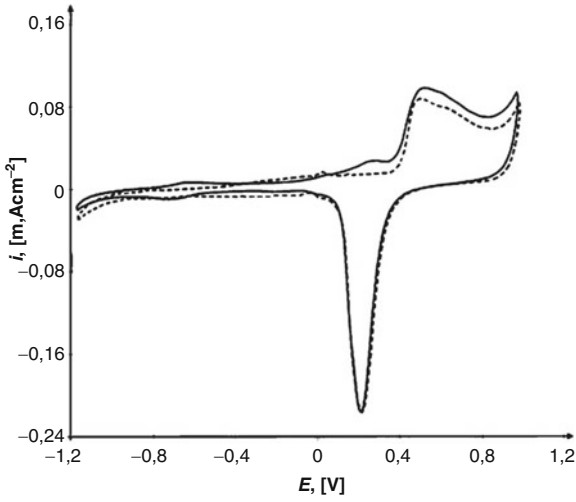

Fig. 2.8 Cyclic voltammogram of an Au electrode in 0.05 M $NaHCO_3$ (*dashed line*) and with the addition of 0.40 mg cm^{-3} erythromycin succinate (*full line*), sweep rate: 50 mVs^{-1}. Cathodic and anodic reaction was observed in the examined range of concentrations (from 0.235 to 0.588 mg cm^{-3}) (Reproduced with a permission from Elsevier) [10]

whole region. A suppression of the anodic and cathodic currents in the region from –0.35 to 0.0 V is more apparent in a case of erythromycin, as well as a suppression of hydrogen evolution. From the decrease of the capacitive currents and the absence of concentration dependence it was supposed that at the electrode surface exists an adsorbed layer of erythromycin/active intermediate species that undergoes transformation. The fouling of the currents after cyclic voltammetry is not observed during 4 h of cycling. Most probable explanation is that the electrode is cleaned in the region of the oxide reduction after each cycle and that erythromycin/active intermediates are not strongly adsorbed. The degradation ability of erythromycin A in different pH solutions suggested that it would be interesting to test its electrochemical behavior in the region of its low stability, acid solution: pH 2.17 and in the region of its high stability, neutral solution, pH 7.14. The second one is close to the pH value of the tested solution (pH 8.55) and is very important for

the possible analyses of biological samples with the same or similar pH values: human blood, urine, and plasma. Erythromycin A in electrolyte at pH 2.12 undergoes immediately to the spontaneous degradation and under the experimental conditions presented in Fig. 2.8. At pH 7.14, erythromycin A exhibited the same electrochemical activity as was observed at pH 8.55. In order to compare the activity of the entire tested macrolides, one can suggest continuing with using of 0.05 M $NaHCO_3$ in the further erythromycin A examination. The electrochemical behavior of commercial erythromycin, Erythromycin®, was studied in the concentration range 0.235–0.588 mg cm^{-3}. The obtained data are useful for the manufacturers of erythromycin A in a case that their commercial products in capsules and tablets contain the same or similar excipients. Due to the presence of excipients, the obtained electrochemical activity differed greatly from that of the basic erythromycin ethyl succinate. It is clear from Fig. 2.9 that the anodic activity at the beginning of the region of the formation of oxides is only small. The appearance of an additional cathodic peak at –0.25 V and an expanded cathodic activity in the region from –0.55 to –1.00 V was observed.

During the electrochemical oxidations of erythromycin A, the amount of starting macrolide decreased while the amount of starting impurities increased and some new products were observed. At the end of the electrochemical oxidations of erythromycin A (5 h), approximately 70 % of the starting compound was recovered. From the obtained results, it is obvious that erythromycin A underwent oxidative degradation. Probably, the first step in the oxidation process is the removal of the electron from one of the nitrogen atoms to form an aminium cation radical:

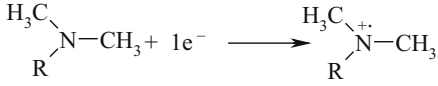

(2.1)

where R is a sugar moiety. Formed aminium radical cation is a very reactive species and rapidly reacts with the environment to form stable products. The formed radical cation can abstract hydrogen atom from the water resulting in salt formation (reaction 2.2) in an overall one-electron process. Hence, the formed cation inhibits further electrochemical oxidation.

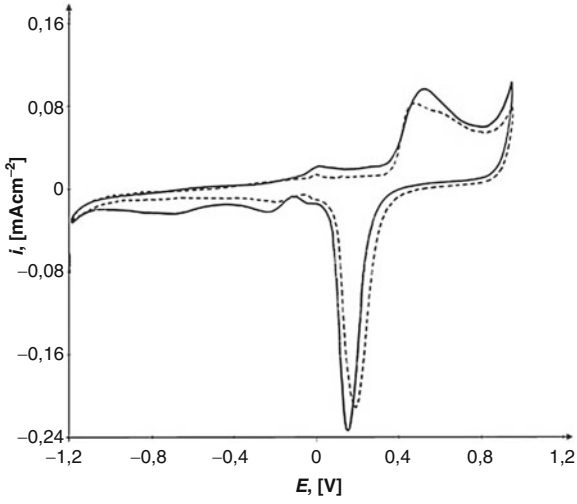

Fig. 2.9 Cyclic voltammogram of an Au electrode in 0.05 M $NaHCO_3$ (*dashed line*) and with the addition of 0.40 mg cm^{-3} Erythromycin® (*full line*) in a concentration of 0.40 mg cm^{-3}, sweep rate: 50 mVs^{-1} (Reproduced with a permission from Elsevier) [10]

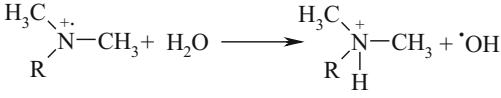

(2.2)

In addition to reaction 2.2, it is probable that the amine group underwent a demethylation reaction, resulting in the corresponding secondary amines. This reaction proceeds via an overall two-electron transfer step (ECE mechanism) (reactions 2.3–2.5). The rate determining steps in these mechanisms are the removal of the α-proton and the formation of an enamine as an intermediate (reactions 2.3 and 2.4).

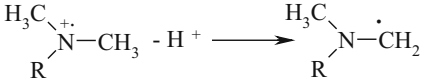

(2.3)

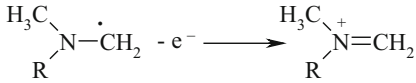

(2.4)

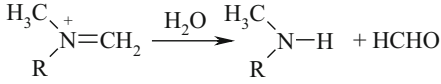

(2.5)

The electrochemical behavior of erythromycin A differs greatly from that of azithromycin dehydrate, which was caused by structural differences. Comparison of the electrochemical activity of basic erythromycin with that of clarithromycin showed that the electrochemical activity of erythromycin is more pronounced than that of clarithromycin. Taking into account that the 6-hydroxy group of erythromycin was methylated to obtain the clarithromycin, it can be assumed that the comparable but more pronounced electrochemical activity of erythromycin is caused by the free hydroxyl group.

Roxithromycin is a semisynthetic 14-membered-ring macrolide antibiotic (Fig. 2.10), in which the erythronolide A lactone ring has been modified by the replacement of the nine keto group with an etheroxime side chain, in order to prevent deactivation in the gastric milieu. The in vitro activity of roxithromycin is well known and is as effective as or more effective than

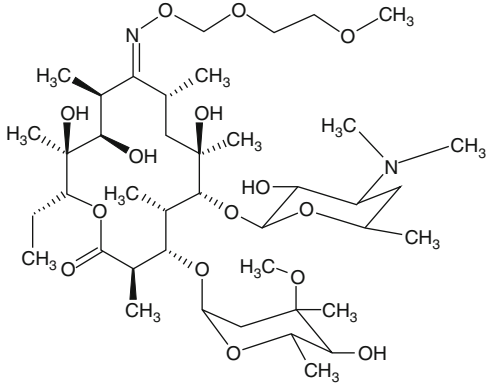

Fig. 2.10 Structure of the roxithromycin

other macrolide antibiotics against a wide range of infections. In vivo, roxithromycin has mostly been used to treat respiratory, urinary, and soft tissue infections. Gastrointestinal disturbances are the most frequent adverse effects but are less frequent than with erythromycin. Roxithromycin exhibits increased chemical stability and higher concentrations of antibiotic in the serum after oral administration compared to erythromycin.

The oxidative behavior of antibiotic roxithromycin standard [11] was studied at a gold electrode in 0.05 M $NaHCO_3$ using cyclic linear sweep voltammetry and differential pulse voltammetry. It was found that the value of the oxidative peak of pure roxithromycin at 0.81 V vs. SCE in 0.05 M $NaHCO_3$ at a scan rate of 50 mVs^{-1} is a linear function of the concentration in a range 0.10006–0.654 mg cm^{-3}.

The cyclic voltammogram of the clean electrode is presented with dashed line and the tested concentrations of roxithromycin standard, continuously added in the same experiment are presented in Fig. 2.11 (full lines). Only the first cycle was recorded. Cyclic voltammograms show two oxidative reactions with maximum current values at 0.5 and 0.8 V vs. SCE. In comparison to the clean electrode, the peak of the gold oxides reduction slightly decreases in the presence of roxithromycin with the increasing of the amount of antibiotic, but it is not a linear function of its concentration. The value of the oxidative peaks of pure roxithromycin at 0.81 V vs. SCE in 0.05 M $NaHCO_3$ at the scan rate of 50 mVs^{-1} is linear function of the concentration in a range of 0.10006–0.654 mg cm^{-3}.

Differential pulse voltammetry was employed in order to verify the results obtained by cyclic voltammetry. Differential pulse voltammograms were recorded at the gold electrode in 0.05 M $NaHCO_3$ solution containing different concentrations of roxithromycin. Potential was scanned from 0.6 to 1.0 V at a scan rate of 2 mVs^{-1}, pulse amplitude of 25 mV, and pulse time of 0.1 s. All voltammograms possess one anodic peak positioned at approximately 0.75 V, as presented in Fig. 2.12.

The deviation of the peak current density from the linear relationship at higher concentrations could be ascribed to the exhaustion of solution during the experiment. Taking into account that each DPV measurement lasted for 13.3 min (eight different

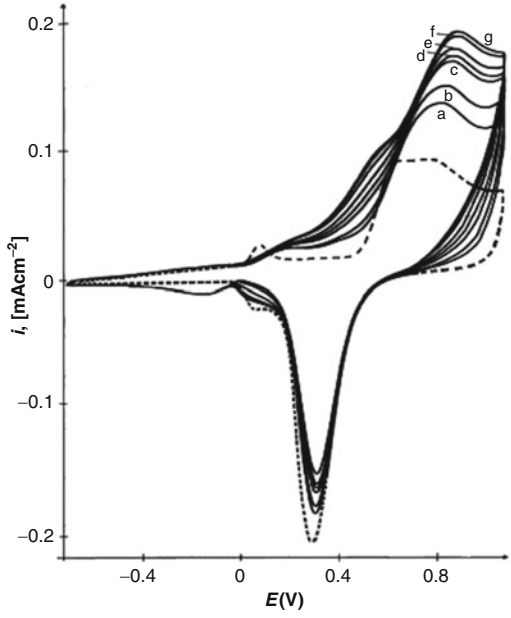

Fig. 2.11 Cyclic voltammogram of an Au electrode in 0.05 M $NaHCO_3$ (*dashed line*) and after the addition of roxithromycin (in the concentration range 0.10006–0.654 mg cm^{-3} (*full lines*, starting from 0.10006, then 0.196, 0.291, 0.385, 0.476, 0.566, and 0.654 mg cm^{-3}), sweep rate: 50 mVs^{-1}. Only the first sweep was recorded (Reproduced with a permission from Elsevier) [11]

concentrations were used) it is most likely that the actual concentration of roxithromycin became significantly lower than the calculated one, i.e., the amount of roxithromycin oxidized during the DPV procedure could not be neglected. Hence, it seems reasonable to assume that the linear range would have been extended to higher concentrations if larger scan rates had been used. It was already published that macrolide antibiotics like roxithromycin which contain a tertiary amino group are detectable.

HPLC analysis of Runac tablets confirmed the data obtained by the analysis of the current peak values vs. concentrations concerning the correlation of the obtained chromatographic peak areas with the investigated concentrations. For the determination of

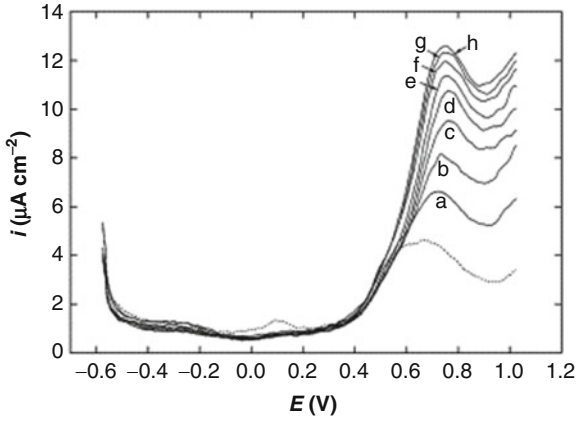

Fig. 2.12 Differential pulse anodic voltammograms obtained at the gold electrode in 0.05 M $NaHCO_3$ (*dashed line*) and in the presence of different concentrations of roxithromycin (*full lines*): (*a*) 0.1006, (*b*) 0.196, (*c*) 0.291, (*d*) 0.385, (*e*) 0.476, (*f*) 0.566, (*g*) 0.654, and (*h*) 0.741 mg cm^{-3}. Initial potential –0.6 V, final potential 1.0 V, scan rate 2 mVs^{-1}, pulse amplitude 25 mV, pulse time 0.1 s (Reproduced with a permission from Elsevier) [11]

roxithromycin in the spiked urine samples, the same values of roxithromycin concentrations (pharmacokinetic concentrations in the range 2.5–10 μg cm^{-3}) were used as in [9], where a sensitive chemiluminescence method was proposed for the determination of roxithromycin. Figure 2.13 represents cyclic voltammograms of the gold electrode in 0.05 M $NaHCO_3$ and after the addition of urine samples spiked with roxithromycin (in the concentration range 2.5–10 μg cm^{-3}). Cyclic voltammograms show that electrochemical oxidation of roxithromycin is represented by anodic peak between 0.60 and 0.90 V (with the current maximum at 0.85 V). This oxidative reaction is in direct correlation with the increasing of antibiotic concentration. It was found that the value of the oxidative peak of urine sample spiked with roxithromycin (at 0.85 V at the scan rate of 50 mVs^{-1}) is a linear function of the concentration in the range 2.5–10 μg cm^{-3}.

Anisomycin is a multifunctional antibiotic isolated from two different species of *Streptomyces* (Fig. 2.14). It is also an inhibitor

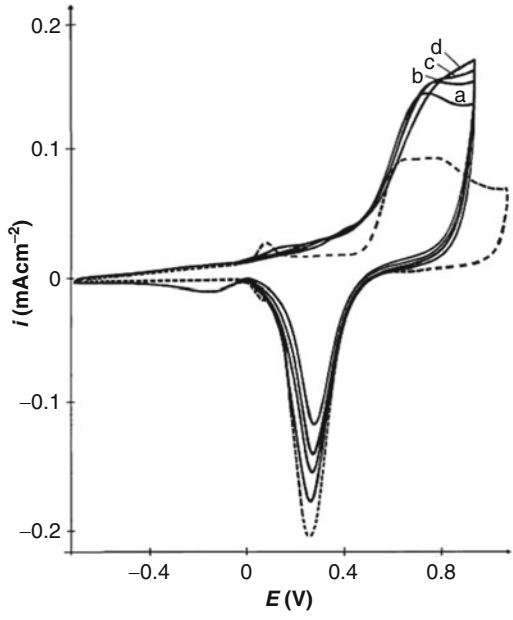

Fig. 2.13 Cyclic voltammogram of an Au electrode in 0.05 M $NaHCO_3$ (*dashed line*) and after the addition of urine samples spiked with roxithromycin (in the concentration range 2.5, 5, 7.5, 10 μg cm^{-3}) (*full lines*, assigned from *a* to *d*), sweep rate: 50 mVs^{-1}. Only the first sweep was recorded (Reproduced with a permission from Elsevier) [11]

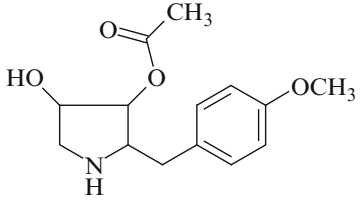

Fig. 2.14 Chemical structure of anisomycin

of protein synthesis and affects memory by inhibiting the consolidation of new memories and causing amnesia. Anisomycin is an immunosuppressant in low doses (<0.1 μM; M = mol dm^{-3}) indicating its possible application in treatment of some autoimmune diseases and in inhibition of the transplantation rejection. It suppresses malignant tumor cell growth and can be used as an antitumor agent. Anisomycin possesses herbicidal activity and selective activity against pathogenic protozoa and fungi.

The electrochemical activity of anisomycin was investigated on gold electrode using cyclic voltammetry in 0.05 M $NaHCO_3$ [12]. Square wave voltammetry was applied for quantitative determination of the drug and in spiked urine samples, followed by high performance liquid chromatography–tandem mass spectrometry (HPLC–MS/MS). The structural identification of anisomycin and its hydrolysis product in 0.05 M $NaHCO_3$ and under the potential cycling conditions in the absence and in the presence of biological sample (urine) was also performed by HPLC–MS/MS.

The CVs (subsequent scans, 1–20) of anisomycin on gold electrode in 0.05 M $NaHCO_3$ alongside the voltammetric response of Au electrode in blank solution (dot line) are presented in Fig. 2.15a. In the presence of anisomycin, the CV in the first cycle was changed so that an apparent current increase occurs in the whole region of the oxide formation and reduction. The changes induced by continuous cycling are expected to be correlated with the surface oxide formation. During the cycling between first and 20th cycles, the voltammograms show a slight decrease of anodic currents in the area of the oxide formation.

Figure 2.15b demonstrates the CVs of anisomycin-containing solution at different scan rates (v). The current density increases with the increased scan rate. In Fig. 2.15c the relationship between peak current and $v^{1/2}$ is displayed showing linearity, indicating that the anisomycin oxidation is diffusion-controlled process. Furthermore, the peak potential increases with increasing scan rate, and a straight line relationship is observed between peak potentials and ln of scan rates (Fig. 2.15d), suggesting that the anisomycin oxidation is an irreversible electrode process. According to the results presented in Fig. 2.15b, the kinetic parameters for the anisomycin oxidation are estimated from Laviron's

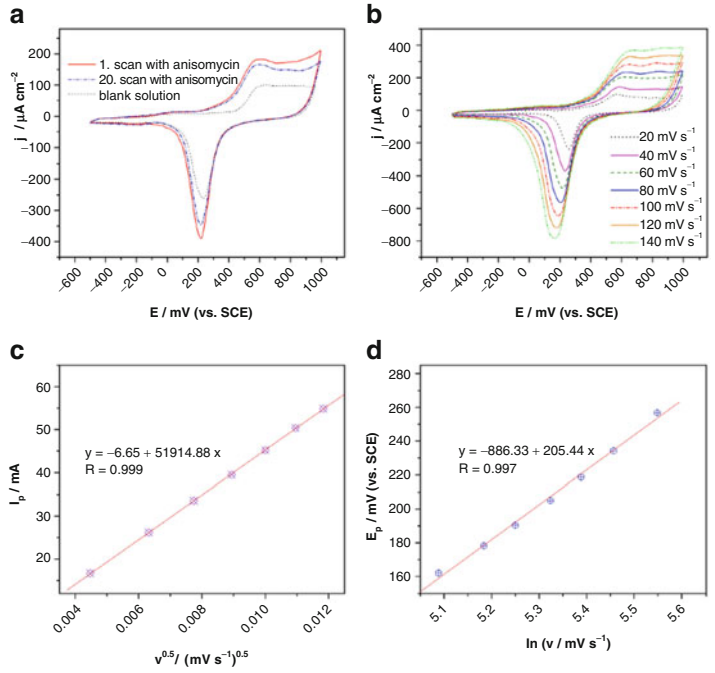

Fig. 2.15 Cyclic voltammogram of Au electrode using 0.05 M $NaHCO_3$ (*dashed line*) and with 0.037 nM anisomycin, (**a**) 1. and 20. scan, scan rate: 50 mV s^{-1}, (**b**) for scan rates: 20, 40, 60, 80, 100, 120, and 140 mV s^{-1}, (**c**) plot of peak current vs. $v^{1/2}$, (**d**) plot of peak potential shift vs. ln of scan rates (Reproduced with a permission from Elsevier) [12]

theory [13]. The value of αn is calculated from the slope of Ep vs. log v. The number of electrons transferred in the electrooxidation of anisomycin was calculated to be 1.1 (approximately equal to 1) assuming that the first electron transfer is rate determining so the transfer coefficient is equal to the symmetry factor which is 0.5. The value of ko (heterogeneous electron-transfer rate constant) is determined from the intercept of the previous plot if the value of Eo is known. The value of Eo is obtained from the intercept of Ep vs. v curve and the value is 267.2 mV. From this, ko was calculated as 0.23 s^{-1}. The HPLC–MS/MS method, used for confirmation of SWV results, exhibited good linearity in the observed concentration range in the absence (R=0.999) and in the presence of biological sample (R=0.978) (Fig. 2.16).

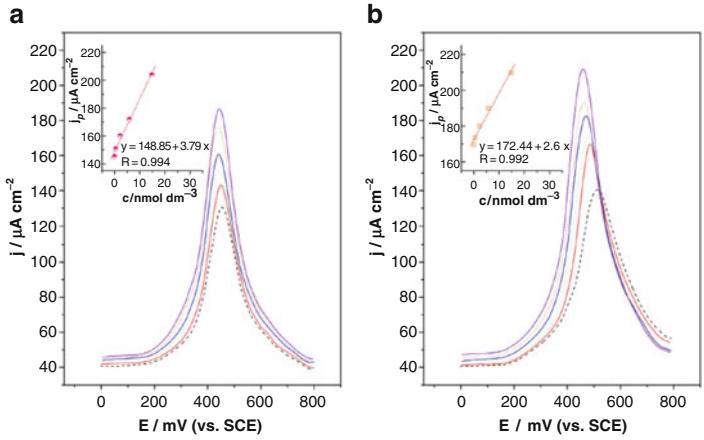

Fig. 2.16 Square wave voltammograms on Au electrode (*dashed line*) using 0.05 M $NaHCO_3$ and with anisomycin (0.037, 0.4, 2.23, 5.84, 14.77 nM) in the absence of biological sample (**a**) and in the presence of biological sample (**b**). Step size 5 mV, pulse size 100 mV, frequency 2 Hz and scan rate 10 mV s^{-1}, accumulation time 200 ms at 0.0 V. *Inset*: linear dependency of anodic peak currents vs. concentration of anisomycin (Reproduced with a permission from Elsevier) [12]

CV during 4 h of anisomycin oxidation (Fig. 2.17a) shows the appearance of the new anodic reactions with the increasing currents compared to Fig. 2.15a, suggesting simultaneous oxidation of anisomycin and the products of its oxidation. SWV (Fig. 2.17b) confirms that effect showing the increasing currents of the anodic peak.

During the cycling, samples of electrolyte were collected and analyzed by HPLC–MS/MS. It was determined that anisomycin hydrolysis occurs, and deacetylanisomycin (*m*/*z* 224) was identified as the hydrolysis product chromatographically separated from anisomycin. Figure 2.18 shows SRM chromatograms and MS/MS spectra of anisomycin (Fig. 2.18a) and its hydrolysis product (Fig. 2.18b) in 0.05 M $NaHCO_3$. Anisomycin hydrolysis under the CV conditions (Fig. 2.17a) is presented in Fig. 2.18c. In the first 2 h, the amount of anisomycin decreases while the amount of hydrolysis product increases. After that, the amounts of both anisomycin and the hydrolysis product decrease and by the end of

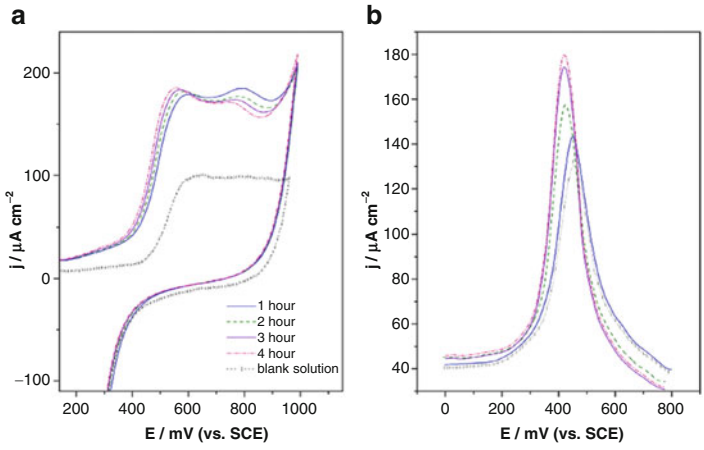

Fig. 2.17 Cyclic voltammograms (**a**) and square wave voltammograms (**b**) of Au electrode in 0.05 M $NaHCO_3$ (*dashed line*) and with 0.037 nM anisomycin, after 1, 2, 3, and 4 h of cycling, scan rate 50 mV s^{-1}. Square wave parameters: step size 5 mV, pulse size 100 mV, frequency 2 Hz and scan rate 10 mV s^{-1}, accumulation time 200 ms at 0.0 V (Reproduced with a permission from Elsevier) [12]

the experiment (4 h) their presence was neglectable. This confirms that after 2 h the electrooxidation products cause the apparent increase of anodic currents in Fig. 2.17. It was also determined that the hydrolysis of anisomycin proceeds in 0.05 M $NaHCO_3$ without electrochemical conditions (Fig. 2.18d). Within the first 30 min, only 3 % of anisomycin is hydrolyzed enabling the correct electroanalytical measurements for at least 30 min. Unlike the electrochemical experiment, the amount of hydrolysis product constantly increases and in 4 h only 69.5 % of anisomycin is hydrolyzed.

2.2.2 Cardiovascular Drugs

Cardiovascular drugs belong also to the most prescribed medications nowadays since various cardiovascular diseases are predominant in developed countries worldwide. In this group the most

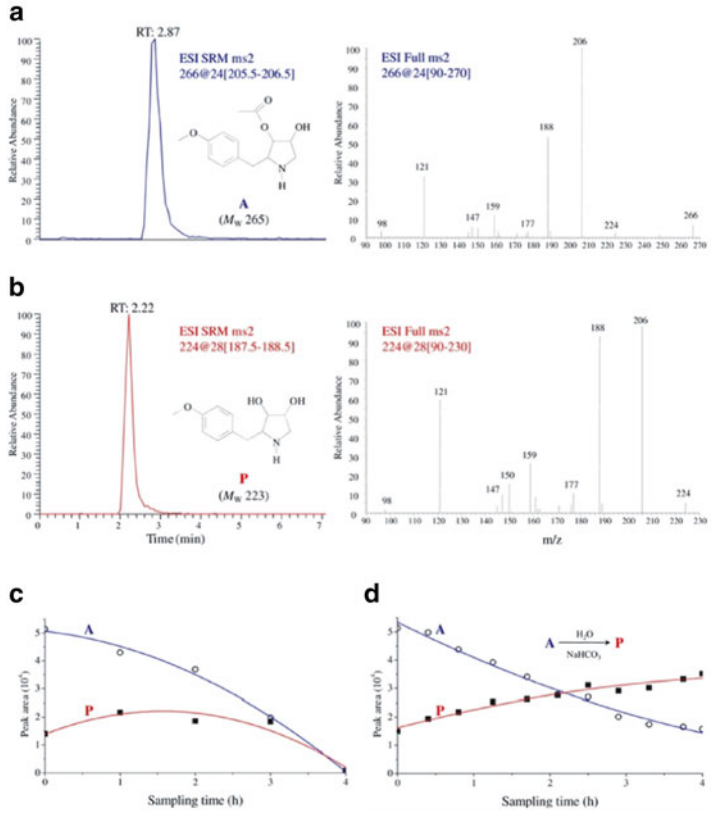

Fig. 2.18 SRM chromatogram and MS/MS spectrum of: (**a**) anisomycin, A, (**b**) the hydrolysis product, *P*. The degradation rate of *A* (*open circle*) and the formation of *P* (*filled square*) in the electrochemical experiment (**c**) and in 0.05 M $NaHCO_3$ (**d**) (Reproduced with a permission from Elsevier) [12]

important drugs are antihypertensives, cardiotonics, antiarrhythmics, anticoagulants, coronary vasodilators, and hypolipemics.

Amlodipine, chemically, 2-[(2-aminoethoxy)methyl]-4-(2-chlorophenyl)-1,4-dihydro-6-methyl-3,5-pyridinedicarboxylic acid, 3-ethyl,5-methylester, besylate (Fig. 2.19), is a dihydropyridine calcium channel blocker, which acts only on the L-type channel to produce their pharmacological effect. Like most of the

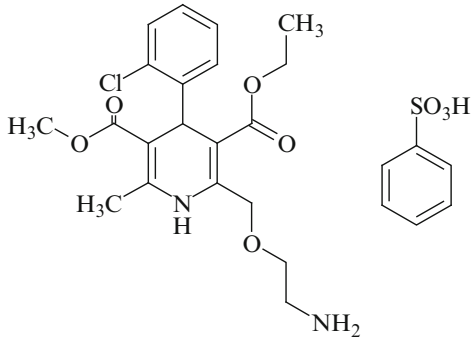

Fig. 2.19 Structure of amlodipine besylate

second-generation dihydropyridine derivatives, it has greater selectivity for the vascular smooth muscle than myocardial tissue and therefore their main effect is vasodilatation. Amlodipine is used alone or in combination with other medicines for the treatment of chronic stable angina, certain types of vasospastic angina, and in the management of mild-to-moderate essential hypertension.

The electrochemical behavior and determination of amlodipine besylate was performed on gold electrode in 0.05 M $NaHCO_3$ [14].

Before voltammetric experiments the electrode surfaces were characterized by AFM. AFM studies were conducted to give insight into the surface topography of the amlodipine/gold and amlodipine/o-MWCNT.

Figures 2.20 and 2.21 show typical two-dimensional (2D) and three-dimensional (3D) AFM images of amlodipine besylate obtained by dropping the water suspension of amlodipine on the gold surface.

The sample of amlodipine besylate/gold is made up of small agglomerates which are compact and uniformly cover the entire substrate (Fig. 2.20), with average diameter of 200 nm (Fig. 2.21).

Gold electrode modified by oxidized multiwall carbon nanotubes was prepared by placing a drop of the water suspension of the nanotubes on the gold surface. As shown in Fig. 2.22, it was clearly seen that randomly oriented MWCNT covered the entire surface of the substrate homogeneously, with average diameter of 100 nm (Fig. 2.23a).

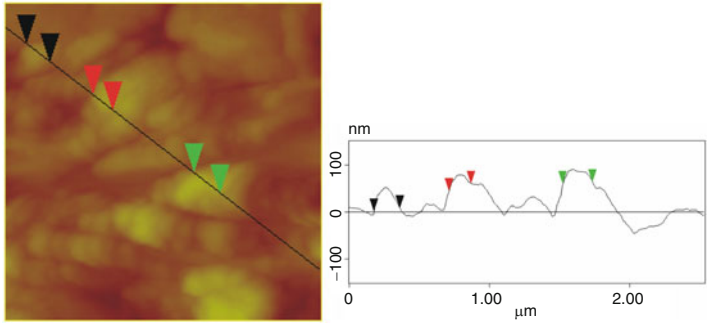

Fig. 2.20 2D AFM image and height profile (3×3×0.3 µm) of amlodipine besylate/Au (Reproduced with a permission from International Journal of Electrochemical Science) [14]

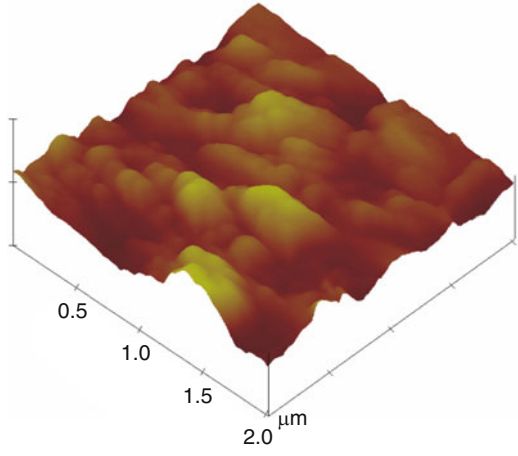

Fig. 2.21 3D image (2×2×0.3 µm) of amlodipine besylate/Au (Reproduced with a permission from International Journal of Electrochemical Science) [14]

The acid treatment of raw MWCNT, using strong oxidizing agent nitric acid, caused severe etching of the graphitic surface of the material, leading to tubes with a population of disordered sites and shortened nanotubes. Shortened o-MWCNT assembles on the

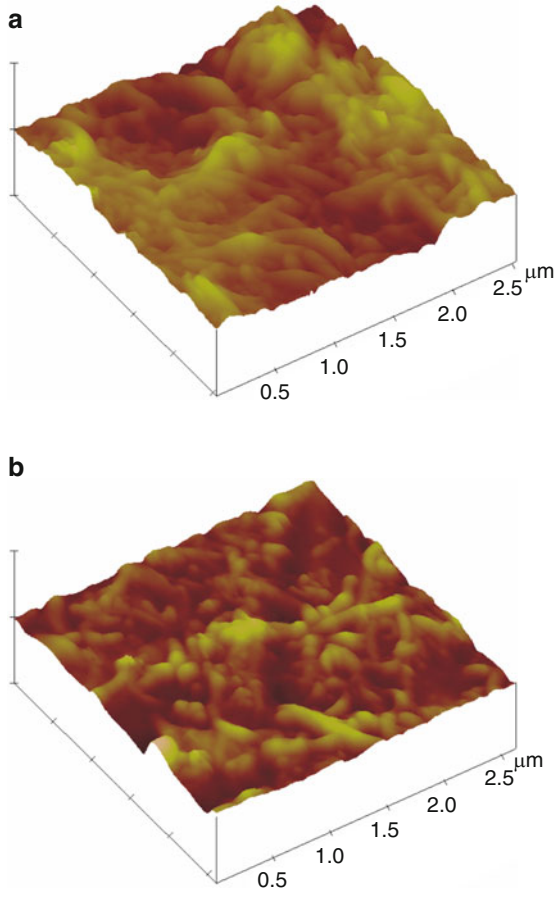

Fig. 2.22 3D AFM images of (**a**) o-MWCNT/Au (2.5 × 2.5 × 0.4 μm) and (**b**) amlodipine besylate/o-MWCNT/Au (2.5 × 2.5 × 0.5 μm) (Reproduced with a permission from International Journal of Electrochemical Science) [14]

gold electrode more easily because of their decreased rigidity and present oxygen functionality contributes better adherence to the gold electrode surface.

However, after adsorbing amlodipine, the diameter of o-MWCNT coated by amlodipine besylate became "wide" as

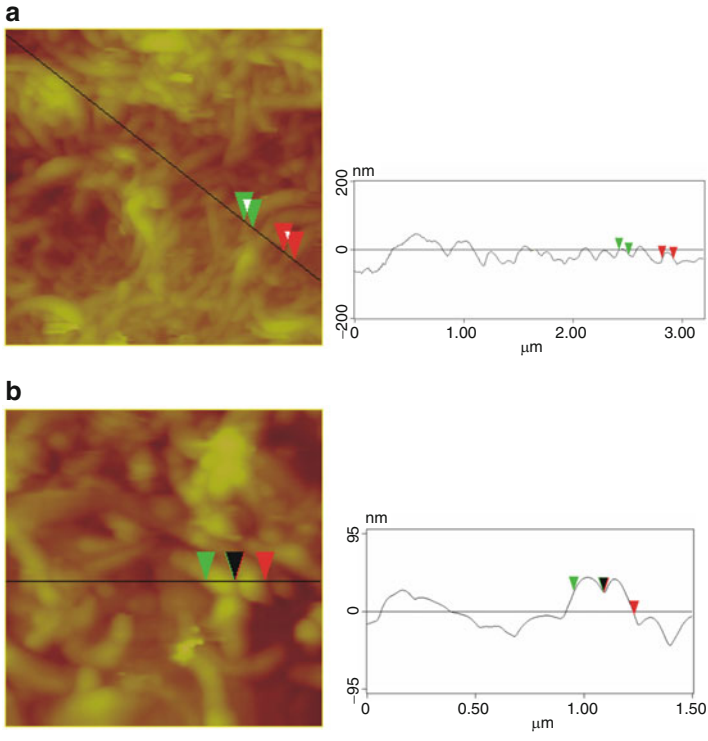

Fig. 2.23 2D images and height profiles of (**a**) o-MWCNT (3×3×0.4 µm) and (**b**) amlodipine besylate/o-MWCNT/Au (1.5×1.5×0.2 µm) (Reproduced with a permission from International Journal of Electrochemical Science) [14]

compared with the o-MWCNT with average diameter of 140 nm (Fig. 2.23b). The sample of amlodipine/o-MWCNT was also well dispersed, implying that the o-MWCNT would connect well the amlodipine on the surface.

Figure 2.24 presents the cyclic voltammograms of amlodipine besylate standard in 0.05 M $NaHCO_3$ obtained without accumulation. The small agglomerates of amlodipine besylate on gold seen by AFM (Fig. 2.20) cover the electrode surface and during the first cycle stay adsorbed on it causing the significantly lower currents in second and consecutive sweeps. In Fig. 2.24 and the following

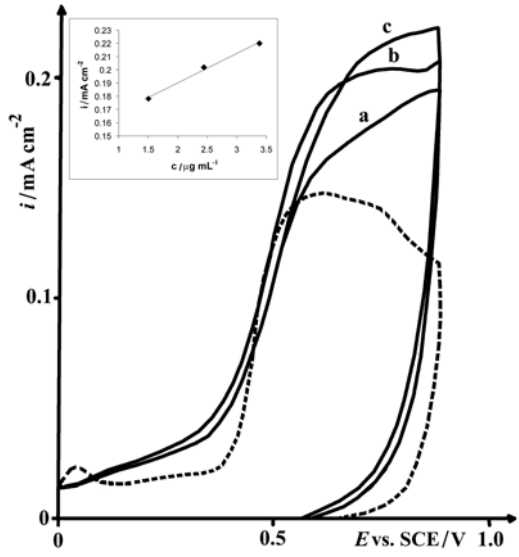

Fig. 2.24 Cyclic voltammogram of gold electrode in 0.05 M $NaHCO_3$ (*dashed line*) and in a presence of amlodipine besylate (*full line*) (*a*) 1.5 μg cm^{-3}, (*b*) 2.439 μg cm^{-3}, (*c*) 3.38 μg cm^{-3}, sweep: 50 mVs^{-1} (Reproduced with a permission from International Journal of Electrochemical Science) [14]

figures, only the first sweep is presented and the electrode surface was prepared for the each presented concentration as is described in experimental part.

The apparent anodic reaction, with wide plateau is observed between 0.5 and 0.85 V for all presented concentrations. In the inset of Fig. 2.24 is presented the linear dependency of the anodic currents vs. concentration in the investigated range (1.50–3.38 μg cm^{-3}), obtained at 0.75 V.

Figure 2.25 presents the cyclic voltammograms of Alopres in 0.05 M $NaHCO_3$ obtained without accumulation. All presented excipients, as was previously published, have no electrochemical activity under the same experimental conditions and amlodipine besylate as a content of Alopres exhibits in their presence also the linear dependency of the anodic current vs. concentration, but for

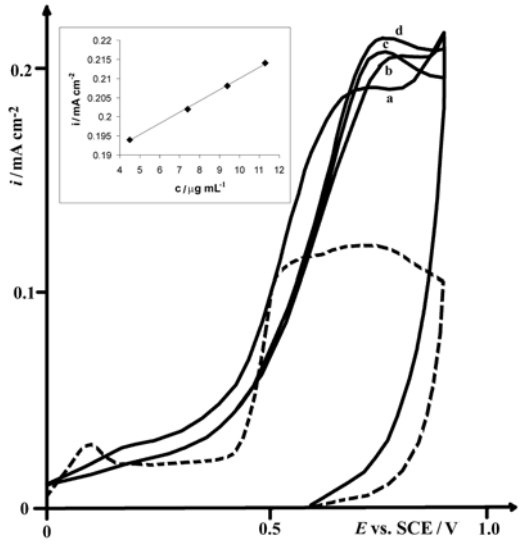

Fig. 2.25 Cyclic voltammogram of gold electrode in 0.05 M $NaHCO_3$ (*dashed line*) and in a presence of amlodipine in Alopres tablet (*full line*) (*a*) 5 μg cm^{-3}, (*b*) 6.5 μg cm^{-3}, (*c*) 9 μg cm^{-3}, (*d*) 12 μg cm^{-3} sweep: 50 mV s^{-1} (Reproduced with a permission from International Journal of Electrochemical Science) [14]

the higher values (4.0–11.5 μg cm^{-3}) obtained at 0.75 V (as is presented in the left corner of Fig. 2.25). Comparing Figs. 2.24 and 2.25 it can be supposed that excipients could cover the electrode surface and in some way prevent the formation of strongly adsorbed agglomerates of amlodipine besylate, causing its anodic reaction to occur at higher concentrations. For higher concentrations in Fig. 2.25 the shape of voltammograms stabilizes, which can be attributed to the reached equilibrium concerning the competitive adsorption between amlodipine besylate and some or all present excipients.

Square wave voltammetry analysis was applied in order to further examine the electrochemical determination of amlodipine in Alopres tablet on a gold electrode in a pH 11 phosphate buffer solution (Fig. 2.26). Voltammograms were recorded in the range of

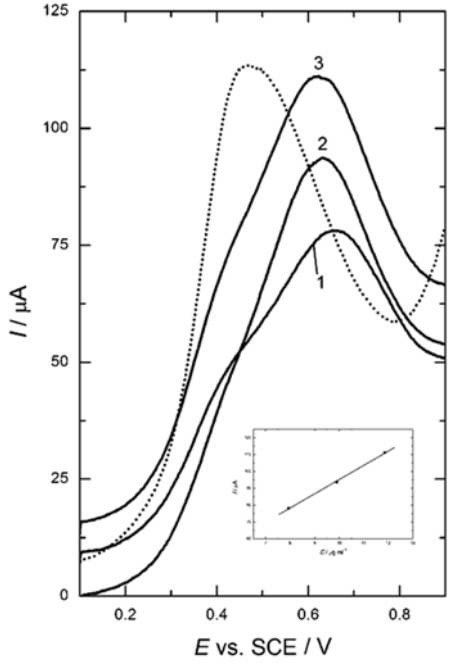

Fig. 2.26 Square-wave anodic stripping voltammograms recorded on a polycrystalline gold electrode for (1) 7.94, (2) 9.90 and (3) 11.86 μg cm^{-3} of amlodipine in Alopres tablet in a phosphate buffer solution pH 11 (the *dotted line* represents a blank solution). Accumulation time: 220 s at $E = +0.1$ V; step size: 2 mV; pulse size: 25 mV; frequency: 50 Hz; scan rate: 100 mVs^{-1} (Reproduced with a permission from International Journal of Electrochemical Science) [14]

potential between +0.1 and +0.9 V for different concentrations of amlodipine in Alopres tablet and before each scan a preconcentration step was performed at the potential of +0.1 V for 220 s in order to accumulate amlodipine besylate on the electrode surface.

In Fig. 2.27 is presented the oxidation of amlodipine in Alopres tablet on Au/o-MWCNT in a pH 11 phosphate buffer solution (7.94 μg cm^{-3}), with accumulation at 0.1 V during 220 s. The anodic activity of amlodipine in Alopres tablet is much lower on Au/o-MWCNT than on a gold electrode.

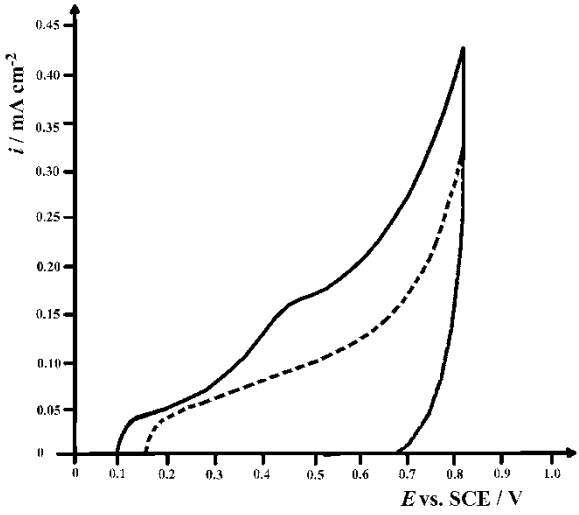

Fig. 2.27 Cyclic voltammograms of Au/o-MWCNT in phosphate buffer (pH = 11) (*dashed line*) and in a presence of amlodipine in Alopres tablet (*full line*), with accumulation at 0.1 V after 220 s, 7.94 μg cm^{-3}, sweep rate; 50 mV s^{-1} (Reproduced with a permission from International Journal of Electrochemical Science) [14]

Figure 2.22 clearly shows that randomly oriented o-MWCNT covered the entire surface of the substrate homogeneously, with the average diameter of 100 nm (Fig. 2.23a). The sample of amlodipine besylate/o-MWCNT was also well dispersed, implying that the o-MWCNT would connect well the amlodipine on the surface and inhibit its oxidation. This explains the better electrocatalytic activity of the gold surface which is covered with small agglomerates. Square wave voltammetry analysis was applied and on Au/o-MWCNT under the same experimental conditions and very low anodic activity of amlodipine in Alopres tablet is obtained, as is presented for cyclic voltammetry in Fig. 2.27. In [15] was published significant anodic oxidation of amlodipine besylate on a glassy carbon electrode modified by o-MWCNT in physiological solution. The results clearly show that glassy carbon electrode

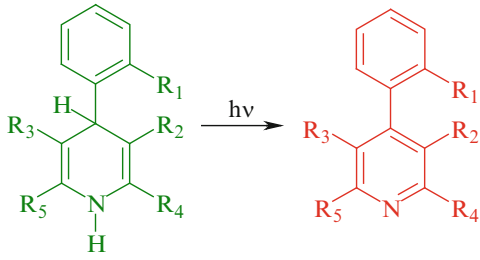

Fig. 2.28 1,4-Dihydropyridine oxidative degradation to pyridine derivative under the influence of light—amlodipine (R_1=Cl; R_2=COOMe; R_3=COOEt; R_4=$CH_2OCH_2CH_2NH_2$; R_5=Me), nifedipine (R_1=NO_2; R_2,R_3=COOMe; R_4,R_5=Me) (Reproduced with a permission from International Journal of Electrochemical Science) [16]

modified by o-MWCNT is better catalyst than gold modified by o-MWCNT for the oxidation of amlodipine besylate and in pharmaceutical preparation.

The electrochemical behavior of inclusion complexes of *nifedipine* (Nif) and *amlodipine* (Aml), a long-acting calcium channel blockers dihydropyridine (DHP) class, with β-cyclodextrin (βCD) and (2-hydroxypropyl)-β-cyclodextrin (HPβCD) (Fig. 2.28), is examined using cyclic and square wave voltammetry in 0.05 M $NaHCO_3$ and phosphate buffer (pH = 11) on a gold electrode [16]. The voltammograms show a single irreversible anodic wave with the current controlled by adsorption. It was found that phosphate buffer favors the electrochemical activity of both complexes of Nif with the linear dependency of the oxidative currents on their concentrations. In phosphate buffer, only HPβCD–Aml complex showed linear dependency of the oxidative currents on the concentration. In 0.05 M $NaHCO_3$ as electrolyte only HPβCD–Nif exhibited apparent activity. The initial potential of the anodic reaction as well as the value of the potential for anodic currents maximum of all the examined complexes in both electrolytes was shifted to the positive direction compared to their standards. In addition, the value of anodic currents decreased.

Nifedipine, dimethyl 1,4-dihydro-2,6-dimethyl-4-(2-nitrophenyl)pyridine-3,5-dicarboxylate, is a dihydropyridine calcium channel blocker. It is a peripheral and coronary vasodilator,

but it has little or no effect on cardiac conduction and negative inotropic activity is rarely seen in therapeutic doses. After oral administration of nifedipine, arterial dilation increases peripheral blood flow, but venous tone does not change. Nifedipine is used in the management of hypertension, angina pectoris, particularly when a vasospastic element is present, as in Prinzmetal's angina, but is not suitable for relief of an acute attack and in the treatment of Raynaud's syndrome.

1,4-Dihydropyridine calcium channel antagonist drugs are characterized by a high tendency to degradation when exposed to light. Oxidative aromatization of dihydropyridine fragment to the pyridine moiety is one of the main degradation pathways of amlodipine and related molecules of 1,4-dihydropyridine family (such as nifedipine) and occurs both in solution and in solid state and is promoted by light. These drugs absorb intensively in the UV-A (some derivates also in the visible) and are known to be photolabile. When amlodipine and corresponding besylate were irradiated in a solution, both in the presence and in the absence of air, it was found to give the aromatized pyridine as the main product. Under exposition of nifedipine to daylight or to certain wavelengths of artificial light it is converted to a nitrosophenylpyridine derivative, while expose to ultraviolet light leads to formation of nitrophenylpyridine derivative.

The inclusion complexes (Fig. 2.29) of nifedipine with β-cyclodextrin (βCD–Nif) or (2-hydroxypropyl)-β-cyclodextrin (HPβCD–Nif) and amlodipine besylate with β-cyclodextrin (βCD–Aml) or (2-hydroxypropyl)-β-cyclodextrin (HPβCD–Aml) were prepared in solid state by coprecipitation with 1:1 mol ratio and characterized by the application of spectroscopic methods FTIR, ^{1}H-NMR, and XRD. Formation of inclusion complexes with cyclodextrin alters the physical properties of the included components such as solubility, dissolution rate, photosensitivity, and stability.

Cyclic voltammograms of βCD–Nif [16] are presented in Fig. 2.30 in phosphate buffer (pH = 11) showing that in anodic direction its electrooxidation begins at 0.25 V with the increasing tendency until the current maximum appearing at the beginning of the oxide formation on gold electrode. This maximum current

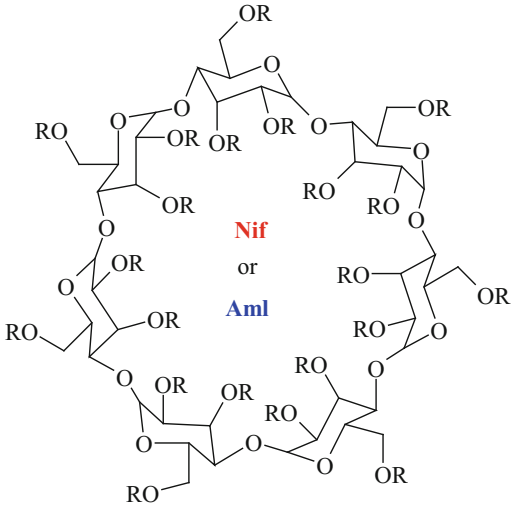

Fig. 2.29 Structure of β-cyclodextrin (βCD) (R=H) and (2-Hydroxypropyl)-β-cyclodextrin (HPβCD) (R=$CH_2CH_2(OH)CH_3$); *Nif* nifedipine, *Aml* amlodipine (Reproduced with a permission from International Journal of Electrochemical Science) [16]

value appears in the whole range of the oxide formation with slightly increasing from 0.9 to 1.0 V. In cathodic direction the presence of βCD–Nif leads to the smaller currents of the oxide reduction which is attributed to the reduction of the species oxidized in anodic direction.

The linear dependency of anodic currents vs. concentration of nifedipine in βCD–Nif in a range: 2.24–5.53 μg cm^{-3} was obtained at 0.77 V from the data in Fig. 2.30. The mentioned linear relationship corresponds to Eq. 1 given in Table 2.1.

Square wave voltammetry, as a fast, sensitive technique with low detection limit, was used for quantitative determination of nifedipine in βCD–Nif on the gold electrode. The square wave anodic stripping voltammograms for different concentrations of nifedipine in βCD–Nif recorded in phosphate buffer in the potential range from 0 to 1.0 V at the scan rate of 15 mV s^{-1} are presented in Fig. 2.31. Before each scan, the compound was

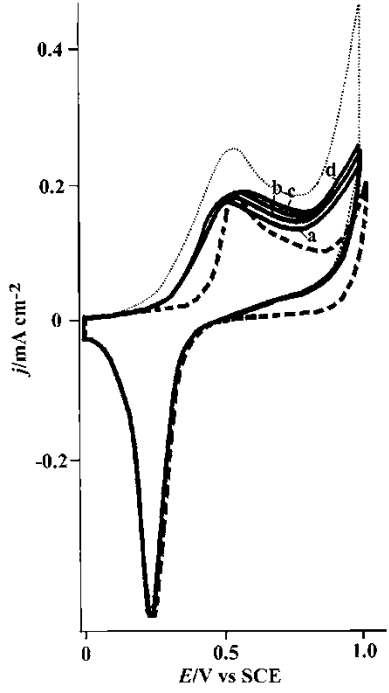

Fig. 2.30 Cyclic voltammogram of gold electrode in phosphate buffer (pH = 11) (*dashed line*) and in a presence of βCD–Nif. Nifedipine concentration: (*a*) 2.24 μg cm^{-3}, (*b*) 3.35 μg cm^{-3}, (*c*) 4.44 μg cm^{-3}, (*d*) 5.53 μg cm^{-3}, sweep: 50 mVs^{-1}; nifedipine standard 2.7 μg cm^{-3} (*dotted line*) (Reproduced with a permission from International Journal of Electrochemical Science) [16]

accumulated at the electrode surface at 0.1 V during 180 s. Each voltammogram is characterized by the well-defined peak at approximately 0.45 V and it is attributed to the oxidation of adsorbed inclusion complex. The current of anodic stripping peak exhibits linear dependence on the βCD–Nif concentration.

The linear dependency of anodic peak currents vs. concentration of nifedipine in βCD–Nif in a range: 4.44–8.72 μg cm^{-3} was obtained from the data in Fig. 2.31. The linear relationship is given by Eq. 2 given in Table 2.1.

Table 2.1 The linear dependency of anodic currents vs. concentration of nifedipine and amlodipine in studied complexes

No.	Complex	Buffer	Method	Equation, j (mA cm^{-2}) = $f(C/\mu$g cm$^{-3})$	R
1	βN[a]	Ph[b]	CV	j = 0.1226 (±0.0025) + 0.0098 (±0.0006) C	0.9962
2	βN	Ph	SWV	j_{pa} = 0.0876 (±0.0003) + 0.0019 (±0.00004) C	0.9998
3	HN[c]	Ph	CV	j = 0.1453 (±0.0018) + 0.0258 (±0.0006) C	0.9996
4	HN	Ph	SWV	j_{pa} = 0. 0727 (±0.0039) + 0.0069 (±0.0014) C	0.9802
5	HN	SBC[d]	CV	j = 0.0782 (±0.0021) + 0.0333 (±0.0011) C	0.9995
6	HN	SBC	SWV	j_{pa} = 0.0706 (±0.0004) + 0.0021 (±0.0001) C	0.9986
7	HA[e]	Ph	CV	j = 0.0679 (±0.0030) + 0.0132 (±0.0004) C	0.9994
8	HA	Ph	SWV	j = 0.0353 (±0.0008) + 0.0006 (±0.00006) C	0.9885

Reproduced with a permission from International Journal of Electrochemical Science [16]

[a]βCD–Nif

[b]Phosphate buffer

[c]HPβCD–Nif

[d]0.05 M $NaHCO_3$

[e]HPβCD–Aml

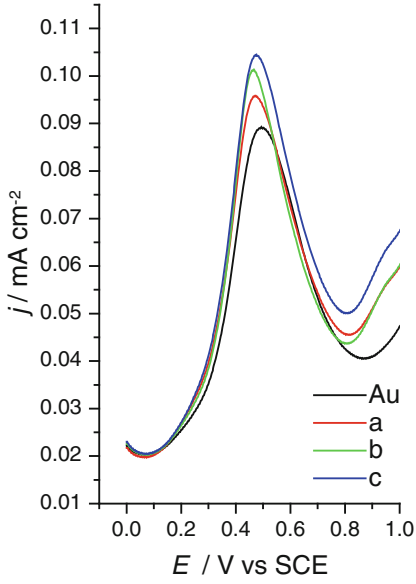

Fig. 2.31 Square wave anodic stripping voltammograms at gold electrode in phosphate buffer (pH = 11) and in a presence of βCD–Nif. Nifedipine concentration: (*a*) 4.44 μg cm^{-3}, (*b*) 6.66 μg cm^{-3}, (*c*) 8.72 μg cm^{-3}. Accumulation time: 220 s at $E = 0.1$ V; step size 2 mV, pulse size 20 mV, frequency 8 Hz, scan rate 15 mV s^{-1} (Reproduced with a permission from International Journal of Electrochemical Science) [16]

Cyclic voltammograms of HPβCD–Nif presented in Fig. 2.32 in phosphate buffer (pH = 11) show the same electrochemical behavior as was observed for βCD–Nif (Fig. 2.30). The linear dependency of anodic currents vs. concentration of nifedipine in HPβCD–Nif in a range: 1.82–3.60 μg cm^{-3} was obtained at 0.65 V from the data given in Fig. 2.32. The linear relationship corresponds to Eq. 3 (Table 2.1).

Although, it was showed earlier that the phosphate buffer is more suitable for the anodic oxidation of dihydropyridine class drugs, so we tested 0.05 M $NaHCO_3$ as electrolyte as well. All the examined inclusion complexes exhibited apparently lower electrochemical activity than in phosphate buffer. The lower activity but good linearity of the currents vs. concentrations was

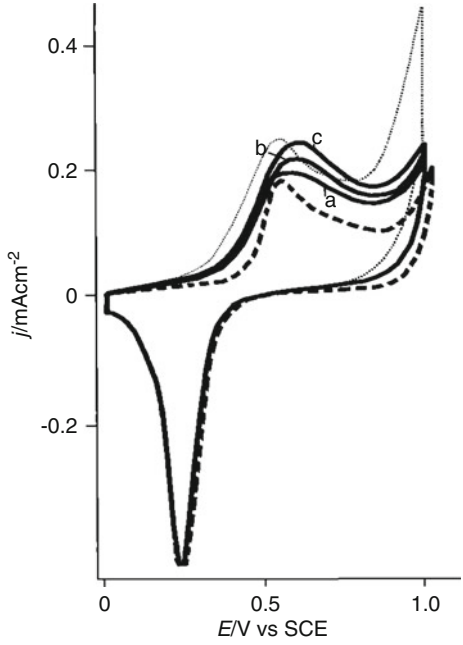

Fig. 2.32 Cyclic voltammogram of gold electrode in phosphate buffer (pH = 11) (*dashed line*) and in a presence of HPβCD–Nif. Nifedipine concentration: (*a*) 1.82 μg cm^{-3}, (*b*) 2.71 μg cm^{-3}, (*c*) 3.60 μg cm^{-3}, sweep: 50 mV s^{-1}; nifedipine standard 2.7 μg cm^{-3} (*dotted line*) (Reproduced with a permission from International Journal of Electrochemical Science) [16]

observed only in the case of the HPβCD–Nif. The linear dependency of anodic currents vs. its concentrations appears at 300 mV more positive potential than was the case in phosphate buffer (Figs. 2.32 and 2.33). The linear dependency in a range: 0.91–2.71 μg cm^{-3} obtained at 0.95 V from the data in Fig. 2.32 is given in Table 2.1 by Eq. 5.

Square wave voltammetry showed also the lower electrochemical activity of nifedipine in HPβCD–Nif in 0.05 M $NaHCO_3$ (lower anodic currents) (Fig. 2.34) than in phosphate buffer (Fig. 2.35). Each voltammogram is characterized by the well-defined peak at approximately 0.6 V which is more than 100 mV shifted to the

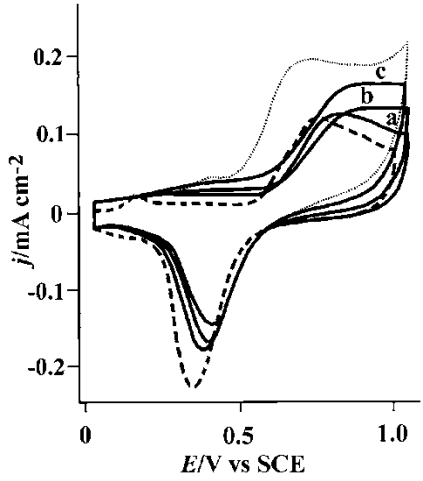

Fig. 2.33 Cyclic voltammogram of gold electrode in 0.05 M $NaHCO_3$ (*dashed line*) and in a presence of HPβCD–Nif (*full line*). Nifedipine concentration: (*a*) 0.91 μg cm^{-3}, (*b*) 1.82 μg cm^{-3}, (*c*) 2.71 μg cm^{-3}, sweep: 50 mVs^{-1}; nifedipine standard 2.7 μg cm^{-3} (*dotted line*) (Reproduced with a permission from International Journal of Electrochemical Science) [16]

positive potential comparing to phosphate buffer. The linear dependency of peak currents vs. concentration of nifedipine in HPβCD–Nif in a range: 0.91–2.71 μg cm^{-3} is presented by Eq. 6 (Table 2.1).

In the form of inclusion complexes, amlodipine exhibited much lower electrochemical activity in both electrolytes compared to nifedipine complexes. Only HPβCD–Aml in phosphate buffer exhibited one apparent electrochemical activity as is presented in Fig. 2.36 and square wave anodic stripping voltammograms are presented in Fig. 2.37. Cyclic voltammograms show an increase in anodic activity in the whole area of the oxide formation on gold electrode with the linear dependency on the concentrations at 0.85 V. The linear dependency of peak currents vs. concentration of amlodipine in HPβCD–Aml in a range: 3.26–9.58 μg cm^{-3} is presented by Eq. 7 (Table 2.1).

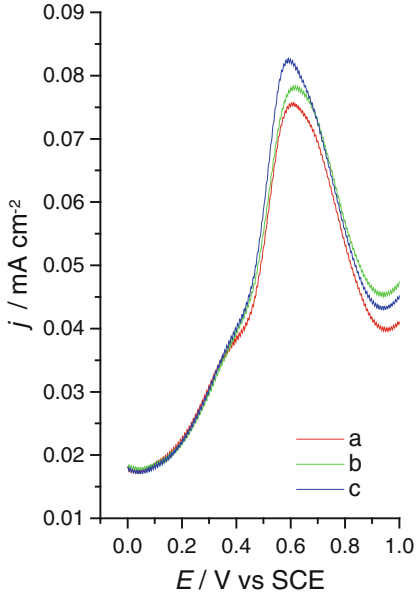

Fig. 2.34 Square wave anodic stripping voltammograms at gold electrode in 0.05 M $NaHCO_3$ and in a presence of HPβCD–Nif. Nifedipine concentration: (*a*) 0.91 μg cm^{-3}, (*b*) 1.82 μg cm^{-3}, (*c*) 2.71 μg cm^{-3}. Accumulation time: 180 s at $E=0.1$ V; step size 2 mV, pulse size 20 mV, frequency 8 Hz, scan rate 15 mV s^{-1} (Reproduced with a permission from International Journal of Electrochemical Science) [16]

By comparing the chemical structures of amlodipine and nifedipine, it is evident that presence of NO_2 group with a strong hydrophobic effect (coefficient hydrophobic substituent, $\pi=-0.85$) significantly decreases the total hydrophobic characteristics of nifedipine. On the other hand, the presence of Cl group as substituent ($\pi=+0.36$) increases the hydrophobic properties of amlodipine. It is important to note that the contribution of the hydrophobic effect to drug/CD complex stability is evident and significant but varies with the structure of drug species. These facts are in good agreements with our experimental data that HPβCD–Aml complex is more subjected to electrochemical adsorption and accumulation.

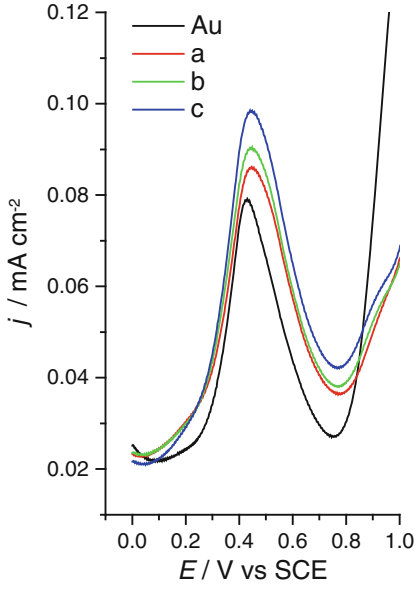

Fig. 2.35 Square wave anodic stripping voltammograms at gold electrode in phosphate buffer (pH = 11) and in a presence of HPβCD–Nif. Nifedipine concentration: (*a*) 1.82 μg cm^{-3}, (*b*) 2.71 μg cm^{-3}, (*c*) 3.60 μg cm^{-3}. Accumulation time: 180 s at $E = 0.1$ V; step size 2 mV, pulse size 20 mV, frequency 8 Hz, scan rate 15 mVs^{-1} (Reproduced with a permission from International Journal of Electrochemical Science) [16]

2.2.3 Central Nervous System Drugs

In modern civilization it is also evident the great demand for different medications related on treatment of various psychoactive states. The drug classes included in this section are depressants and stimulants of central nervous system, various local anesthetics, and also adrenergic and cholinergic agents.

The anodic behavior of *carbamazepine* (CBZ), an anticonvulsant drug (Fig. 2.38), has been studied on gold electrode in 0.1 mol dm^{-3} phosphate buffer of pH 7.0 by using cyclic voltammetry [17]. It has been found that the value of the oxidative current

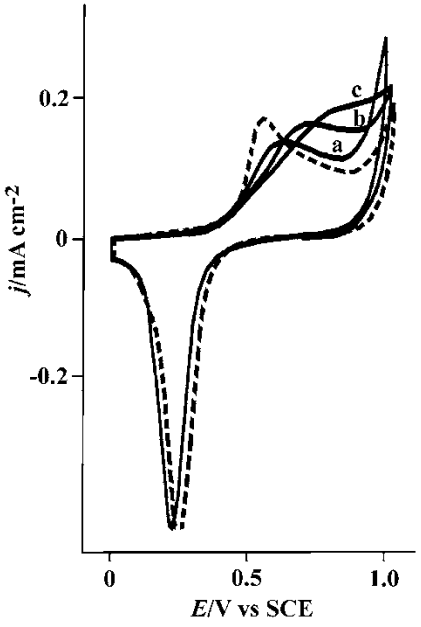

Fig. 2.36 Cyclic voltammogram of gold electrode in phosphate buffer (pH = 11) (*dashed line*) and in a presence of HPβCD–Aml. Amlodipine concentration: (*a*) 3.26 μg cm^{-3}, (*b*) 6.45 μg cm^{-3}, (*c*) 9.58 μg cm^{-3}, sweep: 50 mV s^{-1} (Reproduced with a permission from International Journal of Electrochemical Science) [16]

of pure CBZ at 0.90 V vs. SCE is a linear function of the concentration in a range from 1.0×10^{-7} to 1.0×10^{-4} mol dm^{-3}. The detection of CBZ in the concentration of 1.0×10^{-8} mol dm^{-3} is among the lowest that have been reported for this drug using voltammetric techniques. CBZ as a content of tablet Galepsine® has been quantitatively determined. It has also been demonstrated that the modification of gold electrode with bovine serum albumin (BSA) results in a decrease of the oxidative peak current due to the binding of the drug to BSA.

In the presence of the CBZ standard (at the concentration of 1.0×10^{-8} mol dm^{-3}), the reaction of the oxidation occurs in the area of the oxide formation with the apparent anodic activity from

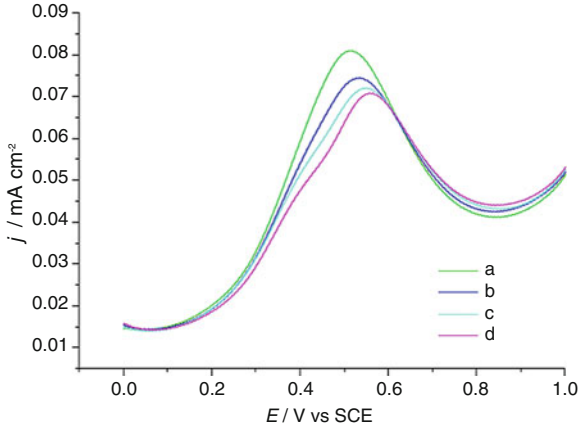

Fig. 2.37 Square wave anodic stripping voltammograms at gold electrode in phosphate buffer (pH = 11) and in a presence of HPβCD–Aml. Amlodipine concentration: (*a*) 9.58 μg cm^{-3}, (*b*) 11.13 μg cm^{-3}, (*c*) 12.65 μg cm^{-3}, (*d*) 14.17 μg cm^{-3}. Accumulation time: 180 s at $E = 0.1$ V; step size 2 mV, pulse size 20 mV, frequency 8 Hz, scan rate 15 mVs^{-1} (Reproduced with a permission from International Journal of Electrochemical Science) [16]

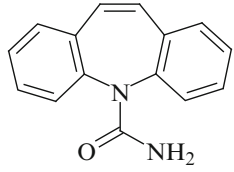

Fig. 2.38 Chemical structure of carbamazepine (5H-dibenzo-[b,f] azepine-5-carboxamide)

0.90 to 1.10 V, as it is presented in Fig. 2.39. The small lowering of the first gold oxide peak at 0.75 V is also apparent only for the concentration of 1.0×10^{-8} mol dm^{-3}. In the reverse sweep, the reaction of the oxide reduction has been decreased in the presence of CBZ at 0.44 V, which may be attributed to the reduction of products formed in the described anodic reactions, as it is the case with macrolide antibiotics [6, 11]. Furthermore, for all of the

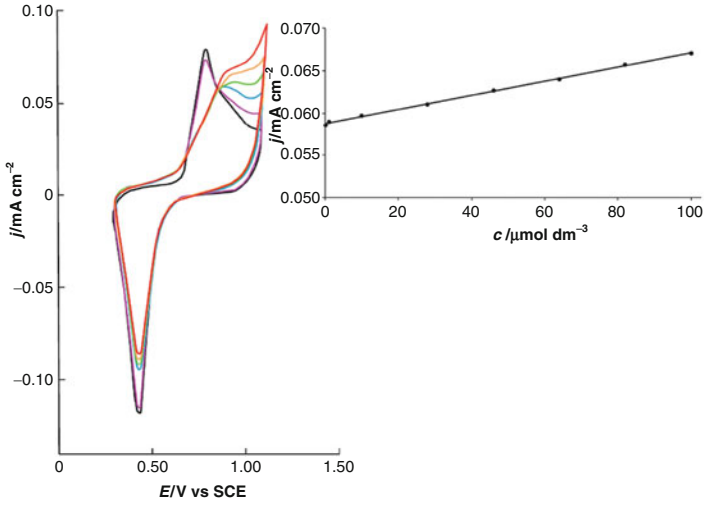

Fig. 2.39 The cyclic voltammograms of bare gold electrode (*black line*) and in the presence of the carbamazepine (CBZ) standard in the concentration from 1.0×10^{-8} to 1.0×10^{-4} mol dm^{-3} (1.0×10^{-8} mol dm^{-3} *pink line*, 1.0×10^{-7} mol dm^{-3} *blue line*, 1.0×10^{-6} mol dm^{-3} *green line*, 1.0×10^{-5} mol dm^{-3} *orange line*, 1.0×10^{-4} mol dm^{-3} *red line*) in 0.1 mol dm^{-3} phosphate buffer (pH 7.0), sweep rate 50 mVs^{-1} (only the first sweep is recorded). *Inset*: The dependency of the value of the oxidative currents of CBZ at 0.90 V on the concentration in the range 1.0×10^{-7}–1.0×10^{-4} mol dm^{-3} (Reproduced with a permission from Association of Chemical Engineers of Serbia) [17]

investigated concentrations of CBZ from 1.0×10^{-7} to 1.0×10^{-4} mol dm^{-3}, in anodic direction, cyclic voltammograms exhibited the changed shape compared to the cyclic voltammograms in the presence of 1.0×10^{-8} mol dm^{-3} of CBZ, as well as in its absence. The increasing anodic current values from 0.30 to 1.10 V due to the increased CBZ concentrations lead to the formation of the current shoulder with the maximum value at 0.95 V. The first gold oxide peak at 0.75 V completely diminished as shown in Fig. 2.39. Because it has tendency to undergo poisoning after the first sweep, gold electrode has been polished between successive additions of suitable aliquots of the working solution of CBZ in phosphate buffer solution to obtain good reproducible results, improved sensitivity, and resolution of voltammetric peaks.

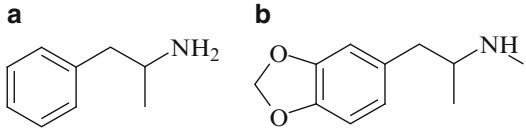

Fig. 2.40 Chemical structures of (**a**) amphetamine and (**b**) 3,4-methylenedio xy-*N*-methylamphetamine

The simple, fast, and cheap voltammetric procedure using gold electrode for the CBZ determination can be further developed as an additional method offering useful combinations with HPLC and with already investigated electrodes, such as glassy carbon electrode.

The abuse of *amphetamine type stimulants* (ATS) is on the rise worldwide. According to UNODC data, the number of ATS users is larger than the number of heroin and cocaine users combined. Amphetamine (A, Fig. 2.40a) and methamphetamine belong to the β-phenyl ethylamine structure sympathomimetic drugs that were utilized as psychostimulants, antidepressants, and appetite suppressants. 3,4-Methylenedioxy-*N*-methylamphetamine (MDMA, Fig. 2.40b) can induce euphoria and diminished anxiety.

There is an increasing interest in the development of rapid, selective, and sensitive methods for the identification and quantification of A and MDMA in illegal market samples. This has been realized using a variety of methodologies: chromatographic techniques, such as HPLC and gas chromatography, capillary electrophoresis, and infrared spectroscopy. Electroanalytical techniques have become powerful tools in modern analytical chemistry for the determination of amphetamine-type drugs. The electrochemical oxidation mechanism of amphetamine-like compounds has not been clarified.

Cyclic voltammetry of some ATS on gold electrode is at the first time performed as is presented in Fig. 2.41 [17].

The value of the oxidative current of the amphetamine standard at 0.80 V vs. SCE in 0.05 M $NaHCO_3$ at the scan rate of 50 mVs^{-1} was a linear function of the concentration in a range of 110.9–258.9 μM.

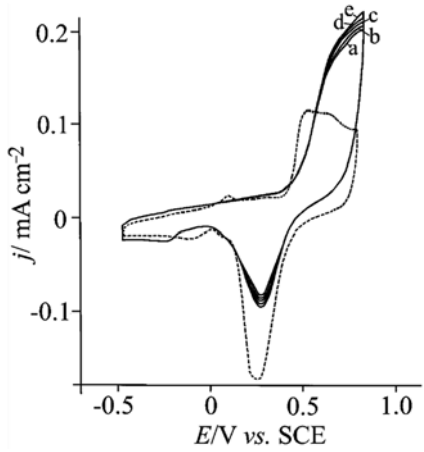

Fig. 2.41 Cyclic voltammogram of the gold electrode in 0.05 M $NaHCO_3$ (*dashed line*) and in a presence of amphetamine standard (*full line*) (*a*) 110.9, (*b*) 147.9 μM, (*c*) 184.9, (*d*) 221.9, and (*e*) 258.9 μM. Sweep rate: 50 mVs^{-1} (Reproduced with a permission from Serbian Chemical Society) [18]

The tested concentrations of the MDMA standard, continuously added in the same experiment, are presented in Fig. 2.42 (full lines). The cyclic voltammograms show an apparent oxidative reaction, with a sharp maximum at the end of the examined oxide region and maximum current values at 0.80 V. Contrary to amphetamine, the oxidation of MDMA began at 0.1 V at the gold electrode surface, 350 mV before oxide formation. This suggests that for MDMA, the gold electrode acted as a catalyst and its molecules were not strongly adsorbed, as in the case of amphetamine.

The urine samples spiked with amphetamine tablets (in the concentration range 110.9–258.9 μM) were analyzed in a same manner as was presented for A. The determination of A in the spiked urine samples was also realized by the standard addition method at two different concentration levels (110.9 and 184.9 μM). Four determinations were performed at each concentration level (Table 2.2). The mean recoveries for the two concentrations were 98.85 % and 97.36 % with relative standard deviations of 0.141 and 1.226, respectively.

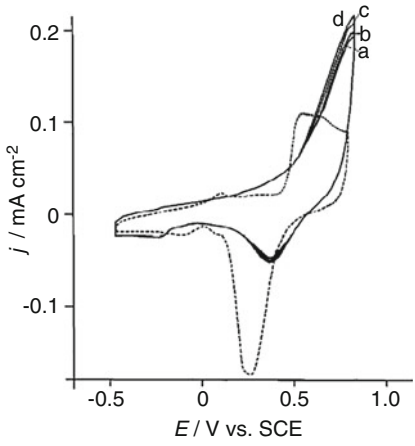

Fig. 2.42 Cyclic voltammogram of the gold electrode in 0.05 M $NaHCO_3$ (*dashed line*) and in a presence of MDMA standard (*full line*) (*a*) 38.7, (*b*) 77.1, (*c*) 153.7, and (*d*) 229.2 μM. Sweep rate: 50 mVs^{-1} (Reproduced with a permission from Serbian Chemical Society) [18]

Table 2.2 Determination of amphetamine in spiked urine samples using the CV method

Taken concentration (μM)	Recovery (%)		SD		RSD	
	CV	HPLC	CV	HPLC	CV	HPLC
110.9	98.25	99.85	0.138	0.100	0.141	0.110
184.9	97.36	99.87	1.201	0.750	1.226	0.805

Reproduced with a permission from Serbian Chemical Society [18]

The urine samples spiked with MDMA standard were analyzed as well and square wave anodic stripping voltammograms of spiked urine samples for the set of concentrations of MDMA presented in Fig. 2.43 are the same as those observed in the absence of urine. The voltammogram for the highest tested concentration of MDMA, 91.6 μM, in Fig. 2.43 shows that a small shoulder that appeared at 0.35 V, attributed to the presence of the urine of healthy volunteers, did not disturb the oxidation of MDMA and had no influence on the value of the oxidation peak. The peak could be slightly shifted to positive potential values (as is presented in Fig. 2.43)

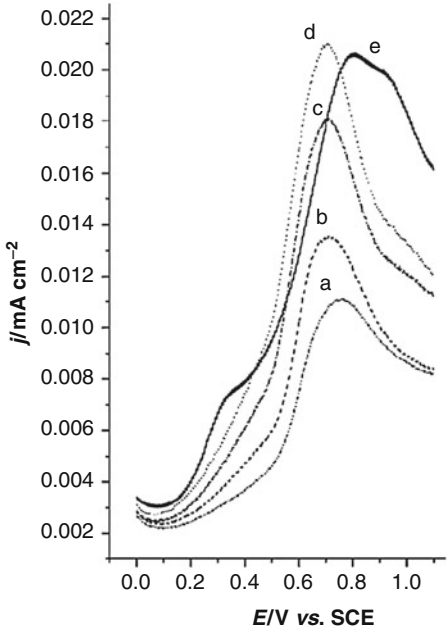

Fig. 2.43 Square wave anodic stripping voltammograms at the gold electrode in 0.05 M $NaHCO_3$ in a presence of MDMA standard, (*a*) 30.9, (*b*) 46.4, (*c*) 76.5, (*d*) 91.6, and (*e*) 91.6 μM spiked with urine. Accumulation time: 220 s at E=0.1 V; step size 2 mV, pulse size 25 mV, frequency 8 Hz, and scan rate 15 mVs^{-1} (Reproduced with a permission from Serbian Chemical Society) [18]

but it did not occur with all spiked urine samples and depended on the urine content, which is common in clinical praxis. The results obtained revealed that SWV could be successfully applied for the quantitative determination of MDMA in urine.

The oxidative ability of *donepezil* (Fig. 2.44), a frequently prescribed drug for the treatment of Alzheimer's disease is reported for the first time at a gold electrode [19]. It was oxidized by cyclic voltammetry and determined by square wave voltammetry in phosphate buffer electrolyte. Electrochemical degradation of donepezil was carried out by long-term potential cycling. The identification and characterization of the major product, isolated by preparative high performance liquid chromatography, was per-

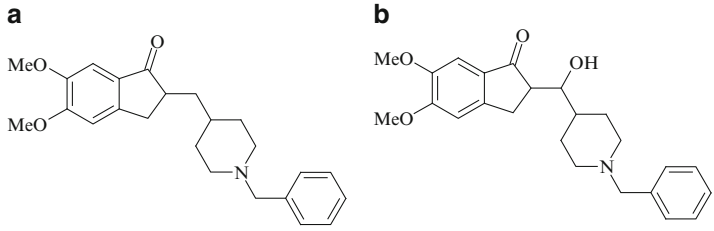

Fig. 2.44 The structures of donepezil (**a**) and the major degradation product (**b**)

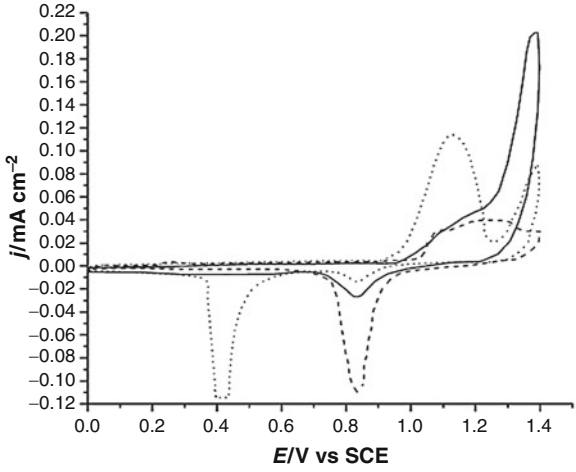

Fig. 2.45 Cyclic voltammogram of gold electrode (*dashed line*) and in a presence of donepezil (50 mg/100 cm^{-3}) in pH 3 phosphate buffer solution before (*dotted line*) and after continuous potential cycling (*full line*). Sweep rate 50 mVs^{-1} (Reproduced with a permission from John Wiley & Sons) [19]

formed by high resolution mass spectrometry and 1D and 2D nuclear magnetic resonance spectroscopy. Donepezil hydroxyl derivative was identified as the major electrochemical oxidation product from donepezil.

The donepezil electroactivity is examined by cyclic voltammetry as is presented in Fig. 2.45 showing in the first sweep an electrooxidation reaction from 0.9 to 1.25 V with the apparent current

maximum at 1.15 V and much smaller, second one at 1.4 V. The first anodic reaction appears before the oxide formation at gold electrode with the current maximum in the area of oxide formation suggesting that gold oxide favors the donepezil oxidation. In the reverse sweep, the apparent cathodic reaction appears at 0.4 V (dotted line). During the long-term potential cycling, the first anodic reaction decreases, the new one appears at 1.25 V, with high currents maximum at 1.4 V. The overlapping with the second anodic reaction cannot be excluded. The cathodic reaction apparently diminishes indicating independency of anodic processes (dotted line). Cyclic voltammetry allows the fast breaking of sites labile toward the oxidation in a donepezil. The linear dependence of the peak currents vs. square roots of sweep rates (25, 50, 100 and 200) mVs^{-1} suggests the diffusion control of the reaction. Electrochemical studies combined with the analysis of the bulk electrolyte after the electrochemical reactions by HPLC were performed. The HPLC method confirmed the existence of several degradation products. The targeted degradation product under study is marked as significant degradation product eluted at retention time of about 11.187 min. Analytical HPLC chromatograms of sample of donepezil bulk drug and sample of donepezil bulk drug electrochemically degraded are obtained by using the HPLC method and are shown in Fig. 2.46. To increase the amount of unknown degradation product of donepezil in the bulk electrolyte, the sample was exposed to 96 h of continuous potential cycling in electrochemical cell. A simple reverse phase semi-preparative chromatographic system was used for isolation of the degradation product from bulk electrolyte. In this chromatographic system, the degradation product eluted at about 14.0 min. The degradation product fraction was collected and then concentrated at room temperature under high vacuum. Purity of the isolated product was tested and found to be 99.0 %, before carrying out spectroscopic and spectrometric experiments. For structure elucidation of the degradation product high resolution mass spectrometry (HRMS) and 1D and 2D NMR experiments were used. Acquisition of HRMS data allowed a determination of the molecular formula. Using high resolution HPLCESI-TOF/MS, the MS spectra of the major degradation product from electro-

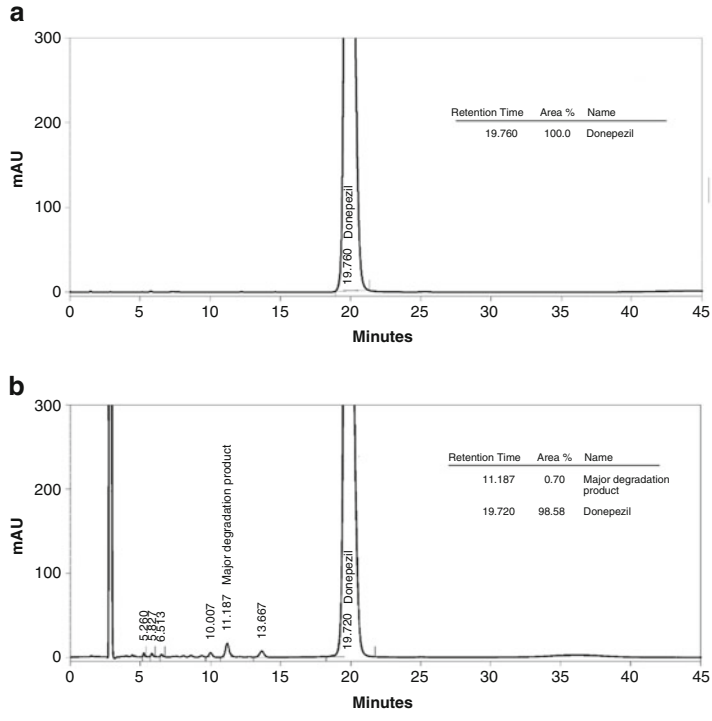

Fig. 2.46 HPLC chromatogram of donepezil bulk in phosphate buffer solution (pH 3) after 14 h of continuous potential cycling in electrochemical cell (**b**) and pure donepezil (**a**) (Reproduced with a permission from John Wiley & Sons) [19]

chemical degradation of donepezil drug substance were recorded in positive and negative mode. MS spectra show precursor ion peak at *m*/*z* 396.2169$[M+H]^+$ in positive mode, and at *m*/*z* 430.1791 $[M+Cl]^-$ and 440.2079 $[M+HCOO]^-$ in negative mode, indicating the molecular formula $C_{24}H_{29}NO_4$. The structure of donepezil degradation product was determined by 1D and 2D NMR spectroscopy.

The ^1H NMR and ^{13}C NMR spectra of the major degradation product are similar to that of donepezil, showing that they have the same basic structure. The corresponding structure of the major

degradation product was characterized as 2-[(1-benzylpiperidin-4-yl)(hydroxy)methyl]-5,6-dimethoxyindan-1-one. This compound has been reported as intermediate in various processes for the synthesis of donepezil and has been investigated for acetylcholine esterase inhibitory activity [20].

Golcu and Ozkan [21] suggested that at glassy carbon electrode the first main anodic reaction could be attributed to the oxidation of the nitrogen atom on the piperidinyl moiety in donepezil. The second anodic oxidation step of donepezil was assigned to the oxidation of alkoxybenzene.

In our study also two anodic reactions were observed. The first main reaction with the current maximum at 1.15 V could be assigned to the oxidation of the nitrogen atom while the second, much smaller anodic reaction (at 1.4 V) could be assigned to the oxidation of alkoxybenzene. This is in agreement with the results presented in [21]. It was suggested that oxidation of alkane to alcohol at Pt electrode [22] proceeds to the formation of secondary carbonium ion in the presence of an acid. Further, carbonium ion reacts with solvent, water, to form an alcohol. We believe that under the applied reaction conditions (acid, water) similar reaction mechanism proceeds at Au electrode during the oxidation of donepezil which leads to the formation of the major oxidation product (Fig. 2.44b). In SWV experiments, deposition times of 120 and 180 s and deposition potentials 0 and 0.2 V were tested but better sensitivity was obtained under conditions presented in Fig. 2.47. SW voltammograms recorded for increasing amount of donepezil (Fig. 2.4a) showed linear increase of peak currents with concentration in the range from 29.1 to 65.4 mg cm^{-3} (Fig. 2.47b).

Phenytoin (5,5-diphenylhydantoin—Fig. 2.48), one of the most frequently used anticonvulsant and antiarrhythmic drug, was examined and determined at bare gold electrode in 0.05 M $NaHCO_3$ using its anodic activity by cyclic voltammetry and square wave voltammetry [23]. Gold electrode is highly sensitive to the phenytoin concentration (the investigated level of concentrations is usually found in human serum of patients treated with phenytoin), providing linear relationships for a set of lower concentrations (0.5, 0.6, 0.8, 1.0 mmol dm^{-3}) and for a set of higher concentrations (10, 20, 30, 40, 50 mmol dm^{-3}). The effects of the substituent

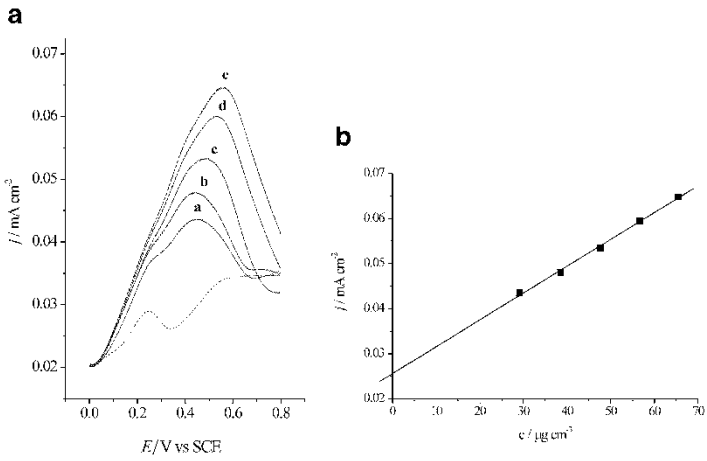

Fig. 2.47 (**a**) Square wave anodic stripping voltammograms of donepezil in concentration range from 29.1 to 65.4 mg cm^{-3} at gold electrode in pH 3 buffer solution (gold electrode: *dashed line*, donepezil concentration: (*a*) 29.1 mg cm^{-3}, (*b*) 38.5 mg cm^{-3}, (*c*) 47.6 mg cm^{-3}, (*d*) 56.6 mg cm^{-3}, (*e*) 65.4 mg cm^{-3}). Accumulation time: 120 s at $E = 0.0$ V; step size 2 mV, pulse size 25 mV, frequency 8 Hz, scan rate 15 mVs^{-1}. (**b**) The linear dependency of anodic peak currents vs. concentration of donepezil (Reproduced with a permission from John Wiley & Sons) [19]

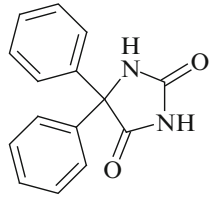

Fig. 2.48 Chemical structure of phenytoin

on the phenyl rings on the electrochemical behavior of two derivatives, 5,5-di(4-chlorophenyl) hydantoin and 5,5-di (4-methylphenyl)hydantoin, were examined by CV. A computational study in correlation with the experimental voltammetric results enabled to propose the oxidation mechanisms: the investigated compounds undergo oxidation involving transfer of $1e^-$ and 1 proton by irreversible, diffusion-controlled process.

Derivatives of hydantoin (imidazolidine-2,4-dione) are important anticonvulsant drugs in the treatment of epilepsy. Depending on the substituents attached to the heterocyclic ring, they can also act as antibacterial and antifungal agents, free radical scavengers, serotonin and fibrinogen receptor antagonists, antiproliferative agents, as well as skeletal muscle relaxants. Phenytoin (5,5-diphenylhydantoin or Dilantin) is a well-known anticonvulsant and antiarrhythmic agent in the treatment of grand mal and psychomotor epilepsy, but its versatile biological effects still attract considerable attention.

Cyclic voltammetry revealed electrochemical activity and concentration dependency of phenytoin in pH 8.4 using 0.05 M $NaHCO_3$ solution and thus possibility for its quantitative determination by square wave voltammetry. In SWV experiments, deposition times of 120 and 25 s and deposition potentials of 0.1 and 0.2 V as well as pulse amplitude of 50 mV were tested but better results were obtained under conditions presented in Figs. 2.49, 2.50, and 2.51.

SW voltammograms recorded for increasing amount of phenytoin for the set of lower concentrations showed linear increase of anodic peak currents to the concentration (insert in Fig. 2.49) with an excellent correlation coefficient ($R=0.995$). Square wave voltammetry also shows that all the lower concentrations of phenytoin start to oxidate at lower potentials than the oxide formation on gold electrode begins to develop as was observed with the cyclic voltammetry (Fig. 2.49). The concentration-dependent anodic peak obtained by SWV appears at the very beginning of the gold oxide formation.

By SWV the linear dependency of the current value of anodic peak on the analyte concentration is obtained with the 20 μM dm^{-3} phenytoin as the highest one. It could be explained by effect of the accumulation time which is long enough to accumulate higher amount of the phenytoin molecules at the gold electrode surface and at the interface with the electrolyte. When concentrations higher than 20 μM dm^{-3} of phenytoin are tested, the peak height observed by SWV increases slowly and it is not concentration dependent.

To investigate the influence of substituent on phenytoin, derivatives with electroaccepting and electron-donating functional

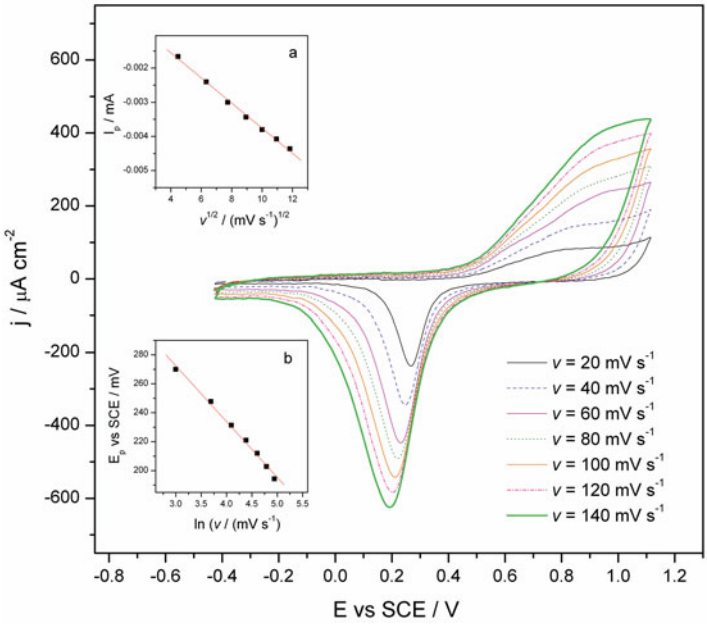

Fig. 2.49 CVs of 20 mmol dm^{-3} of phenytoin on gold electrode using 0.05 M $NaHCO_3$ for scan rates: 20, 40, 60, 80,100, 120, and 140 mVs^{-1}. Insets: plots of current vs. $v^{1/2}$ (*a*) and peak potential shift vs. ln of scan rates (*b*) (Reproduced with a permission from Elsevier) [23]

groups in the phenyl rings were synthesized. The synthesized derivatives of phenytoin (**1**), 5,5-di(4-chlorophenyl) hydantoin (**2**) and 5,5-di(4-methylphenyl) hydantoin (**3**), were investigated by cyclic voltammetry and compared with phenytoin (Fig. 2.52). The chloro derivative exhibits the quite similar voltammetric behavior as was observed with phenytoin (Figs. 2.49 and 2.52) with the little bit lower anodic currents and with the neglectable lowering of the currents of gold oxide reduction. The methyl derivative shows two anodic waves in the area of the gold oxide formation with the little bit higher currents than was observed with phenytoin and with the increased currents of gold oxide reduction. Both derivatives exhibit the higher currents at 1.1 V than phenytoin.

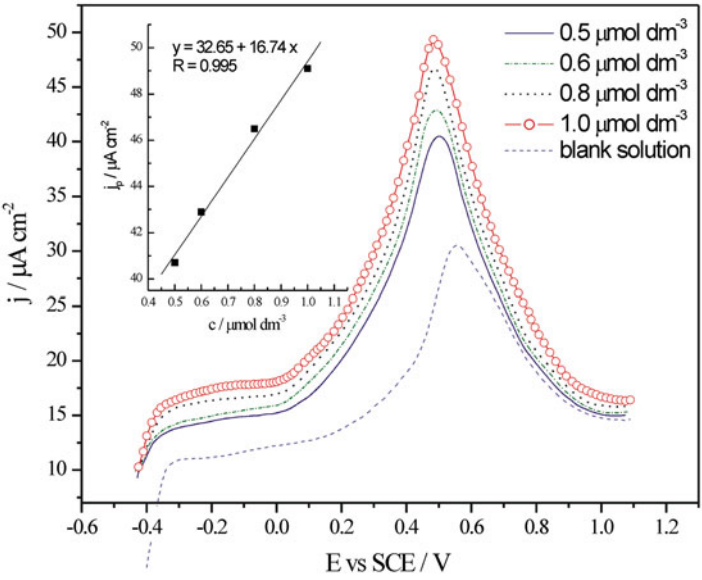

Fig. 2.50 Square wave anodic stripping voltammograms of phenytoin (5, 10, 15, 20) μM dm^{-3} obtained with the Au electrode (*dashed line*) at pH 8.4 using 0.05 M $NaHCO_3$. Accumulation time: 0.2 s at $E = 0.0$ V; step size 5 mV, pulse size 25 mV, frequency 10 Hz, scan rate 50 mVs^{-1}. *Insert*: The linear dependency of anodic peak currents vs. concentration of phenytoin (Reproduced with a permission from Elsevier) [23]

To compare the energy differences between systems involved into the oxidation mechanism, DFT M06-2X calculations with 6-311++G(d,p) basis set are carried out. To keep systems on the same level, the energy of H_2O molecule was added to the energy of hydantoin molecule (G) and corresponding radical cation (R^+) and the energy of H_3O^+ ion was added to the energy of radical and anionic species.

From the M06-2X results can be seen that the formation of radical in position N1 (RN1) is thermodynamically favored instead of the formation of radical in position N3 (RN3). The differences of the energy for formation of RN1 and RN3 radicals are 13.1 and

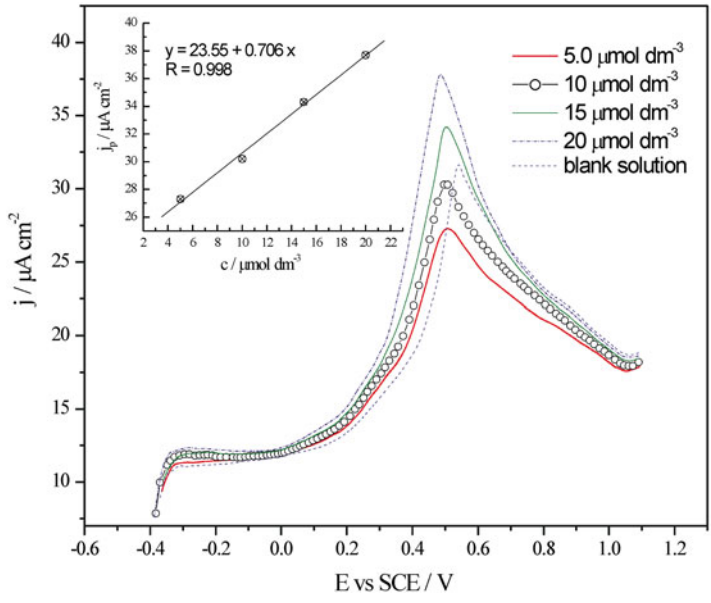

Fig. 2.51 Square wave anodic stripping voltammograms of phenytoin (5, 10, 15, 20 mmol dm^{-3}) obtained with the Au electrode using 0.05 M $NaHCO_3$. Accumulation time: 0.2 s at E=0.0 V; step size 5 mV, pulse size 25 mV, frequency 10 Hz, scan rate 50 mVs^{-1}. Inset: the linear dependency of anodic peak currents vs. concentration of phenytoin (Reproduced with a permission from Elsevier) [23]

13.0 kcal mol^{-1} in vacuum and water for phenytoin. The mechanism of electrolytic oxidation can be divided in two steps: electrochemical abstraction of electron and abstraction of proton. The order of these steps can kinetically favor formation of the corresponding radical. The first route which consisted of abstraction of electron followed by abstraction of proton, from main molecule (G) via intermediate radical cation (R^+) leads to thermodynamically more stable radical RN1.

From the other side, second route considers the abstraction of proton in the first step and formation of anion on N1 (AN1) or N3 (AN3) as intermediates. The formation of AN3 is thermodynamically favored. Differences of the energy for formation of AN1 and

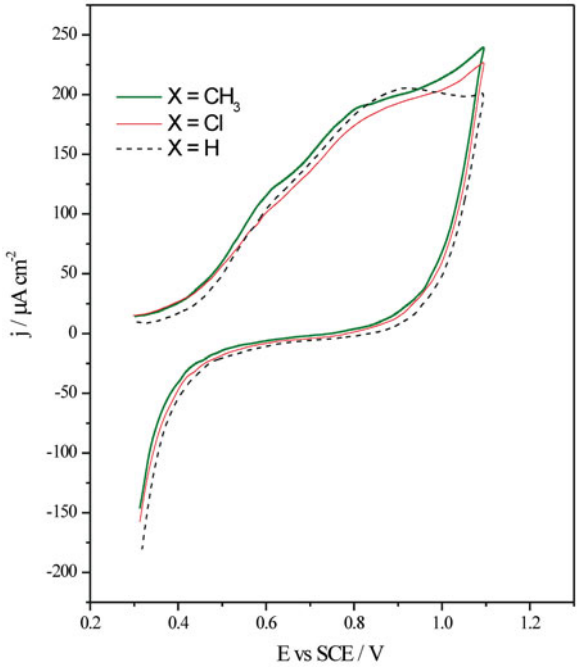

Fig. 2.52 CVs (first scan) of 20 mmol dm^{-3} phenytoin and its derivatives on gold electrode using 0.05 M $NaHCO_3$, scan rate: 50 mVs^{-1} (Reproduced with a permission from Elsevier) [23].

AN3 from phenytoin are −4.6 and −7.3 kcal mol^{-1} in vacuum and water and correspond with acidity of N1–H and N3–H bonds of hydantoins. Second step, electrochemical abstraction of electron needs 82.3 and 126.4 kcal mol^{-1} energy for formation of radical RN1 and 82.3 or 126.4 kcal mol^{-1} energy for formation of radical RN3 in vacuum and water for phenytoin.

The energy for abstraction of electron is dependent on the mechanistic path involved in. As both the paths are feasible, the ratio of the paths is in direct correlation to concentration of hydantoin and its anionic forms. The second mechanistic path slightly favors formation of RN3 radical.

These findings are in good correlation with experimental findings which show that voltammetric response depends on pH of solution of hydantoins. Voltammetric response of solution on

lower pH is on the bigger values and increase of pH leads to decrease of value of voltammetric response.

The energies of the frontier molecular orbital, HOMO and LUMO, are important parameters of the molecular electronic structure, because both are taking part in the chemical reaction. The molecule that has the lower HOMO energy has the weakest donating electron ability; otherwise, a higher HOMO energy implies that the molecule is a good electron donor. Energy of HOMO is a useful diagnostic criterion for oxidation. It has been reported that negative value of HOMO energy (equal to ionization potential) is directly proportional to oxidation potential. As well the energy difference between LUMO and HOMO orbital energies determines the chemical reactivity.

The HOMO orbital of all investigated molecules is π-like orbital and they are mainly localized on the phenyl groups and just partly distributed over the hydantoin ring. The HOMO and LUMO orbitals of investigated hydantoins are shown pictorially in Fig. 2.53.

An examination of HOMO energy values, from B3LYP/6-311++G(d.p) calculations, listed in Table 2.3 reflects that the hydantoin oxidation follows the same order as obtained from voltammetric results. Modulation of HOMO energy with changing functional group suggests that incorporation of substituent on phenyl rings can affect the oxidation potential.

The comparatively easier oxidation of 5,5′-(4,4′-dimethyl-diphenyl) hydantoin is evident from its lower negative HOMO energy (−6.75 eV) than phenytoin (−7.06 eV) due to the electron-donating effect of methyl groups.

Energy of HOMO in 5,5′-(4,4′-dichloro-diphenyl) hydantoin (**3**) is under the influence of two opposing effects (positive mesomeric and negative inductive) resulting in slightly higher negative value in vacuum (−7.11 eV) and lower in water (−7.02 eV) than phenytoin (**1**). This can be explained by the influence of solvation sphere of water which lower inductive effect as a result of electrostatic interaction with Cl groups of hydantoin **3**. As the COSMO model does not include electronic contribution for the creation of the hydrogen bonds, the overall effect is considerably smaller then expected. Nevertheless, predicted effect of electron-donating ability of Cl group in water has the same direction as the experimental results and supports the experimental findings.

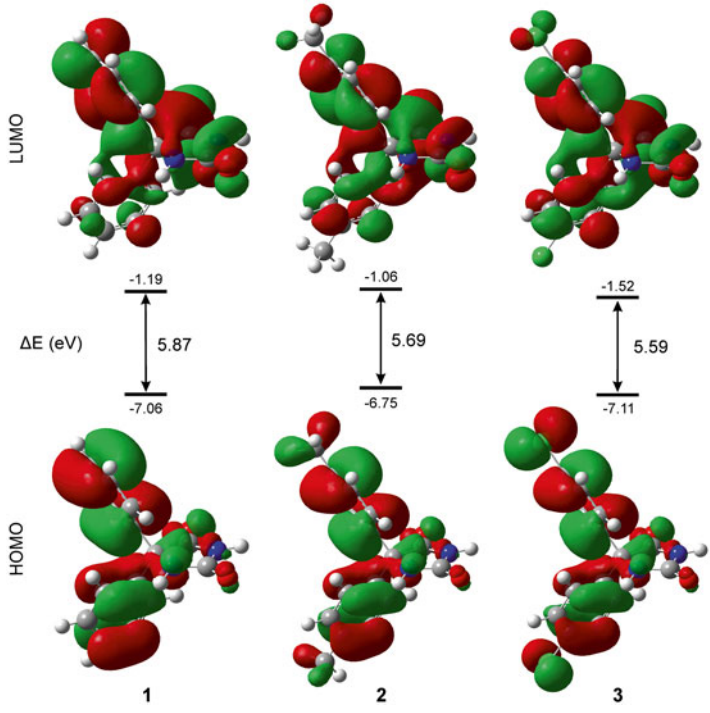

Fig. 2.53 The HOMO and LUMO molecular orbitals, their energies, and energy gaps for investigated hydantoins (Reproduced with a permission from Elsevier) [23]

The spin density distribution is an important quantum property of the radical species. SD maps can show the delocalization of the electron spin which determines stability of radicals and indicates its reactive sites. It can be seen from Fig. 2.54 that the SD of radical cation is delocalized over both phenyl group indicating on that way big influence of substituent to its stability. Energy difference of R^+ from UM06-2X/6-311++G(d,p) calculation for **1**, **2** and **3** is around 10 and 7 kcal/mol for vacuum and water. On the other side, the SD of radical RN1 and RN2 is mostly distributed between corresponding nitrogen atom and atoms of nearby carbonyl groups. Stability of RN1 and RN2 shows very small influence of substituent

Table 2.3 Energy values for HOMO, LUMO orbitals and their energy gap [eV], ionization potential (IP) [kcal mol^{-1}], and NBO charges [e^-] for the investigated hydantoins obtained from B3LYP/6311++G(d,p) calculations

	Energy				NBO charge						
Compd.	HOMO	LUMO	Gap	IP	N1	C2	O2	N3	C4	O4	C5
1	−7.06	−1.19	5.87	194.83	−0.658	0.815	−0.605	−0.658	0.711	−0.572	0.044
2	−6.75	−1.06	5.69	185.44	−0.661	0.814	−0.608	−0.659	0.712	−0.575	0.033
3	−7.11	−1.52	5.59	194.93	−0.661	0.815	−0.599	−0.657	0.710	−0.570	0.044

Reproduced with a permission from Elsevier [23]

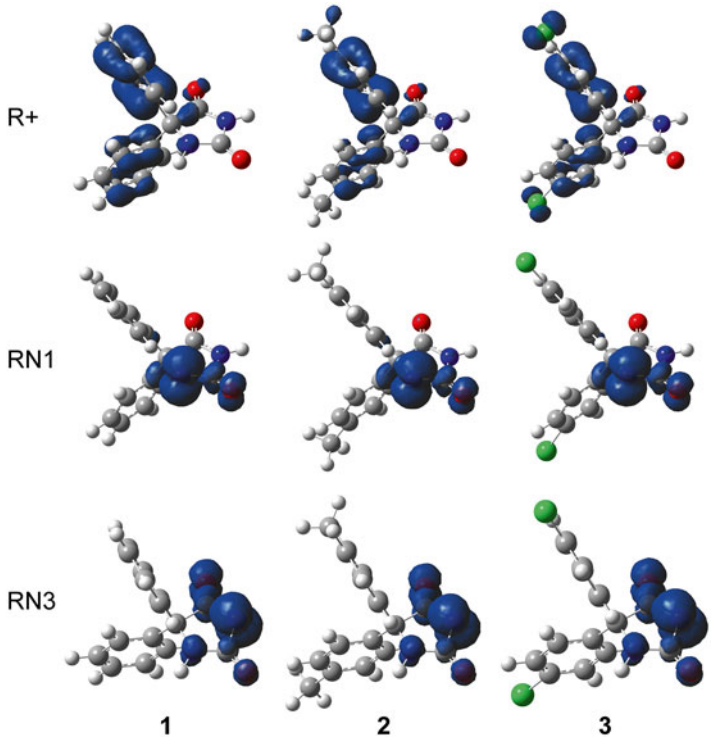

Fig. 2.54 Distribution maps of spin density (squared) for radical species for studied hydantoins (R^+—radical cation; RN1—radical in position N1; RN3—radical in position N3) (Reproduced with a permission from Elsevier) [23]

for correspondent radical, less than 0.7 kcal mol^{-1}, in all cases. As the SD maps for RN1 and RN2 show lot of similarity with HOMO orbital plots for AN1 and AN3 anions, the same conclusion can be derived for the electrochemical abstraction of electron from corresponding anions (second route in mechanism of electrolytic oxidation) especially for water as solvent. Energy difference for abstraction of electron from corresponding anion in water for **1**, **2,** and **3** is less than 2.5 kcal mol^{-1}.

The proposed mechanism for the oxidation of hydantoin derivatives is given at the following scheme (Fig. 2.55).

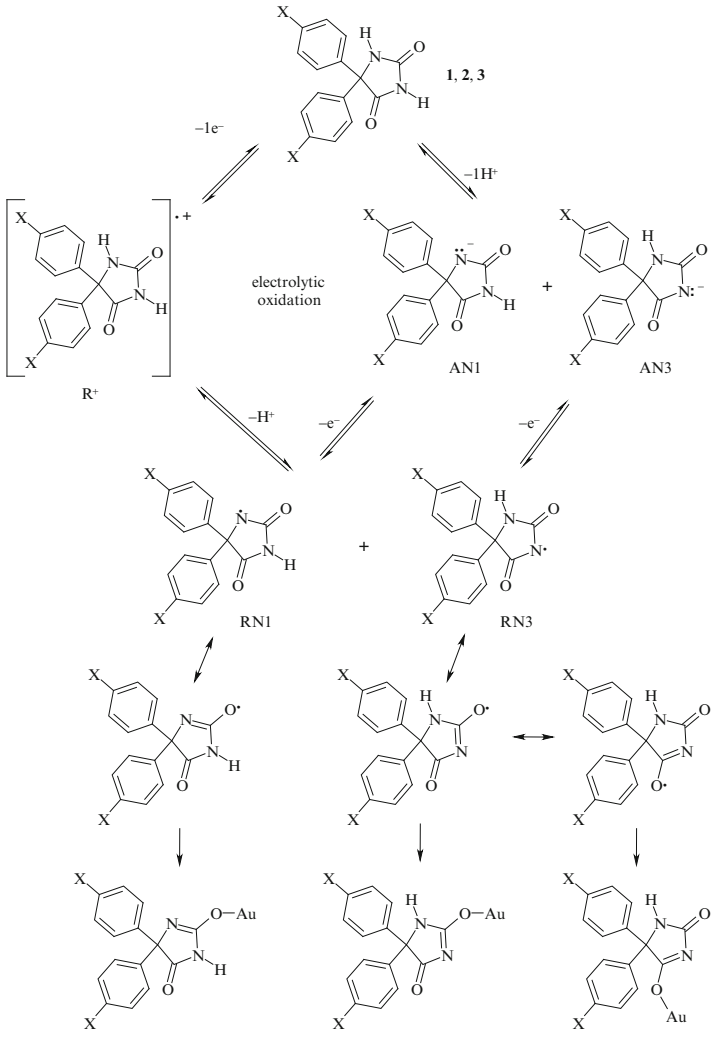

Fig. 2.55 Proposed mechanism for the oxidation of hydantoin derivatives (Reproduced with a permission from Elsevier) [23]

Many requests for the determination of the anticonvulsant drugs arise as a result of problems in the therapy of neurological disorders. Phenobarbital has a narrow therapeutic range, so its concentration needs to be monitored in order to adjust the dose to the optimal level for effective therapeutic control but with minimal side effects such as neurological toxicity [24]. The drug is frequently used in combination with paracetamol since its presence reduces the recurrence risk of simple febrile seizures [25]. DPV has been successfully applied for the determination of phenobarbital and paracetamol in pharmaceuticals [26]. Raoof et al. [27] have prepared a modified electrode by incorporation of multiwalled carbon nanotube and Pt-nanoparticles into a paste matrix. The DPV response of a drug mixture reveals two well-distinguished oxidation peaks, corresponding to the oxidation of phenobarbital and paracetamol, which allow their individual determination.

2.2.4 Anticancer Drugs

The chemotherapy of cancer and neoplastic disease has become very important in recent years. Most antineoplastic drugs are highly toxic to the patient and must be administered with extreme cautions. In this section, are noted several representative drugs with different structures and significant antitumor activity.

Idarubicin is an antracycline drug (Fig. 2.56) which exerts significant antitumor activity. The effect of surface modifications on the electrochemical behavior of the anticancer drug idarubicin was studied at multiwalled carbon nanotubes modified glassy carbon and edge plane pyrolytic graphite electrodes. The surface morphology of the modified electrodes was characterized by scanning electron microscopy [28]. The modified electrodes were constructed for the determination of idarubicin using adsorptive stripping differential pulse voltammetry. The experimental parameters such as supporting electrolyte, pH, accumulation time and potential, and amount of carbon nanotubes for the sensitive assay of idarubicin were studied as details.

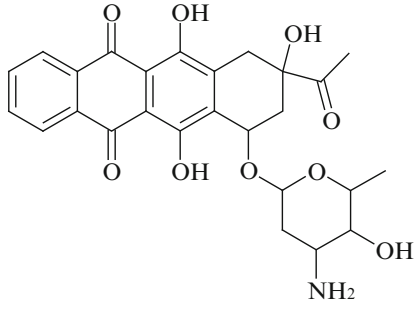

Fig. 2.56 Molecular structure of idarubicin

The results revealed that the modified electrodes showed an obvious electrocatalytic activity toward the oxidation of idarubicin by a remarkable enhancement in the current response compared with bare electrodes.

Under the optimized conditions, idarubicin gave a linear response in the range 9.36×10^{-8} to 1.87×10^{-6} M for modified glassy carbon and 9.36×10^{-8} to 9.36×10^{-7} M for modified edge plane pyrolytic graphite electrodes. The detection limits were found as 1.87×10^{-8} and 3.75×10^{-8} M based on modified glassy carbon and edge plane pyrolytic graphite electrodes, respectively. Interfering species such as ascorbic acid, dopamine, and aspirin showed no interference with the selective determination of idarubicin. The analyzing method was fully validated and successfully applied for the determination of idarubicin in its pharmaceutical dosage form. The possible oxidation mechanism of idarubicin was also discussed. The results revealed that the modified electrodes showed an obvious electrocatalytic activity toward the oxidation of idarubicin by a remarkable enhancement in the current response compared with bare electrodes.

Anthracyclines were originally isolated from a pigment producing *Streptomyces* and are among the most widely used anticancer agents. Idarubicin (IDA) is an anthracycline, which exerts antitumor activity in several solid tumors and hematological malignancies. Because the molecule is more lipophilic than the other anthracyclines it can be administered orally. IDA (Fig. 2.57), a

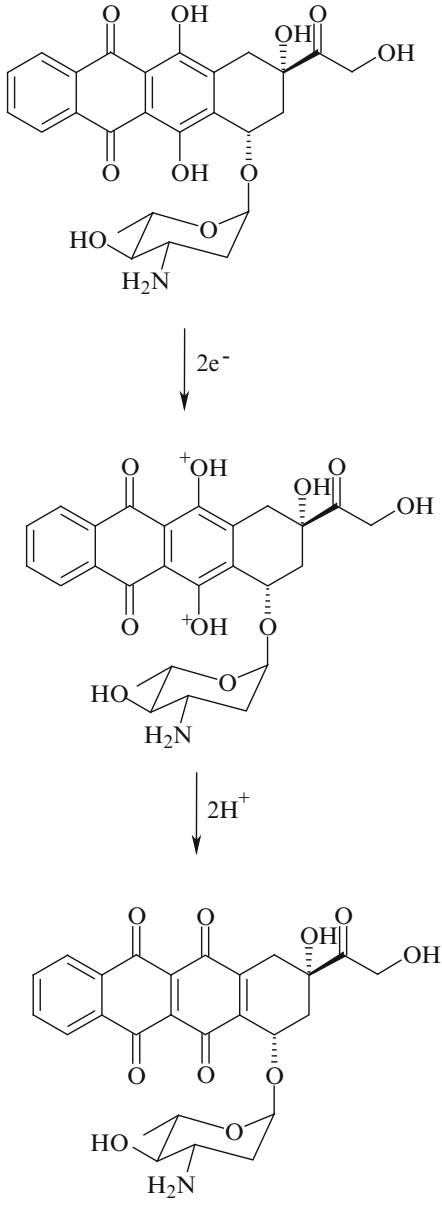

Fig. 2.57 The possible electrooxidation pathway of idarubicin on solid electrodes (Reproduced with a permission from John Wiley & Sons) [28]

synthetic analog of daunorubicin, acts by intercalating between DNA base pairs and inhibiting topoisomerase II. Additionally, it induces free oxygen radicals leading to destruction of DNA and cell membrane.

Idarubicin contains anthracycline and phenol moieties to exclude the possibility of the oxidation part of IDA. Moreover, IDA contains highly electroactive hydroxyl groups on the benzene rings. In general, the oxidation of phenol in a solution at high pH values will generate the phenoxy radical giving an additional oxidation and reduction process similar to anthracyclines such as epirubicin, doxorubicin, and daunorubicin. Therefore, voltammetric techniques are most suitable for investigating the redox properties of drug active compounds. This can give insight into the metabolic fate or in vivo redox process of pharmaceutical activity. The interest in developing electrochemical sensing devices for use in clinical assays is growing rapidly. Electrochemical sensors based on nanomaterial can cope for real samples, which did not have a complex composition and time-consuming preparation steps. The adsorptive stripping differential pulse voltammetric (AdSDPV) technique has been reemergent among electroanalytical techniques through the use of carbon nanotube-modified electrodes where a thin porous layer of nanotubes is in electrical contact with a suitable electrode.

Tamoxifen, [Z]-2-[4-(1,2-diphenyl-1-butenyl)-phenoxy]-*N*,*N*-dimethylethylamine (Tam), a nonsteroidal antiestrogen, has been the most important hormonal agent for treatment of breast cancer for more than two decades, and recently has been approved as a long-term chemopreventive agent for breast cancer in healthy women at high risk for developing breast cancer (Fig. 2.58). Tam undergoes chemical transformation to its phase I metabolites in vivo, resulting in a series of modified species, predominately through methylation or hydroxylation of the benzene rings on the tamoxifen structure, to structures such as 4-hydroxytamoxifen.

The electrochemical investigation of Tam at the glassy carbon electrode and ruthenium oxide (RuO_2) doped on Ebonex electrode in phosphate buffered solution has been studied, based on the adsorption behavior of Tam at the glassy carbon electrode surface [29]. The cyclic voltammetric behavior shows well-defined

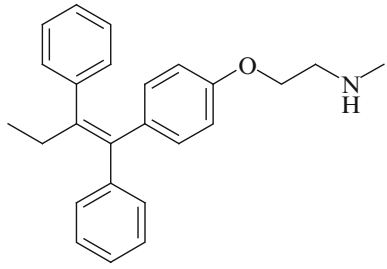

Fig. 2.58 Chemical structure of tamoxifen

irreversible anodic peak at 1.12 V, so to the cyclization reaction to form the corresponding phenanthrene derivative. A fully validated, simple, sensitive, selective, fast, and low-cost differential pulse and square wave adsorptive anodic stripping voltammetric methods were developed for determination of Tam in bulk form, and in spiked human urine and serum. The described methods could be recommended for use in trace analysis, quality control, and clinical laboratories. The phase I metabolite TamOH was shown to be significantly separated from Tamoxifen, being oxidized at a lower potential, but its lower adsorptive character and interfering species at its stripping potential limits our ability to validate a method for its determination.

The electrooxidative behavior of tamoxifen and 4-hydroxytamoxifen (TamOH) was investigated by cyclic, differential-pulse adsorptive anodic stripping (DPAdAS) and square-wave adsorptive anodic stripping (SWAdAS) voltammetric techniques. [29] The anodic oxidation peak of tamoxifen was attributed to the cyclization reaction to form the corresponding phenanthrene derivative and the mechanism of oxidation was postulated on the basis of controlled potential electrolysis and isolation of the oxidative product. Oxidative stripping analysis was successfully applied to the determination of tamoxifen in a bulk pharmaceutical formulation, and sensitivity in human urine and serum was validated. The achieved limits of detection (LOD) of bulk tamoxifen were 1.8×10^{-6} and 2.4×10^{-6} mol dm^{-3} for DPAdAS and SWAdAS, respectively. The LOD values for tamox-

ifen in human urine and serum sample analysis were 4.75×10^{-7} and 2.63×10^{-7} and 1.98×10^{-7} and 3.28×10^{-7} mol dm^{-3} for DPAdAS and SWAdAS, respectively. 4-hydroxytamoxifen is oxidized at more positive potentials than Tamoxifen, separated from the Tamoxifen stripping peak, and its adsorption to the glassy carbon electrode is less pronounced. This affects the ability to determine this important phase I metabolite in serum and urine samples.

2.2.5 Anti-inflammatory Drugs

Anti-inflammatory, especially nonsteroidal drugs continue to be of the more widely used groups of therapeutic drugs. The medicinal drugs covered in this section represent a major market in both prescription and nonprescription drugs.

As the very first electrochemical investigation of *oxaprozin*, nonsteroidal anti-inflammatory drug, using cyclic voltammetry on gold electrode in 0.05 mol dm^{-3} $NaHCO_3$, the synthesized drug, its analytical standard, and its content in Duraprox® tablets were characterized with one oxidation reaction and the three reduction reactions [30]. All they exhibited the linear concentration dependency of anodic currents at 0.83 V for the analytical standard and 0.85 V for Duraprox® tablets in the range of concentrations 8.44–32.78×10^{-6} mol dm^{-3}. The strong adsorption of bovine serum albumin (BSA) on gold electrode in 0.1 mol dm^{-3} phosphate buffer solution (pH 7.4) is shown and concentration dependency of anodic currents of oxaprozin standard on BSA/Au is studied. Following the Langmuir adsorption thermodynamic equation, the binding constants of oxaprozin on BSA/Au electrode was calculated with the results 1.23×10^5 dm^3 mol^{-1}.

Oxaprozin, 3-(4,5-diphenyl-1,3-oxazol-2-yl)propanoic acid (Fig. 2.59), is one of the leading nonsteroidal anti-inflammatory drugs (NSAIDs) in the US market, which is used in the treatment of a number of inflammatory musculoskeletal diseases, including rheumatoid arthritis, osteoarthritis, ankylosing spondylitis, tendinitis, and bursitis. It exhibits several advantages over other NSAIDs (e.g., aspirin, diclofenac, ibuprofen) including a low incidence of

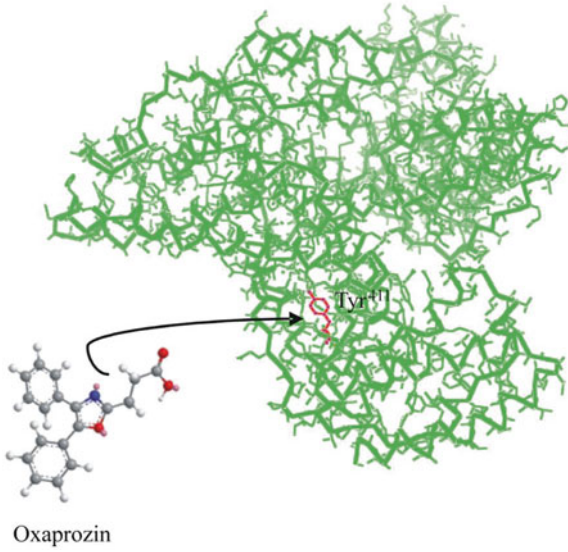

Fig. 2.59 Interaction of oxaprozin with serum albumin. The 3D structure was obtained using Pymol vs. 0.99 and data obtained from Protein Data Bank (PDB). PDB code of serum albumin: 2BXM (Reproduced with a permission from International Journal of Electrochemical Science) [30]

gastrointestinal side effects, a long half-life with long duration of action, and good patient compliance with a once-daily oral regimen. Several chromatographic methods have been presented in the literature for the determination of oxaprozin and its impurities in the bulk drug as well as in biological fluids.

As is presented in Fig. 2.60a, the cyclic voltammogram shows that on gold electrode in the presence of oxaprozin standard, the apparent reaction of the oxidation occurred in the area of the oxide formation with big anodic current plateau between +0.6 and +0.9 V. In the reverse sweep, the reaction of the oxide reduction was decreased in the presence of oxaprozin which can be attributed to the reduction of products formed in described anodic reaction. In the cathodic direction in reverse sweep, the two additional reduction reactions occurred: the first with the cathodic peak at −0.2 V and second one, with cathodic peak at −0.55 V. By cyclic

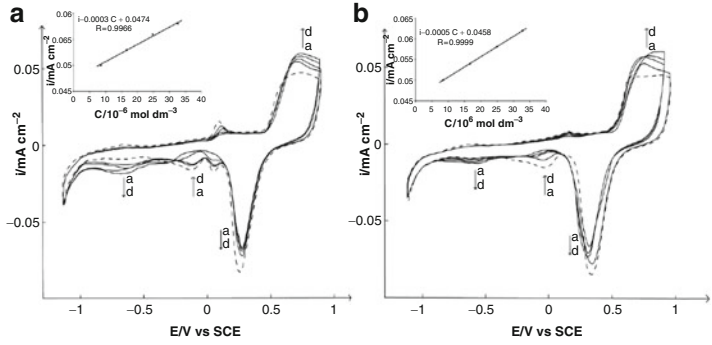

Fig. 2.60 The cyclic voltammograms on bare gold electrode (*dashed line*) as well as in the presence of oxaprozin standard (**a**) and oxaprozin tablets (Duraprox®) (**b**) (*full lines*) in the range of concentrations: $a = 8.44$ mol dm^{-3}; $b = 16.71$ mol dm^{-3}; $c = 24.83$ mol dm^{-3}; $d = 32.78$ mol dm^{-3} in 0.05 mol dm^{-3} $NaHCO_3$, sweep rate 50 mVs^{-1} (only the first sweep is recorded) (Reproduced with a permission from International Journal of Electrochemical Science) [30]

voltammetry on gold electrode, the synthesized oxaprozin as well as its analytical standard was characterized with one oxidation reaction and the three reduction reactions. The synthesized oxaprozin and analytical standard exhibited the identical electrochemical behavior and the concentration dependency of anodic currents at 0.83 V in the range of concentrations 8.44–32.78×10^{-6} mol dm^{-3}. This linearity is presented in the left corner of Fig. 2.60a. In Fig. 2.60b is shown the voltammetric characterization of the content of oxaprozin tablets (Duraprox®). Cyclic voltammograms of oxaprozin standard and as a content of Duraprox® tablets show an identical electrochemical activity of examined drugs and clearly indicate that the present excipients in tablets have no any influence on oxaprozin activity. Excipients were examined separately and did not exhibit any electrochemical activity under the experimental conditions presented in Fig. 2.2b and in [6, 11]. The concentration dependency of anodic currents of content of oxaprozin tablets (Duraprox®) at 0.85 V in the range of concentrations 8.44–32.78×10^{-6} mol dm^{-3} is linear. This linearity is shown in the left corner of Fig. 2.60b.

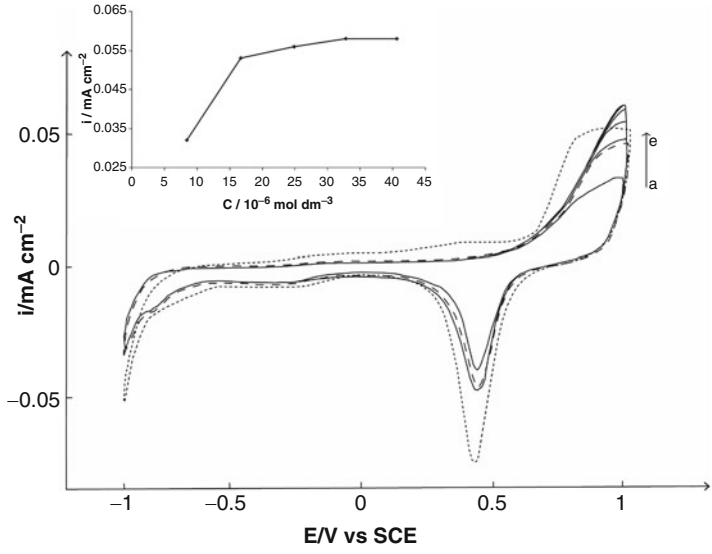

Fig. 2.61 The cyclic voltammogram of bare gold electrode (*d*) (*dotted line*) nd modified with BSA (*dashed line*) as well as in the presence of oxaprozin standard (full lines) in the range of concentrations: $a = 8.44$ mol dm^{-3}; $b = 16.71$ mol dm^{-3}; $c = 24.83$ mol dm^{-3}; $d = 32.78$ mol dm^{-3} in 0.1 mol dm^{-3} phosphate buffer solution (pH 7.4), sweep rate 50 mVs^{-1} (only the first sweep is recorded) (Reproduced with a permission from International Journal of Electrochemical Science) [30]

In Fig. 2.61 is presented the cyclic voltammogram of bare gold electrode (dotted line) and modified with BSA (dashed line) as well as in the presence of different concentrations of oxaprozin standard (full lines) in 0.1 mol dm^{-3} phosphate buffer solution (pH 7.4). It is clear that gold modified by BSA exhibited two times lower currents in the whole region of the applied potential which shows the strong adsorption of BSA on gold. As is shown in Fig. 2.61, the oxidative peak current increased gradually with the concentrations 8.44–24.83 mol dm^{-3} and then reached its saturation value at the concentration of oxaprozin more than 32.78×10^{-6} mol dm^{-3}, which indicated that the binding of oxaprozin with BSA had reached its equilibrium.

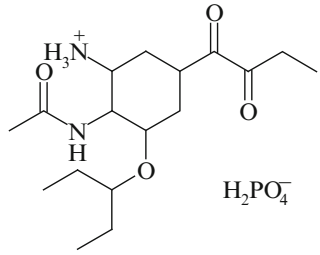

Fig. 2.62 Structural formula of oseltamivir phosphate

A gold electrode was also used in the voltammetric determination of *oseltamivir phosphate* (Fig. 2.62) standard in 0.05 M $NaHCO_3$ [31]. Oseltamivir phosphate as a standard and as a component of Tamiflu® capsule exhibited the identical cyclic voltammogram. The peaks originating from excipients in the capsule did not appear under the applied electrochemical conditions. An electrochemical method for the qualitative determination of oseltamivir phosphate in Tamiflu® capsules by cyclic voltammetry was developed. The presence of oseltamivir phosphate as standard and as a content of Tamiflu® capsule in electrolyte as well as their concentrations was simultaneously checked by HPLC. The lack of the current/concentration dependency was established. The non-pretreated glassy carbon electrode cannot be used for the determination of oseltamivir phosphate under identical experimental conditions presented for the gold electrode.

It is known that antivirals are valuable supplementation to vaccines for the control and prevention of influenza and are likely to be active against a new pandemic variant. Oseltamivir phosphate is the best known orally active neuraminidase inhibitor antiviral drug that slows the spread of influenza virus between cells in the body by stopping the virus from chemically cutting ties with its host cell median time to symptom alleviation is reduced by 0.5–1 days. The neuraminidase inhibitors are effective against both influenza A and B and are considered less toxic and less likely to promote development of drug-resistant influenza than adamantanes.

In our study of electrochemical behavior of oseltamivir phosphate and development of the appropriate method, a solution of oseltamivir phosphate standard was prepared and used in the cyclic voltammetry measurements. In the first part of the work, the gold electrode was used. The cyclic voltammogram of the clean gold electrode of oseltamivir phosphate (0.025 mg cm^{-3}) is presented in Fig. 2.63. Simultaneous HPLC analysis of the bulk of electrolyte confirmed that 0.025 mg cm^{-3} oseltamivir phosphate is presented in the electrolyte. Starting from −1.2 V one can observe an apparent reversible oxidative/reductive reaction between −0.5 and −0.7 V. In the anodic direction, the anodic current increases from 0.4 V and reaches the maximum starting from the area of the oxides formation. In the entire region of oxides formation at the gold electrode, the oxidative activity of oseltamivir phosphate is obvious. The lowering of the oxides reduction currents can also be noticed from the cyclic voltammogram. Starting from −0.8 V the exact same reactions were observed as it was obtained starting from −1.2 V, and as it is presented in Fig. 2.3. The potential was cycled continuously for 2 h and the cyclic voltammogram was quite stable in both cases. Holding the potential for 10 min at the peak potentials and in the area of oxide formation did not affect the voltammogram even in the first sweep. The cyclic voltammogram of oseltamivir phosphate at the gold electrode in 0.05 M $NaHCO_3$ (Figs. 2.63 and 2.64) is quite reproducible. With the addition of the next two aliquots of stock solution of oseltamivir phosphate containing 2.5 mg cm^{-3}, the linearity of the current–concentration dependency was not observed, and even the voltammogram remained the same. With the simultaneous HPLC analysis of the bulk of electrolyte, the presence of the added concentrations was confirmed.

The simple and fast voltammetric method for the qualitative determination of oseltamivir phosphate was developed and applied for the qualitative determination of oseltamivir phosphate in Tamiflu® capsules. Starting from −1.2 V as well as from −0.8 V, an apparent reversible oxidative/reductive reaction between −0.5 and −0.7 V occurs. In the anodic direction, the anodic current increases from 0.4 V and reaches a maximum starting from the area of the oxides formation. In the entire region of the oxides

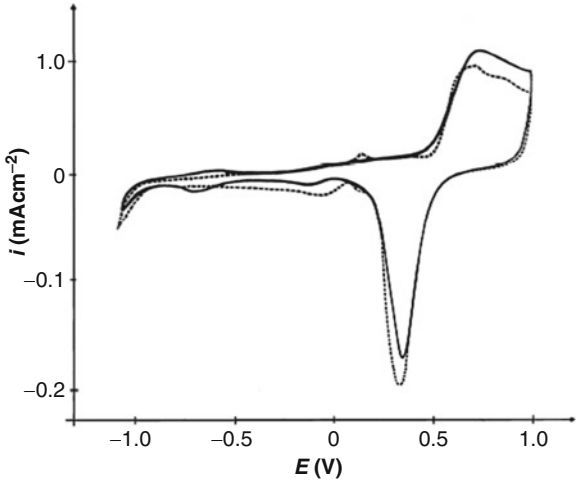

Fig. 2.63 Cyclic voltammogram of the clean gold electrode in 0.05 M $NaHCO_3$ (*dashed line*) and in the presence of 0.025 mg cm^{-3} oseltamivir phosphate (*full line*) in the area of the potential from −1.2 to 1.0 V, sweep rate 50 mVs^{-1} (Reproduced with a permission from Association of Chemical Engineers of Serbia) [31]

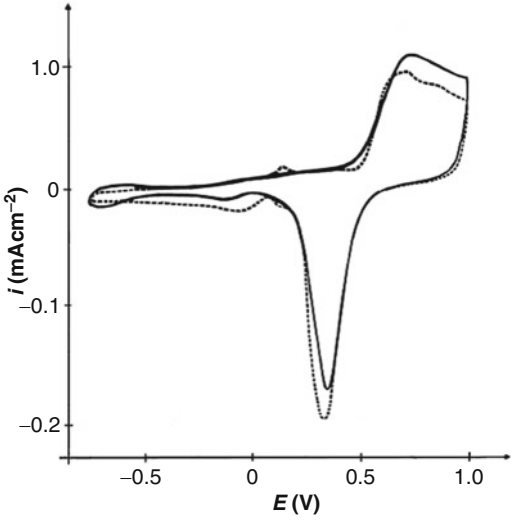

Fig. 2.64 Cyclic voltammogram of the clean gold electrode in 0.05 M $NaHCO_3$ (*dashed line*) and in a presence of 0.025 mg cm^{-3} oseltamivir phosphate (*full line*) in the area of the potential from –0.8 to 1.0 V, sweep rate 50 mVs^{-1} (Reproduced with a permission from Association of Chemical Engineers of Serbia) [31]

formation at the gold electrode, this maximum oxidative current of oseltamivir phosphate remains unchanged. The lowering of the oxides reduction currents is also noticed. The identical cyclic voltammograms of oseltamivir phosphate standard and of Tamiflu® capsule content showed that oseltamivir phosphate is qualitatively determined in Tamiflu® capsule content at the gold electrode in 0.05 M $NaHCO_3$. The glassy carbon electrode cannot be used as working electrode and did not exhibit any affinity to the oxidative/reductive reactions of oseltamivir phosphate starting from −1.2 V as well as from −0.8 V.

2.2.6 Miscellaneous Drugs

In this part, selected miscellaneous drugs with different pharmacological action are presented.

Clopidogrel methyl (+)-(*S*)-*α*-(*o*-chlorophenyl)-6,7-dihydrothieno-[3,2-*c*]pyridine-5(4*H*)-acetate (Fig. 2.65), is an antiplatelet agent widely used in the prevention of ischemic stroke, myocardial infarction, and stroke. It inhibits platelet aggregation by selectively preventing the binding of adenosine diphosphate (ADP) to its platelet receptor. This drug reduces thrombotic events in a wide range of patients (e.g., recent myocardial infarction, established peripheral arterial disease, and acute coronary syndrome). Clopidogrel is an inactive prodrug, and a biotransformation by the liver is necessary to induce expression of its antiaggregating activity. It is rapidly absorbed and undergoes extensive metabolism after oral administration and its plasma concentration goes down considerably rapidly.

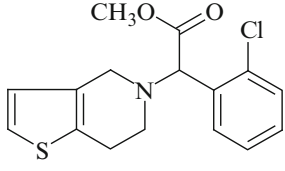

Fig. 2.65 Structure of clopidogrel

The determination of clopidogrel, an antiplatelet agent, was performed at a gold electrode in pH 3.7 acetate buffer using cyclic voltammetry and square wave voltammetry [32]. Each voltammogram was characterized by the well-defined peak at approximately 1.0 V. The current of anodic stripping peak exhibited a linear dependence on the clopidogrel concentration in the range from 317.89 to 935.16 μg cm^{-3}. The obtained linearity was applied to determine clopidogrel in the tablet form of the pharmaceutical preparation (Plavix®). The results were compared to the UV spectrophotometric and HPLC methods.

The electrochemical behavior of the pure standard of clopidogrel on gold electrode was first studied by cyclic voltammetry in pH 3.7 acetate buffer. As is presented in Fig. 2.66, clopidogrel exhibited an apparent oxidative ability in this electrolyte on a gold electrode. The cyclic voltammogram shows the beginning of anodic activity of clopidogrel in double layer region from 0.2 to 0.6 V. An apparent anodic current maximum appears at 1.0 V before oxide formation on the gold electrode and second one at 1.17 V in the area of oxide formation. The rapid increase of anodic current on gold oxide at 1.30 V in the presence of clopidogrel was observed as well as its shift by 0.1 V to a more negative potential, compared to a clean gold electrode (dashed line in Fig. 2.66).

The application of square wave voltammetry for the quantitative determination of clopidogrel on the gold electrode is presented in Fig. 2.67. The SW voltammograms for different concentrations of clopidogrel were recorded in pH 3.7 acetate buffer in the potential range from 0 to 1.5 V at a scan rate of 15 mVs^{-1}. Before each scan, the compound was accumulated at the electrode surface at 0 V for 180 s. Under these conditions, the oxidation of clopidogrel proceeded before oxide formation on Au and reached maximum currents at the onset potential of Au oxide formation. Each voltammogram was characterized by a well-defined peak at approximately 1.0 V. The currents of anodic stripping peak exhibited a linear dependence on the clopidogrel concentration, as shown in the inset of Fig. 2.67.

The voltammetric behavior of clopidogrel as the content of commercial tablets Plavix® was also in a first stage investigated by cyclic voltammetry. Its voltammetric behavior even in the pres-

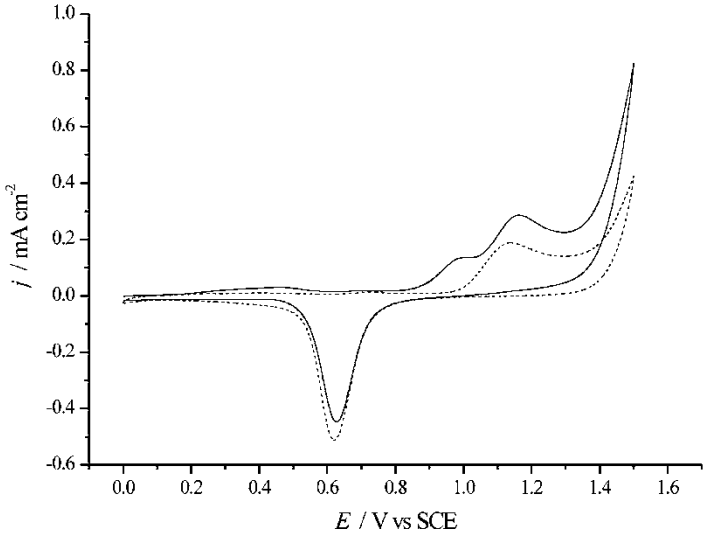

Fig. 2.66 Cyclic voltammogram of an Au electrode in pH 3.7 acetate buffer, *dashed line*, and after the addition of clopidogrel (concentration 32.0 μg cm^{-3}), *full line*; sweep rate: 50 mVs^{-1}. Only the first sweep is presented (Reproduced with a permission from Serbian Chemical Society) [32]

ence of the excipients present in Plavix® showed the same anodic activity as the standard substance, presented in Fig. 2.66, with a negligible reduction in the values of the current maximums.

Similarly as for clopidogrel, the oxidation of Plavix® at a gold electrode using square wave voltammetry proceeded at potentials before the formation of oxide on the Au. The square wave voltammogram was characterized by a well-defined peak at approximately 1.0 V.

The obtained linear relationship between current and concentration of clopidogrel in acetate buffer (pH 3.7) by SW voltammetry within the concentration range 0.317–0.935 mg cm^{-3} (Table 2.4) was used for the determination of clopidogrel in tablet form (Plavix®) and the results were compared with those obtained by the UV and HPLC methods. The validation of the SW procedure was carried out by evaluation of the limit of detection (*LOD*), limit

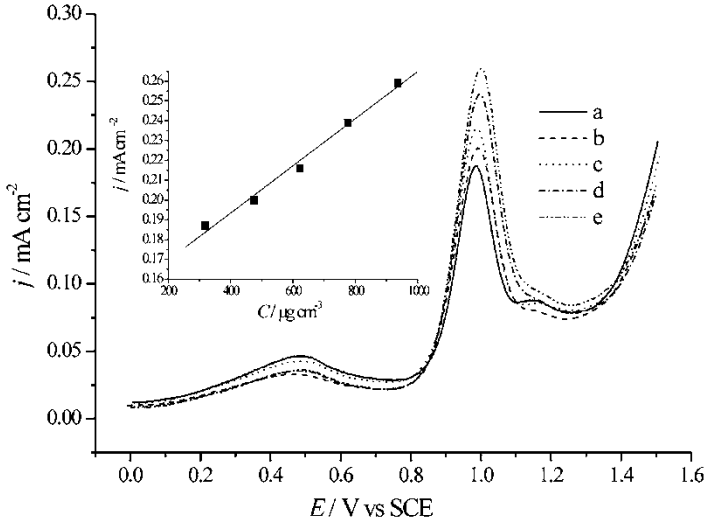

Fig. 2.67 Square wave anodic stripping voltammograms of clopidogrel at a gold electrode in acetate buffer (pH 3.7). Clopidogrel concentration: (*a*) 317.89, (*b*) 474.49, (*c*) 622.03, (*d*) 775.63, and (*e*) 935.16 μg cm^{-3}. Accumulation time: 180 s at $E = 0.0$ V; step size 2 mV, pulse size 20 mV, frequency 8 Hz, scan rate 15 mVs^{-1}. *Inset*: The linear dependency of the anodic peak current vs. concentration of clopidogrel (Reproduced with a permission from Serbian Chemical Society) [32]

of quantification (*LOQ*), and recovery. The *LOD* and *LOQ* were calculated from the calibration curves as kSD/b where $k = 3$ for *LOD* and 10 for *LOQ*, *SD* is the standard deviation of the intercept and b is the slope of the calibration curve. The *LOD* and *LOQ* values for the SW voltammetry method were 117.50 and 391.66 μg cm^{-3}, respectively.

Recovery studies were also performed to judge the accuracy of the SW voltammetry method by performing six measurements at low, intermediate, and high CLP concentrations (317.89, 622.03 and 935.16 μg cm^{-3}). Mean percentage recoveries of 99.6 % with relative standard deviation of 1.11 % were found and are presented in Table 2.4.

Table 2.4 Determination of clopidogrel by SWV, UV-spectrophotometry, and HPLC

Parameter	SWV	UV	HPLC
Range (mg cm^{-3})	0.317–0.935	0.030–0.747	0.032–0.962
Regression equation[a]			
Slope	0.00012	1.8104	233358783.00
S.D. of slope	7.09×10^{-6}	0.0003	0.0026
Intercept	0.1457	0.0076	36117.71
S.D. of intercept	0.0047	0.0001	0.0030
Regression coefficient	0.9947	0.9999	0.9999
Recovery (%)	99.6	99.94	99.57
S.D. (%)	1.11	1.65	1.38
LOD (μg cm^{-3})	117.50	8.56	8.24
LOQ (μg cm^{-3})	391.66	30.46	29.28

Reproduced with a permission from Serbian Chemical Society [32]

[a] $Y = a + bC$ where C is concentration of clopidogrel in mg cm^{-3}; Y is current per area unit (mA cm^{-2}), absorbance (A) and peak area unit (mAu), for SWV, UV, and HPLC methods, respectively. S.D.: standard deviation

Some selected examples of various applications of electrochemical methods in pharmaceutical analysis are given in following Table 2.5.

2.3 Conclusion

Recent trends in development of electrochemical methods for analysis of pharmaceuticals are listed with the highlights of electrochemical methods of analysis of antibiotics, cardiovascular drugs, central nervous system drugs, anticancer drugs, anti-inflammatory drugs, and miscellaneous drugs on gold electrode in neutral electrolytes. A polycrystalline gold electrode was selected as the optimal working electrode for the examination of the pharmaceutical compounds because it is defined with a completely reproducible cyclic voltammograms and, consequently, all the electrochemical reactions at this electrode can be attributed only to

Table 2.5 Selected papers of electrochemical methods for analysis of pharmaceuticals (2006–2015)

No	Analytes/drugs	Electrochemical methods	Electrode type	Medium	application	Reference
2.1. Antibiotics						
1	Ciprofloxacin (norfloxacin)	CV	GC	Aqueous solution 0.14 Phosphate buffer (pH 7.0)	Biological fluids	[33]
2	Netilmicin	LSASV	HMDE	BR buffer (pH=8.7)	Spiked humane urine, serum injectable formulations	[34]
3	Azithromycin	CV	Au	0.05 $NaHCO_3$ 0.05 $NaHCO_3$/CH_3OH 50/50	Standard capsules	[6]
4	Cephalosporins (cephalexin, cephalothin)	CV, DPV	CPE CPE/CoSal	Buffered solution (pH 3.0)	Human serum	[35]
5	Tetracyclines	CV	MWCNT-GCE	Phosphate buffer (pH 2.5)	Standards Water samples	[36]
6	Tetracyclines	CV	Au modified	Strong acidic electrolyte	Wastewater residues	[37]
7	Clarithromycin	CV	Au	0.05 M $NaHCO_3$	Standard tablets	[9]
8	Perfloxacin	CV, DPV, SWV	GC, BDDE	0.05 M $H2SO_4$ Acetate buffer pH 4 Acetate buffer pH 6	Tablet, ampule human serum	[38]

(continued)

Table 2.5 (continued)

No	Analytes/drugs	Electrochemical methods	Electrode type	Medium	application	Reference
9	Erythromycin A	CV	Au	0,05 $NaHCO_3$	Tablets	[10]
10	Ciprofloxacin	CV	MWCNT/GCE	Phosphate buffer (pH 7.0)	Urine/serum	[39]
11	Roxythromycin	CV, DPV	Au	0.05 M NaHCO3	Solid dosage form	[11]
12	Macrolide antibiotics	CV	Au	0.05 M $NaHCO_3$	Capsule, tablet	[40]
13	Macrolide antibiotics	CV	Au	0.05 M $NaHCO_3$	Solid dosage forms	[41]
14	Midecamycin	CV	Au	0.05 M $NaHCO_3$	Standard solid dosage forms	[42]
15	Rifampicin	Ads SV, SWV	GC, Pb-film electrode	Acetate buffer (pH 5.0)	Pharmaceutical formulations	[43]
16	Cefdinir	CV, SW adsv	HMDE	Phosphate buffer	Urine	[44]
17	Doxycycline	DPV, CV	MIP, NIP	BR buffer (pH 2.0–4.0)	Pharmaceutical samples	[45]
18	Cefixime	DPV, SWV, CV	GC	Acetate buffer (pH 3.5–5.5)	Serum, urine, breast milk	[46]
				BR buffer (pH 2.32–8.0)		
2.2. Cardiovascular drugs						
19	Atenolol	DPV	Graphite-polyurethane (60 %, w/w) composite	Universal buffer pH 10.0 phosphate buffer pH 7.4	Pharmaceutical formulations (tablets)	[47]

20	Antihypertensive drugs	CV	GC	BR buffer pH 2–11	Effect of surfactant Urine, tablets	[48]
21	Verapamil	DPV, OSWV	GC	Sulfuric acid (0.1, 0.5 M) acetate buffer (0.2 M, pH 3.51–5.71), phosphate buffer (0.2 M pH 2.5–12.01)	Ampule, tablets	[49]
22	Bisoprolol	DPV	GC, SWNT	BR buffer (0.04 M, pH 2.20–11.04), phosphate buffer pH 3.4–10	Urine	[50]
23	Cinnarizine	CV, ADSV	GC	BR buffer (pH 2.5–11.5)	Commercial formulations Spiked serum	[51]
24	Cinnarazine	CV, DPV	MWCNT	BR buffer pH 2.5	Pharmaceutical formulations, urine	[52]
25	Amlodipine	CV, SWV	MWCNT-modified	pH 7.2	Tablets, urine	[53]
26	Atorvastatin	CV, Ads DPV Ads SWV	GC	BR buffer pH 2.5	Dosage forms urine, serum	[54]

(continued)

Table 2.5 (continued)

No	Analytes/drugs	Electrochemical methods	Electrode type	Medium	application	Reference
27	Amlodipine	SWV, CV	Au	Phosphate buffer (pH 11)	Tablet	[14]
			Au-/o-MWCNT	0.05 M $NaHCO_3$	Standards	
28	Metoprolol	CV, SWV, DDP	HMDE, GCE	BR buffer pH 10.5, 3.0	Tablets, human serum	[55]
29	Amlodipin, Nifedipin	CV, SWV	Au	Phosphate buffer (pH 11)	Cyclodextrin, inclusion complexes	[16]
				0.05 M $NaHCO_3$		
30	Atorvastatin	CV, DPAdsv	VACNT-GO	Phosphate buffer (pH 2.0)	Tablet	[56]
31	Atorvastatin Amlodipine	DPV, SWV	GC	0.5 M H_2SO_4 pH 5.0	Binary mixtures	[57]
				BR buffer 3.0–9.0		
32	Verapamil	SWAdasv	MWCNT-PAH	0.25 M H_2SO_4	Tablets	[58]
	Propranolol	DPAdasv	GCE			
33	Valsartan	CV, DPP	HMDE	BR buffer (pH 6.0)	Tablets	[59]
34	Carvedilol	CV, LSW	Pt-electrode	Acetonitrile/0.1 M	Pharmaceutical preparations	[60]
				Tetrabutylammonium perchlorate		
2.3. Central nervous system drugs						
35	Carbidopa, Levodopa	DPV, CV	GC	0.1 M $HClO_4$	Pharmaceutical products	[61]

36	Lorazepam	DPV	HMDE	BR buffer (pH = 2.0)	Pharmaceutical preparations, tablets, urine, plasma	[62]
37	Paroxetine	SWAdsv, FIA-SWAdsv	HMDE	pH 8.8/borate buffer, 0.2 mol/L	Pharmaceutical products	[63]
38	Flavoxate	DPV, CV	HMDE	pH 4 acetate buffer	Tablets	[64]
39	Promethazine	CV, DPV	DNA/GCE (ox)	0,1 M acetate buffer pH = 5.0	Human blood samples	[65]
40	1,4-Benzodiazepines	CV	CPE-modified	Br buffer (pH 2.5/10.0)	Plasma, urine, standards	[62]
41	Fluoxetine	SWAdsSV	HMDE	phosphate buffer (pH 12.0)	Standards, human plasma	[66]
42	Clozapine	CV, DPV	Au-modified	0.05 M tris–HCl (pH 8.1)	Tablets	[67]
43	Domperidone	DPV, CV	GC	BR buffer (pH 2.6–10.3)	Tablets/waste water	[68]
44	Tetrazepam	DPP, ADSCV, DPV, SWV	HMDE	pH 11, pH 7	Tablet, bulk form, human serum	[69]
45	Trazodone	CV, DPV	MWCNT-modified GCE	Phosphate buffer 0.2 M, pH 7.0	Tablets, urine	[70]
46	Gabapentin	CV, DPV	Au	pH 12.0, 0.2 M buffer	Standards, urine	[71]

(continued)

Table 2.5 (continued)

No	Analytes/drugs	Electrochemical methods	Electrode type	Medium	application	Reference
47	Sertindole	CV	GC, BDDE	0.1 M H_2SO_4	Tablets	[72]
				BR buffer (pH = 3; 5), phosphate buffer		
48	Amphetamine drugs	DPV	GC	phosphate buffer pH 7.3	Tablets, standards, human serum	[73]
49	Pyridostigmine-bromide	SWCADSV DPCADSV, ADSV	Hg	BR buffer (pH 3.8)	Pharmaceutical dosage forms	[74]
50	Naratriptan	DPV	GC	BR buffer 0.1 M	Tablets	[75]
51	Ziprasidone	CV, DPV, SWV	BDDE, GCE	0.1 M H_2SO_4	Capsule, spiked serum	[76]
				Acetone buffer pH 4.75		
52	1,4-benzodiazepine	SWV	GCE-modified	0.15 M acetate buffer, pH 4.75	Pharmaceutical formulations	[77]
53	Methyldopa	SWV	MWCNT modified	0.1 M phosphate buffer	Tablets, urine	[78]
54	Carbamazepine	CV	Au	phosphate buffer (pH 7.0)	Tablets	[17]
55	Amphetamine	CV, SWV	Au	0.5 M $NaHCO_3$	Tablets, spiked urine	[18]

56	Donepezil	CV, SWV	Au	pH 3 phosphate buffer	Tablets	[19]
57	Levodopa, Cabergoline	CV, SWV	CPE-modified graphene nanosheets	pH 7.0	Human serum, urine, pharmaceutical formulations	[79]
58	Haloperidol	DPV, SWV	CPE-modified, MWCNT	BR buffer (pH 4.5–8.5)	Pharmaceutical samples, biological fluids	[80]
59	Amphetamine/ecstasy	SWV	GC	BR buffer (pH 1.2–12.2)	Spiked human serum	[16]
2.4. Anticancer drugs						
60	Rutin	CV, CASV	HMDE	BR buffer (pH 2–12), phosphate buffer (pH acetate buffer 2–8)	Tablets, human urine, blood serum	[81]
61	Acetylspiramycin	CV, DPV	GCE/MWNT/DHP	pH 4.0–8.0 phosphate buffer	Tablets	[82]
62	Gemcitabine	CV, DPV	GCE	Phosphate buffer (pH 7.4), BR buffer (pH 2–11)	Bulk/pharmaceutical formulations, injections	[83]
63	Gemcitabine	CV, DPV	Au	Phosphate buffer (pH 3.0–12.0)	Pharmaceutical formulations	[84]
64	Danusertib	CV, DPV, SWV	Au	0.1 M phosphate buffer (pH 7.0)	Pharmaceutical formulation	[85]
65	Picoplatin	CV, DPV	MWNT/GCE	0.05 mol/L KCl (pH 7.4)	Injection	[86]

(continued)

Table 2.5 (continued)

No	Analytes/drugs	Electrochemical methods	Electrode type	Medium	application	Reference
66	Idarubicin	CV, DPV, Ads DPV	GCE, MWCNT/GC	Phosphate buffer (pH 3.0)	Injection	[28]
67	Zanosar	DPP, CV	HMDE	pH 4.0	Urine samples, pharmaceutical preparations	[87]
68	Tamoxifen	DPADASV SWADASV, CV	GCE	BR buffer (pH 2–10)	Tablets, human blood	[29]
69	Temozolomide	DPV	GC	0.1 M phosphate buffer pH 7.0	Biosensor	[88]
2.5. Anti-inflammatory drugs						
70	Nimesulide	CV, DPV	GCE, CNT/GCE	0,05 M H_2SO_4	Human serum, tablets	[89]
71	Lidocaine	SWV, CV	BDDE	BR buffer (0.1 M) + 2 M NaOH	Pharmaceutical preparation	[90]
72	Meloxicam	CV, ASV	GC	Phosphate buffer (pH 6.0), BR buffer (pH 2–8)	Tablets, urine, plasma	[91]
73	Meloxicam	CV	GCE	Phosphate buffer	Standard	[92]
74	Sumatriptan	CV	PGE/MWCNT	BR buffer (pH 7,4)	Tablets	[93]

75	Ketoprofen	CV	DDDE, Pt	pH 6.0	Standard	[94]
76	Mefenamic acid, indomethacin, diclofenac	CV, DPV	GC	Phosphate buffer	Standards	[95]
77	NSAID-s	CV	ANMGC, Pt	0.1 M $LiClO_4$	Standards	[94]
				MeOH, EtOH, CH_3CN, mixture/H_2O		
78	Ibuprofen	CV, DPV	BDDE	BR buffer (pH 2–10)	Standards	[96]
79	Oxaprozin	CV	Pt, BSA-modified	0.05 M $NaHCO_3$	Standards	[30]
80	Paracetamol	DPV, CV	CILE, TCPE	pH = 4.6	Tablets, urine samples	[97]
2.6. Miscellaneous drugs						
81	Abacavir	DPAdsV, CV	MWCNT/EPPGE	BR buffer (pH 2.5), (0.04 M, pH 2–9), 0.1 M H_2SO_4	Tablets, human serum	[98]
82	Spironolactone drugs (aldactone)	CV, DPPAdsV	HMDE	BR buffer (pH 2.5)	Tablets, spiked urine, serum	[99]
83	Chloroquine	CV, DPV	DNA-modified CP	0.1 M phosphate buffer (pH 5.5)	Tablets	[100]
	Primaquine		CPE-modified (Cu-Nw-CPE)			

(continued)

Table 2.5 (continued)

No	Analytes/drugs	Electrochemical methods	Electrode type	Medium	application	Reference
84	Fosamprenavir	CV	GC, BDDE	0.1 M H_2SO_4	Tablets, urine samples	[101]
				Phosphate buffer pH 2.0		
85	Metformin	SWV, LSP, DPV	Pt	Acetate buffer pH 4.7	Urine, tablets	[102]
				MOPS buffer (pH 3.8–8.0)		
86	Nandrolone	SWV, CV, DPV	Fullerene-C60 modified electrode	0.1 M phosphate buffer (pH 2.0–10.0)	Blood and urine samples injection	[103]
87	Fluvastatin	CV, DPV, SWV	BDDE	BR buffer (pH 10.0)	Tablets, human serum	[104]
88	Valacyclovir	CV, DPV, SWV	GC	0.2 M Na_2SO_4	Tablets, gastric fluid, serum	[105]
				BR buffer pH 10.0		
				Phosphate buffer, pH 4.2		
89	Epinephrone/ascorbic acid	CV, SWASV, SLSV	SAM/Au	Sodium borate buffer (pH 4.4)	Simultaneous determination	[106]
					Standards/mixture	
90	Simvastatin	CV, SWV	Graphite electrode Hg	0.1 M $Na_2B_4O_7$-KH_2PO_4, pH 7.0, (buffer)	Pharmaceutical dosage formulations	[107]

91	Lamivudine	CV	HMDE	pH 3.4 (phosphate buffer)	Pharmaceutical formulations	[108]
92	Abacivir	LSV	HMDE	0.1 M sulfuric acid, acetate buffer, phosphate buffer, borate buffer	Tablets	[98]
93	Glipizide	CV, SWV-AdSV	HMDE	BR buffer (pH 6.0)	Tablets	[109]
94	Prednisolone	CV, OSWV	GC	0.4 M H_2SO_4 (pH 0,56)	Tablets, human serum	[110]
95	Danazol	SWV, CV, Sw-AdSv	HMDE	BR buffer (pH 2)	Capsules	[111]
96	Tinidazole	CV	poly (carmine) film modified GCE	Phosphate buffer (pH 5.7)	Tablets, ampule	[112]
97	Acyclovir	CV, LSV	MWNT-DHP film, GCE	Citrate–sodium hydrogen phosphate buffer (pH 7.36)	Tablets	[113]
98	Estrogens	CV, LSV, SWV	MWNT/GCE Pt/ MWNT/GCE	Phosphate buffer solution (pH 7.0)	Sensor	[114]
99	Oseltamivir	CV	Au	0.05 M $NaHCO_3$	Capsule	[31]
100	Omeprazol	DPP, CV	SMDE	Buffered solution 0,05 M pH 8	Standard acid decomposition	[115]

(continued)

Table 2.5 (continued)

No	Analytes/drugs	Electrochemical methods	Electrode type	Medium	application	Reference
101	Omeprazol	DPP, CV	GC	Acetic acid/sodium acetate buffer pH 5.10	Enteric-coated tablets	[116]
102	Prednisone/Prenisolone	OSWV	GC	Phosphate buffer (pH 7.2)	Pharmaceutical formulations, serum	[117]
103	Clopidogrel	CV, SWASV	Au	Acetate buffer (pH 3.7)	Solid dosage forms	[32]

BR buffer-Britton Robinson buffer, *CV* cyclic voltammetry, *GC* glassy carbon, *Au* gold, *LSASV* linear sweep adsorptive stripping voltammetry, *CPE/Cosal* carbon paste electrode modified with Co salophen, *HMDE* hanging mercury drop electrode, *MWCNT-GCE* multiwalled carbon nanotube modified electrode, *Ni-DIA* diamond thin film electrode modified with nickel, *BDDE* boron doped diamond electrode, *UME* ultramicroelectrode, *SMDE* static mercury drop electrode, *DPP* differential pulse polarography, *DPV* differential pulse voltammetry, *GC* glassy carbon, *OSW* osteryoung square wave voltammetry, *ADSSWV* adsorptive square wave voltammetry, *VACNT-GO* vertically aligned carbon nanotube/graphene oxide, *DPADSV* differential pulse adsorptive stripping voltammetry, *MWCNT-PAH/GCE* glassy carbon electrode modified with functionalized multiwalled, *SWADSV* square wave adsorptive stripping voltammetry, *FIA* flow injection analysis, *DPP* differential pulse polarography, *DNA/GCE(ox)-ds* DNA-modified electrode/pretreated glassy carbon, *Si-TipH* silica gel modified with titanium phosphate, *ADSCV* adsorptive cathodic stripping electrode, *CASV* cathodic stripping voltammetry, *SWNT* single wall carbon nanotubes, *DHP* dihexadecyl hydrogen phosphate, *DPAdSV* differential pulse adsorptive anodic stripping voltammetry, *CNT/GCE* carbon nanotubes modified GCE, *CILE* carbon ionic liquid electrode, *ANMGC* alumina nanoparticle modified glassy carbon, *EPPGE* edge plane pyrolitic graphite electrode, DNA-modified CP, *Cu-Nw-CPE* CPE modified by $Cu(OH)_2$ nanowire, *LSV* linear sweep voltammetry, *SAM/Au* self-assembled monolayer, *OSWV* osteryoung square wave voltammetry modified, *MWNT/GCE* multiwalled carbon nanotubes modified glassy carbon electrode

the studied molecule in the analysis of these drugs. CV, SWV, and DPV were used in combination with HPLC, AFM, FTIR, and MS–MS in the investigations of aforementioned drugs. The presented data show that different electrochemical methods with the use of gold as working electrode combined with spectroscopic, spectrometric, and chromatographic techniques gave a fast quantitative and qualitative response of the investigated standards as well as of the commercial drugs. With the drugs analysis in biological samples the very important data were collected for the further clinical investigations.

Acknowledgments The work was supported by the Ministry of Education, Science and Technological Development of the Republic of Serbia (Grant No. ON172013).

References

1. Ozkan SA (2012) Electroanalytical methods in pharmaceutical analysis and their validation. HNB, New York
2. Gupta V, Jain R, Radhapyari K, Jadon N, Agarwal S (2011) Voltammetric techniques for the assay of pharmaceuticals—a review. Anal Biochem 408:179–196
3. Barek J, Fischer J, Navratil T, Peckova K, Yosypchuk B, Zima J (2007) Nontraditional electrode materials in environmental analysis of biologically active organic compounds. Electroanalysis 19:2003–2014
4. Gupta AK, Dubey RS, Malik JK (2013) Application of modern electroanalytical techniques: recent trend in pharmaceutical and drug analysis. Int J Pharm Sci Res 4:2450–2458
5. Avramov-Ivić M, Jovanović V, Vlajnić G, Popić J (1997) The electrocatalytic properties of the oxides on noble metals in electrooxidation of some organic molecules. J Electroanal Chem 423:119–124
6. Avramov Ivic ML, Petrovic SD, Mijin DZ, Zivkovic PM, Kosovic IM, Drljevic KM, Jovanovic MB (2006) Studies on electrochemical oxidation of azithromycin and Hemomycin® at gold electrode in neutral electrolyte. Electrochim Acta 51:2407–2416
7. Antonio A, Mazzone MG, Moschetti V, Blanco AR (2001) Process for the preparation of aqueous formulations for ophthalmic use. US patent 6,277,829
8. Dawson CR, Bowman LM (2003) Topical treatment or prevention of ocular infections. US patent 6,569,443

9. Avramov Ivic ML, Petrovic SD, Vonmoos F, Mijin DZ, Zivkovic PM, Drljevic KM (2007) The qualitative electrochemical determination of clarithromycin and spectroscopic detection of its structural changes at gold electrode. Electrochem Commun 9:1643–1647
10. Avramov Ivic ML, Petrovic SD, Mijin DZ, Vanmoos F, Orlovic DZ, Marjanovic DZ, Radovic VV (2008) The electrochemical behavior of erythromycin A on a gold electrode. Electrochim Acta 54:649–654
11. Drljevic-Djuric KM, Jovic VD, Lacnjevac UC, Avramov Ivic ML, Petrovic SD, Mijin DZ, Djordjevic SB (2010) Voltammetric and differential pulse determination of roxithromycin. Electrochim Acta 56:47–52
12. Tolić LJ, Lović J, Petrović S, Mijin D, Grujić S, Laušević M, Avramov Ivić M (2015) Investigation of electrochemical behavior of anisomycin on gold electrode followed by HPLC–MS/MS analysis. Electrochem Commun 58:20–24
13. Laviron E (1979) The use of linear potential sweep voltammetry and of a.c. voltammetry for the study of the surface electrochemical reaction of strongly adsorbed systems and of redox modified electrodes. J Electroanal Chem 100:263–270
14. Stoiljković ZŽ, Avramov Ivić ML, Petrović SD, Mijin DŽ, Stevanović SI, Lačnjevac UČ, Marinković AD (2012) Voltammetric and square-wave anodic stripping determination of amlodipine besylate on gold electrode. Int J Electrochem Sci 7:2288–2303
15. Goyal RN, Bishnoi S (2010) A novel multi-walled carbon nanotube modified sensor for the selective determination of epinephrine in smokers. Bioelectrochemistry 79:234–240
16. Stoiljković ZZ, Jovanović VM, Mijin DŽ, Nikolić V, Nikolić LJ, Petrović SD, Avramov Ivić ML (2013) The electrochemical investigation of inclusion complexes of nifedipine and amlodipine with β-cyclodextrin and (2-hydroxypropyl)-β-cyclodextrin. Int J Electrochem Sci 8:9543–9557
17. Trišović NP, Božić BĐ, Petrović SD, Tadić SJ, Avramov Ivić ML (2014) Electrochemical characterization and determination of carbamazepine as pharmaceutical standard and tablet content on gold electrode. Hem Ind 68:207–212
18. Nevešćanin MM, Avramov Ivić ML, Petrović SD, Mijin DŽ, Banović Stević SN, Jovanović VM (2013) The use of a gold electrode for the determination of amphetamine derivatives and application to their analysis in human urine. J Serb Chem Soc 78:1373–1385
19. Mladenovic AR, Mijin DZ, Drmanic SZ, Vajs VE, Jovanovic VM, Petrovic SD, Avramov Ivic ML (2014) Electrochemical oxidation of donepezil and its voltammetric determination at gold electrode. Electroanalysis 26:893–897
20. Iimura Y, Naito T, Senaga M, Yamanishi Y (1997) Aralkylpiperidine derivative. JP Patent 09268176, CAN127:293137
21. Golcu A, Ozkan SA (2008) Electroanalytical determination of donepezil HCl in tablets and human serum by differential pulse and osteryoung square wave voltammetry at a glassy carbon electrode. Pharmazie 61:760–765

22. Grimshaw J (2000) Electrochemical reactions and mechanisms in organic chemistry. Elsevier, Amsterdam
23. Trišović NP, Božić BDJ, Lović JD, Vitnik VD, Vitnik ŽJ, Petrović SD, Avramov Ivić ML (2015) Electrochemical characterization of phenytoin and its derivatives on bare gold electrode. Electrochim Acta 161:378–387
24. Zhang J, Heineman WR, Halsall HB (1999) Capillary electrochemical enzyme immunoassay (CEEI) for phenobarbital in serum. J Pharm Biomed Anal 19:145–152
25. Clinical Practice Guidelines (2008) Febrile seizures: clinical practice guideline for the long-term management of the child with simple febrile seizures. Pediatrics 121:1281–1286
26. Ni Y, Wang Y, Kokot S (2004) Differential pulse stripping voltammetric determination of paracetamol and phenobarbital in pharmaceuticals assisted by chemometrics. Anal Lett 37:3219–3235
27. Raoof JB, Baghayeri M, Ojani R (2012) A high sensitive voltammetric sensor for qualitative and quantitative determination of phenobarbital as an antiepileptic drug in presence of acetaminophen. Colloids Surf B Biointerfaces 95:121–128
28. Kurbanoglu S, Dogan-Topal B, Uslu B, Can A, Ozkan SA (2013) Electrochemical investigations of the anticancer drug idarubicinusing multiwalled carbon nanotubes modified glassy carbonand pyrolytic graphite electrodes. Electroanalysis 25:1473–1482
29. Sharma DK, Mourya GL, Jhankal KK, Jones LA, Bhargava SK (2012) Electrochemical behaviour and validated determination of the anticancer drug tamoxifen. Der Pharm Lett 4:1599–1606
30. Bozic BDJ, Avramov Ivic ML, Trisovic NP, Petrovic SD, Uscumlic GS (2012) Electrochemical characterization of oxaprozin on bare gold electrode and electrode modified with bovine serum albumin. Int J Electrochem Sci 7:11609–11616
31. Avramov Ivić ML, Petrović SD, Mijin DŽ, Drljević-Đurić KM (2011) The qualitative determination of oseltamivir phosphate in Tamiflu® capsule by cyclic voltametry. Hem Ind 65:87–91
32. Mladenović AR, Jovanović VM, Petrović SD, Mijin DŽ, Drmanić SŽ, Avramov Ivić ML (2013) Determination of clopidogrel using square wave voltammetry at a gold electrode. J Serb Chem Soc 78:2131–2140
33. Torriero AAJ, Salinas E, Raba J, Silber JJ (2006) Sensitive determination of ciprofloxacin and norfloxacin in biological fluids using an enzymatic rotating biosensor. Biosens Bioelectron 22:109–115
34. Sun N, Mo W, Hu B, Shen Z (2006) Adsorptive stripping voltammetric determination of netilmicin in the presence of formaldehyde. Anal Bioanal Chem 385:161–167
35. Jamasbi ES, Rouhollahi A, Shahrokhian S, Haghgooc S, Aghajani S (2007) The electrocatalytic examination of cephalosporins at carbon paste electrode modified with CoSalophen. Talanta 71:1669–1674
36. Vega D, Agüí L, González-Cortés A, Yáñez-Sedeño P, Pingarrón JM (2007) Voltammetry and amperometric detection of tetracyclines at

multi-wall carbon nanotube modified electrodes. Anal Bioanal Chem 389:951–958
37. Wang H, Zhao H, Quan X (2012) Gold modified microelectrode for direct tetracycline detection. Front Environ Sci Eng 6:313–319
38. Uslu B, Topal BD, Ozkan SA (2008) Electroanalytical investigation and determination of perfloxacin in pharmaceuticals and serum at boron-doped diamond and glassy carbon electrodes. Talanta 74:1191–1200
39. Fotouhi L, Alahyari M (2010) Electrochemical behavior and analytical application of ciprofloxacin using a multi-walled nanotube composite film-glassy carbon electrode. Colloid Surf B 81:110–114
40. Avramov Ivić ML, Petrović SD, Mijin DŽ (2007) A study of the electrochemical activity of some macrolide antibiotics on a gold electrode in a neutral electrolyte. J Serb Chem Soc 72:1427–1436
41. Avramov Ivić ML, Petrović SD, Živković PM, Mijin DŽ, Drljević KM (2010) A study of the catalytic role of a gold electrode in the electrochemical activation of four macrolide antibiotics in sodium bicarbonate solution. Chem Ind Chem Eng Q 16:111–116
42. Drljevic Djuric KM, Avramov Ivic ML, Petrovic SD, Mijin DZ, Jadranin MB (2011) A voltammetric method for the quantitative determination of midecamycin compared to its simultaneous HPLC determination. Russ J Electrochem 47:781–786
43. Tyszczuk K, Korolczuk M (2009) New protocol for determination of rifampicine by adsorptive stripping voltammetry. Electroanalysis 21:101–106
44. Jain R, Radhapyari K, Jadon N (2007) Electrochemical evaluation and determination of cefdinir in dosage form and biological fluid at mercury electrode. J Electrochem Soc 154:F199–F204
45. Gurler B, Ozkorucuklu SP, Kir E (2013) Voltammetric behavior and determination of doxycycline in pharmaceuticals at molecularly imprinted and non-imprinted overoxidized polypyrrole electrodes. J Pharm Biomed Anal 84:263–268
46. Golcu A, Dogan B, Ozkan SA (2005) Anodic voltammetric behavior and determination of cefixime in pharmaceutical dosage forms and biological fluids. Talanta 67:703–712
47. Cervini P, Ramos LA, Cavalheiro ETG (2007) Determination of atenolol at a graphite–polyurethane composite electrode. Talanta 72:206–209
48. Atta NF, Darwish SA, Khalil SE, Galal A (2007) Effect of surfactants on the voltammetric response and determination of an antihypertensive drug. Talanta 72:1438–1445
49. Demircan Ş, Kır S, Ozkan SA (2007) Electroanalytical characterization of verapamil and its voltammetric determination in pharmaceuticals and human serum. Anal Lett 40:1177–1195
50. Goyal RN, Tyagi A, Bachheti N, Bishnoi S (2008) Voltammetric determination of bisoprolol fumarate in pharmaceutical formulations and urine using single-wall carbon nanotubes modified glassy carbon electrode. Electrochim Acta 53:2802–2808

51. Hegde RN, Hosamani RR, Nandibewoor ST (2009) Voltammetric oxidation and determination of cinnarizine at glassy carbon electrode modified with multi-walled carbon nanotubes. Colloid Surf B 72:259–265
52. El-Sayed GO, Yasin SA, El Badawy AA (2008) Voltammetric behavior and determination of cinnarizine in pharmaceutical formulations and serum. Anal Lett 41:3021–3033
53. Goyal RN, Bishnoi S (2010) Voltammetric determination of amlodipine besylate in human urine and pharmaceuticals. Bioelectrochemistry 79:234–240
54. Eskikoy D, Durmus Z, Kilic E (2011) Electrochemical oxidation of atorvastatin and its adsorptive stripping determination in pharmaceutical dosage forms and biological fluids. Collect Czech Chem Commun 76:1633–1649
55. Zorluoglu SL, Tasdemir IH, Ece A, Kiliç E (2013) A cooperative computational and experimental investigation on electrochemical behavior of metoprolol and its voltammetric determination. Can J Chem 91:951–959
56. Silva TA, Zanin H, Vicentini FC, Corat EJ, Fatibello-Filho O (2014) Differential pulse adsorptive stripping voltammetric determination of nanomolar levels of atorvastatin calcium in pharmaceutical and biological samples using a vertically aligned carbon nanotube/graphene oxide electrode. Analyst 139:2832–2841
57. Dogan-Topal B, Bozal B, Demircigil T, Uslu B, Ozkan S (2009) Electroanalytical studies and simultaneous determination of amlodipine besylate and atorvastatine calcium in binary mixtures using derivative of the ratio-voltammetric methods. Electroanalysis 21:2427–2439
58. Oliveira GS, Azzi DC, Vicentini FC, Sartori ER, Fatibello-Filho O (2013) Voltammetric determination of verapamil and propranolol using a glassy carbon electrode modified with functionalized multiwalled carbon nanotubes within a poly (allylamine hydrochloride) film. J Electroanal Chem 708:73–79
59. Habib IHI, Weshay SA, Toubar SS, El-Alamin MM (2008) Stripping voltammetric determination of valstartan in bulk and pharmaceutical products. Pharmazie 63:337–341
60. Yilmaz B, Ekinci D (2010) Voltammetric behavior of carvedilol in nonaqueous media and its analytical determination in pharmaceutical preparations. Rev Anal Chem 30:187–193
61. Socorro M, Quintino M, Yamashita M, Angnes L (2006) Voltammetric studies and determination of levodopa and carbidopa in pharmaceutical products. Electroanalysis 18:655–661
62. Ghasemi J, Niazi A, Ghorbani R (2006) Determination of trace amounts of lorazepam by adsorptive cathodic differential pulse stripping method in pharmaceutical formulations and biological fluids. Anal Lett 39:1159–1169
63. Nouws HPA, Delerue-Matos C, Barros AA, Rodrigues JA (2006) Electroanalytical determination of paroxetine in pharmaceuticals. J Pharm Biomed Anal 42:341–346

64. Ghoneim MM, El-Attar MA, Razeq SA (2006) Voltammetric quantitation at the mercury electrode of the anticholinergic drug flavoxate hydrochloride in bulk and in pharmaceutical formulation. Cent Eur J Chem 5:496–507
65. Yang ZS, Zhao J, Zhang DP, Liu YC (2007) Electrochemical determination of trace promethazine hydrochloride by a pretreated glassy carbon electrode modified with DNA. Anal Sci 23:569–572
66. Nouws HPA, Delerue-Matos C, Barros AA, Rodrigues JA, Santos-Silva A, Borges F (2007) Square-wave adsorptive-stripping voltammetric detection in the quality control of fluoxetine. Anal Lett 40:1131–1146
67. Huang F, Qu S, Zhang S, Liu B, Kong J (2007) Sensitive detection of clozapine using a gold electrode modified with 16-mercaptohexadecanoic acid self-assembled monolayer. Talanta 72:457–462
68. El-Shahawi MS, Bahaffi SO, El-Mogy T (2007) Analysis of domperidone in pharmaceutical formulations and wastewater by differential pulse voltammetry at a glassy-carbon electrode. Anal Bioanal Chem 387:719–725
69. Ghoneim M, El-Desoky HS, El-Ries MA, Abd-Elaziz AM (2008) Electrochemical determination of muscle relaxant drug tetrazepam in bulk form, pharmaceutical formulation, and human serum. Chem Pap 62:127–134
70. Hegde RN, Shetti NP, Nandibewoor ST (2009) Electro-oxidation and determination of trazodone at multi-walled carbon nanotube-modified glassy carbon electrode. Talanta 79:361–368
71. Hegde RN, Kumara Swamy BE, Shetti NP, Nandibewoor ST (2009) Electro-oxidation and determination of gabapentin at gold electrode. J Electroanal Chem 635:51–57
72. Altun Y, Dogan-Topal B, Ozkan SB (2009) Anodic behavior of sertindole and its voltammetric determination in pharmaceuticals and human using glassy carbon and boron-doped diamond electrodes. Electrochim Acta 54:1893–1903
73. Garrido EMPJ, Garrido JMPJ, Milhazes N, Borges F, Oliveira-Brett AM (2010) Electrochemical oxidation of amphetamine-like drugs and application to electroanalysis of ecstasy in human serum. Bioelectrochemistry 79:77–83
74. Jain R, Gupta VK, Jadon N, Radhapyari K (2010) Adsorptive stripping voltammetric determination of pyrodistigmine bromide in bulk, pharmaceutical formulations and biological fluid. J Electroanal Chem 648:20–27
75. Velasco-Aguirre C, Álvarez-Lueje A (2010) Voltammetric behavior of naratriptan and its determination in tablets. Talanta 82:796–802
76. Kul D, Gumustas M, Uslu B, Ozkan SA (2010) Electroanalytical characteristics of antipsychotic drug ziprasidone and its determination in pharmaceuticals and serum samples on solid electrodes. Talanta 82:286–295
77. Lozano-Chaves ME, Palacios-Santander JM, Cubillana-Aguilera LM, Naranjo-Rodrıguez I, Hidalgo-Hidalgo-de-Cisneros JL (2006) Modified carbon-paste electrodes as sensors for the determination of 1,4-benzodi-

azepines: Application to the determination of diazepam and oxazepam in biological fluids. Sens Actuator B Chem 115:575–583
78. Fouladgar M, Karimi-Maleh H (2013) Ionic liquid/multiwall carbon nanotubes paste electrode for square wave voltammetric determination of methyldopa. Ionics 19:1163–1170
79. Tajik S, Taher MA, Beitollahi H (2014) First report for electrochemical determination of levodopa and cabergoline: application for determination of levodopa and cabergoline in human serum, urine and pharmaceutical formulations. Electroanalysis 26:796–806
80. Bagheri H, Afkhami A, Panahi Y, Khoshsafar H, Shirzadmehr A (2014) Facile stripping voltammetric determination of haloperidol using a high performance magnetite/carbon nanotube paste electrode in pharmaceutical and biological samples. Mater Sci Eng C 37:264–270
81. Temerk YM, Ibrahim HSM, Schuhmann W (2006) Cathodic adsorptive stripping voltammetric determination of the antitumor drug rutin in pharmaceuticals, human urine, and blood serum. Microchim Acta 153:7–13
82. Peng Y, Lu C, Hu B, Wang Z, Hu S (2007) Development of an acetylspiramycin sensor based on a single-walled carbon nanotubes film electrode. Microchim Acta 158:79–84
83. Kalanur SS, Katrahalli U, Seetharamappa J (2009) Electrochemical studies and spectroscopic investigations on the interaction of an anticancer drug with DNA and their analytical applications. J Electroanal Chem 636:93–100
84. Naik K, Nandibewoor ST (2013) Electro-oxidation and determination of gemcitabine hydrochloride, and anticancer drug at gold electrode. J Ind Eng Chem 19:1933–1938
85. Popa OM, Diculescu VC (2013) Electrochemical and spectrophotometric characterisation of proteinkinase inhibitor and anticancer drug danusertib. Electrochim Acta 112:486–492
86. Ye L, Xiang M, Zhang Y, Luo L, Gao Y, Yu J, Cha J (2013) A novel electrochemical method for sensitive detection of anticancer drug picoplatin with graphene multi-walled carbon nanotubes modified glassy carbon electrode. Int J Electrochem Sci 8:12726–12734
87. Reddy CN, Prasad PR, Sreedhar NY (2013) Electrochemical analysis of antichemotherapeutic drug zanosar in pharmaceutical and biological samples by differential pulse polarography. J Anal Methods Chem 2013:Article ID 420761
88. Lopes IC, Oliveira SCB, Oliveira-Brett AM (2012) In situ electrochemical evaluation of anticancer drug temozolomid and its metabolits-DNA interaction. Anal Bioanal Chem 405:3783–3790
89. Wang C, Shao X, Liu Q, Qu Q, Yang G, Hu X (2006) Differential pulse voltammetric determination of nimesulide in pharmaceutical formulation and human serum at glassy carbon electrode modified by cysteic acid/CNTs based on electrochemical oxidation of l-cysteine. J Pharm Biomed 42:237–244

90. Oliveira RTS, Salazar-Banda GR, Ferreira VS, Oliveira SC, Avaca LA (2007) Electroanalytical determination of lidocaine in pharmaceutical preparations using boron-doped diamond electrodes. Electroanalysis 19:1189–1194
91. Farhadi K, Karimpour A (2007) Electrochemical determination of meloxicam in pharmaceutical preparation and biological fluids using oxidized glassy carbon electrodes. Chem Pharm Bull 55:638–642
92. Cristian A, Iorgulescu EE, Mihailciuc C (2010) Electrochemical studies using activated glassy carbon I. meloxicam. Rev Roum Chim 55:329–334
93. Ghalkhani M, Shahrokhian S, Ghorbani-Bidkorbeh F (2009) Voltammetric studies of sumatriptan on the surface of pyrolytic graphite electrode modified with multi-walled carbon nanotubes decorated with silver nanoparticles. Talanta 80:31–38
94. Tsopelas F, Ochsenkühn-Petropoulou M, Zikos N, Spyropoulou E, Andreadou I, Tsantili-Kakoulidou A (2011) Electrochemical study of some non-steroidal anti-inflammatory drugs: solvent effect and antioxidant activity. J Solid State Electrochem 15:1099–1108
95. Tabeshnia M, Heli H, Jabbari A, Moosavi-Movahedi AA (2010) Electrooxidation of some non-steroidal anti-inflammatory drugs on an alumina nanoparticle-modified glassy carbon electrode. Turk J Chem 34:35–45
96. Lima AB, Faria EO, Montes RHO, Cunha RR, Richter EM, Munoz RAA, dos Santos WTP (2013) Electrochemical oxidation of ibuprofen and its voltammetric determination at a boron-doped diamond electrode. Electroanalysis 25:1585–1588
97. Messina GA, De Vito IE, Raba J (2006) On-line microfluidic sensor integrated with an enzyme-modified pre-cell for the monitoring of paracetamol in pharmaceutical samples. Anal Chim Acta 559:152–158
98. Dogan B, Uslu B, Ozkan SA, Zuman P (2008) Electrochemical determination of HIV drug abacavir based on its reduction. Anal Chem 80:209–216
99. Al-Ghamdi AH, Al-Ghamdi AF, Al-Omar MA (2008) Electrochemical studies and square-wave adsorptive stripping voltammetry of spironolactone drug. Anal Lett 41:90–103
100. Mashhadizadeh MH, Akbarian M (2009) Voltammetric determination of some anti-malarial drugs using a carbon paste electrode modified with Cu(OH)2 nano-wire. Talanta 78:1440–1445
101. Gumustas M, Ozkan SA (2010) Electrochemical evaluation and determination of antiretroviral drug fosamprenavir using boron-doped diamond and glassy carbon electrodes. Anal Bioanal Chem 397:189–203
102. Skrzypek S, Mirceski V, Ciesielski W, Sokołowski A, Zakrzewski R (2007) Direct determination of metformin in urine by adsorptive catalytic square-wave voltammetry. J Pharm Biomed 45:275–281
103. Goyal RN, Gupta VK, Bachheti N (2007) Fullerene-C60-modified electrode as a sensitive voltammetric sensor for detection of nandrolone—an anabolic steroid used in doping. Anal Chim Acta 597:82–89

104. Dogan B, Tuncel S, Uslu B, Özkan SA (2007) Selective electrochemical behavior of highly conductive boron-doped diamond electrodes for fluvastatin sodium oxidation. Diam Relat Mater 16:1695–1704
105. Uslu B, Ozkan SA, Senturk Z (2006) Electrooxidation of the antiviral drug valacyclovir and its square-wave and differential pulse voltammetric determination in pharmaceuticals and human biological fluids. Anal Chim Acta 555:341–347
106. Sun YX, Wang SHF, Zhang XH, Huang YF (2006) Simultaneous determination of epinephrine and ascorbic acid at the electrochemical sensor of triazole SAM modified gold electrode. Sens Actuator B Chem 113:156–161
107. Komorsky-Lovric S, Nigovic B (2006) Electrochemical characterization of simvastatin by abrasive stripping and square-wave voltammetry. J Electroanal Chem 593:125–130
108. Jain R, Jadon N, Radhapyari K (2007) Cathodic adsorptive stripping voltammetric studies on lamivudine: an antiretroviral drug. J Colloid Interface Sci 313:254–260
109. Ghoneim EM, El-Attar MA, Hammam E, Khashaba PY (2007) Stripping voltammetric quantification of the anti-diabetic drug glipizide in bulk form and pharmaceutical formulation. J Pharm Biomed 43:1465–1469
110. Yilmaza S, Skrzypek S, Dilgin Y, Yagmura S, Coskun M (2007) Electrochemical oxidation of prednisolone at glassy carbon electrode and its quantitative determination in human serum and tablets by Osteryoung square wave voltammetry. Curr Anal Chem 3:41–46
111. Alghamdi AH, Belal FF, Al-Omar MA (2006) Square-wave adsorptive stripping voltammetric determination of danazol in capsules. J Pharm Biomed 41:989–993
112. Wang C, Wang F, Li C, Xu X, Li T, Wang C (2007) Voltammetric sensor for tinidazole based on poly(carmine) film modified electrode and its application. Dyes Pigments 75:213–217
113. Wang F, Chen L, Chen X, Hu S (2006) Studies on electrochemical behaviors of acyclovir and its voltammetric determination with nanostructured film electrode. Anal Chim Acta 576:17–22
114. Lin X, Li Y (2006) A sensitive determination of estrogens with a Pt nano-clusters/multi-walled carbon nanotubes modified glassy carbon electrode. Biosens Bioelectron 22:253–259
115. Qaisi AM, Tutunji MF, Tutunji LF (2006) Acid decomposition of omeprazole in the absence of thiol: a differential pulse polarographic study at the static mercury drop electrode (SMDE). J Pharm Sci 95:384–391
116. Yan JL (2006) Electrochemical behavior and the determination of omeprazole using glassy carbon electrode. J Appl Sci 6:1625–1627
117. Goyal RN, Bishnoi S (2009) Simultaneous voltammetric determination of prednisone and prednisolone in human body fluids. Talanta 79:768–774